



UNIVERSITÉ DE  
STRASBOURG



ÉCOLE DOCTORALE MS2I  
ICUBE – CNRS UMR 7357- LABORATOIRE DES  
SCIENCES DE L'INGENIEUR, INFORMATIQUE ET  
IMAGERIE

**THÈSE** présentée par:

**John Mwangi WANDETO**

soutenue le **14** septembre 2018

pour obtenir le grade de: **Docteur de l'Université de Strasbourg**  
Discipline/ Spécialité: **Informatique**

**Self-Organizing Map Quantization Error Approach for Detecting  
Temporal Variations in Image Sets**

**THÈSE dirigée en cotutelle par:**

MME Birgitta **DRESP** Directeur de Recherche, CNRS Strasbourg, FRANCE (Supervisor)  
M Henry Okola **NYONGESA** Professor of Computer Science and Systems Engineering,  
DeKUT, Nyeri, KENYA (Co-supervisor)

**RAPPORTEUR-E-S:**

M Paul **ROSIN** Professor of Computer Vision, Cardiff University, UK  
MME Rachele **ALLENA** PhD, HDR, MCF ENSAM, Paris, FRANCE

---

**AUTRES MEMBRES DU JURY:**

M Daniel **GEORGE** (examinateur) PhD, HDR, MCF Strasbourg University, FRANCE  
M José **RAGOT** (examinateur) Professor Emeritus of Automatics, Nancy University,  
FRANCE

# Abstract

A new approach for image processing, dubbed SOM-QE, that exploits the quantization error (QE) from self-organizing maps (SOM) is proposed in this thesis. SOM produce low-dimensional discrete representations of high-dimensional input data. QE is determined from the results of the unsupervised learning process of SOM and the input data. SOM-QE from a time-series of images can be used as an indicator of changes in the time series. To set-up SOM, a map size, the neighbourhood distance, the learning rate and the number of iterations in the learning process are determined. The combination of these parameters that gives the lowest value of QE, is taken to be the optimal parameter set and it is used to transform the dataset. This has been the use of QE. The novelty in SOM-QE technique is fourfold: first, in the usage. SOM-QE employs a SOM to determine QE for different images - typically, in a time series dataset - unlike the traditional usage where different SOMs are applied on one dataset. Secondly, the SOM-QE value is introduced as a measure of uniformity within the image. Thirdly, the SOM-QE value becomes a special, unique label for the image within the dataset and fourthly, this

label is used to track changes that occur in subsequent images of the same scene. Thus, SOM-QE provides a measure of variations within the image at an instance in time, and when compared with the values from subsequent images of the same scene, it reveals a transient visualization of changes in the scene of study. In this research the approach was applied to artificial, medical and geographic imagery to demonstrate its performance. Changes that occur in geographic scenes of interest, such as new buildings being put up in a city or lesions receding in medical images are of interest to scientists and engineers. The SOM-QE technique provides a new way for automatic detection of growth in urban spaces or the progressions of diseases, giving timely information for appropriate planning or treatment. In this work, it is demonstrated that SOM-QE can capture very small changes in images. Results also confirm it to be fast and less computationally expensive in discriminating between changed and unchanged contents in large image datasets.

Pearson's correlation confirmed that there was statistically significant correlations between SOM-QE values and the actual ground truth data. On evaluation, this technique performed better compared to other existing approaches. This work is important as it introduces a new way of looking at fast, automatic change detection even when dealing with small local changes within images. It also introduces a new method of determining QE, and the data it generates can be used to predict changes in a time series dataset.

**Keywords:** change detection, self-organizing map, quantization error, time series images, change prediction, difficulty to detect changes.

# Dedication

To my Dad, Wandeto and my Mum, Wanja for being the most practical problem-solving coaches.

To my family: Mercy, Elizabeth, Ann, Maria and Martha; as you are the world's greatest team.

# Acknowledgements

I would like to acknowledgement Birgitta DRESP and Henry NYONGESA, the supervisors of the development of this thesis. It was largely due to their univocal guidance, criticism and encouragement that constant progress was made in the research that culminates in this thesis. In particular, it was encouraging when they promptly replied to my queries, providing clear and straightforward comments that ensured smooth planning, implementation, analysis and reporting of the experiments. Special thanks to the French government, who through their embassy in Nairobi, Kenya awarded me the scholarship to study and do this research work in France. I also recognize efforts by the two universities involved in this research: Dedan Kimathi University of Technology, Nyeri Kenya and the University of Strasbourg, France. They provided good working environment that enabled timely completion of the studies. I will also like to pass special thanks to two radiologists: Dr. Philippe Choquet (PhD) from Hôpital de Hautepierre, and ICube UMR 7357 CNRS-UdS, Strasbourg France, who provided valuable insight and expertise for this research, and Dr. Christian Goetz (PhD) also of Hôpital de

Hautepierre as at December 2015, for playing a crucial role in shaping the idea behind the thesis. Both provided information on how radiologist manage, acquire and utilize information gleaned from images. It was through watching them manipulate medical images, and listening to them talk about gathering information from the images that I gained the confidence and the conviction to work on this thesis. I also thank them for suggesting and directing me to possible and relevant medical image datasets. Last but not least, I thank Yves REMOND, Professor of Mechanics, Strasbourg University, for regularly providing advice on the process and as the head of the doctoral school, provided guidance on administrative matters pertaining to PhD studies at Strasbourg.

# Contents

<b>List of Figures</b>	<b>xi</b>
<b>List of Tables</b>	<b>xv</b>
<b>1 Introduction</b>	<b>1</b>
1.1 Application of Artificial Intelligence on Images . . . . .	2
1.2 Review of change detection work . . . . .	7
1.3 Motivation for this work . . . . .	15
1.4 Objectives of the study . . . . .	16
1.5 Statement of the problem . . . . .	17
1.6 Scope . . . . .	18
1.7 Assumptions . . . . .	19

1.8	Limitations . . . . .	19
1.9	Thesis organization . . . . .	20
<b>2</b>	<b>Self-Organizing Map and the Quantization Error (SOM-QE)</b>	<b>21</b>
2.1	Brain maps and vector quantization . . . . .	22
2.2	SOM . . . . .	25
2.3	SOM learning: winner-takes-all . . . . .	30
2.4	Network architecture . . . . .	32
2.5	The trained SOM: final synaptic weights . . . . .	38
2.6	The quantization error (QE) . . . . .	41
2.7	The SOM-QE concept . . . . .	44
2.8	Hypothesis: SOM-QE value reflects critical variations in image content and it predicts future image status. . . . .	54
<b>3</b>	<b>Experimental Methodology</b>	<b>56</b>
3.1	Change detection problems detectable by SOM-QE . . . . .	58
3.1.1	Materials and methods . . . . .	59
3.1.2	Results . . . . .	66



3.2	How sensitive is SOM-QE? Comparing SOM-QE to human de- tection . . . . .	75
3.2.1	Subjects . . . . .	76
3.2.2	Materials and methods . . . . .	76
3.2.3	Results . . . . .	79
3.2.4	Discussion . . . . .	89
3.3	Change detection in time series of medical images . . . . .	90
3.3.1	Materials and methods . . . . .	94
3.3.2	Results . . . . .	98
3.3.3	Discussion . . . . .	102
3.4	Change detection in time series of satellite images . . . . .	105
3.4.1	Determining urban growth variability through Atlas maps	106
3.4.2	Regions in Las Vegas . . . . .	107
3.5	Using SOM-QE to tell future occurrences . . . . .	132
3.5.1	Method . . . . .	135
3.5.2	Results . . . . .	136
3.6	Evaluating SOM-QE performance . . . . .	138

3.6.1	Carbon dioxide gas measurements . . . . .	138
3.6.2	Challenging change-detection image dataset . . . . .	145
3.7	The SOM-QE algorithm: New method to determine QE in time series images . . . . .	146
3.7.1	Introduction . . . . .	146
3.7.2	Method . . . . .	149
3.7.3	Results . . . . .	150
<b>4</b>	<b>Discussion of results</b>	<b>154</b>
<b>5</b>	<b>Conclusions and Contribution</b>	<b>158</b>
	<b>Bibliography</b>	<b>162</b>
	<b>Appendix A List of publications the thesis has produced</b>	<b>180</b>
	<b>Appendix B Sample code: The Python code used in section 2.7</b>	<b>183</b>
	<b>Appendix C Real medical images: set 1</b>	<b>195</b>
	<b>Appendix D Real medical images: set 2</b>	<b>198</b>

<b>Appendix E</b>	<b>Real medical images with added 1 ‘lesion’</b>	<b>201</b>
<b>Appendix F</b>	<b>Real medical images with global ‘lesions’</b>	<b>204</b>
<b>Appendix G</b>	<b>Satellite images: Las Vegas City Center ROI</b>	<b>207</b>
<b>Appendix H</b>	<b>Satellite images: Lake Mead ROI</b>	<b>210</b>
<b>Appendix I</b>	<b>Satellite images: Residential North of Las Vegas ROI</b>	<b>213</b>
I.1	Résumé . . . . .	216
I.1	Résumé en anglais . . . . .	246

# List of Figures

2.1	SOM learning . . . . .	26
2.2	Reducing sensitivity from point of touch . . . . .	32
2.3	Trained SOM . . . . .	40
2.4	Histogram of change . . . . .	46
2.5	Two images compared using SOM-QE . . . . .	48
2.6	SOM-QE set up . . . . .	50
3.1	Image with local contrast . . . . .	60
3.2	Object added to image . . . . .	62
3.3	Objects increasing in size . . . . .	63
3.4	Growing object in a scene . . . . .	64

3.5	Object with varied light intensity . . . . .	65
3.6	SOM-QE vs extent of contrast . . . . .	68
3.7	SOM-QE vs number of objects . . . . .	69
3.8	SOM-QE vs object size . . . . .	70
3.9	SOM-QE vs contrast area . . . . .	71
3.10	SOM-QE vs contrast intensity . . . . .	72
3.11	Paired random-dot images . . . . .	77
3.12	Average hit rate . . . . .	82
3.13	SOM-QE vs dot size . . . . .	86
3.14	Image dataset used by Pohl et al. [2011a] . . . . .	88
3.15	Images with local 'lesions' . . . . .	96
3.16	Real medical images . . . . .	98
3.17	SOM-QE on real images . . . . .	99
3.18	SOM-QE on images with 1 'lesion' and with 2 'lesions' . . . . .	100
3.19	Images with global 'lesions' . . . . .	101
3.20	Las Vegas ROIs . . . . .	109

3.21	Las Vegas photos . . . . .	114
3.22	SOM-QE on Las Vegas city . . . . .	116
3.23	Visitors in Las Vegas city . . . . .	118
3.24	Visitors in Las Vegas . . . . .	119
3.25	SOM-QE vs number of visitors . . . . .	121
3.26	SOM-QE vs population trend in Las Vegas . . . . .	122
3.27	SOM-QE on Las Vegas image series . . . . .	123
3.28	Water levels in Lake Mead . . . . .	125
3.30	SOM-QE on Las Vegas Residential North . . . . .	127
3.31	Population trend in Residential North . . . . .	128
3.32	SOM-QE vs the Residential North population . . . . .	129
3.33	Regions of change/no change detected by SOM-QE . . . . .	131
3.34	SOM-QE dataset for prediction . . . . .	133
3.35	SOM-QE values: current vs previous . . . . .	134
3.36	SOM-QE prediction . . . . .	137
3.37	Sample images from the challenging change detection dataset . . .	146

3.38	New and old methods of QE determination . . . . .	150
3.39	Changes detected by the two methods . . . . .	151
3.29	SOM-QE vs Lake Mead water levels . . . . .	153
I.1	Régions de changement/aucun changement détecté par SOM-QE .	234
I.2	Exemples d'images provenant de l'ensemble de données de détection des changements difficiles à détecter . . . . .	238
I.3	Nouvelles et anciennes méthodes de détermination de l'QE . . . .	243
I.4	Changements détectés par les deux méthodes . . . . .	244
I.5	Regions of change/no change detected by SOM-QE . . . . .	261
I.6	Sample images from the challenging change detection dataset . . .	265
I.7	New and old methods of QE determination . . . . .	269
I.8	Changes detected by the two methods . . . . .	270

# List of Tables

3.1	Novice response rate for 5 percent change . . . . .	80
3.2	Novice response rate for 10 percent change . . . . .	80
3.3	Novice response rate for 30 percent change . . . . .	81
3.4	Expert response rate for 5 percent change . . . . .	83
3.5	Expert response rate for 10 percent change . . . . .	84
3.6	Expert response rate for 30 percent change . . . . .	84
3.7	SOM-QE on dataset by Pohl et al. [2011a] . . . . .	88
3.8	SOM-QE on Berlin and Strasbourg changes . . . . .	107
3.9	Sampled SOM-QE values of regions in Residential North . . . . .	130
3.10	Predicted versus actual observation . . . . .	138
3.11	Evaluating SOM-QE performance . . . . .	143



I.1	Sampled SOM-QE valeurs des régions dans le Nord résidentiel . .	233
I.2	Sampled SOM-QE values of regions in Residential North . . . .	260

# Chapter 1

## Introduction

Radiologists use time-series of medical images to monitor a patient's condition. They compare information gleaned from sequences of images to gain insight on progression or remission of the lesions, thus evaluating the progress of a patient's condition or response to therapy. Visual methods of determining differences between one series of images to another can be subjective or fail to detect very small differences. Similarly, city administrators, planners and politician, among others, require to monitor infrastructure distribution within their cities and determine the changes in city status with time. They need to know the effects of resources, for instance road networks, on the residents' lives in the different parts of the city. In this thesis, the application of SOM-QE technique to assist the radiologist and the city managers to mine information from an image at a particular time and thereafter, monitor subsequent changes occurring with time in the patient and in the

city is demonstrated. Medical images and satellite images are directly analysed to eliminate intermediate procedural bias and to produce fast results.

The concept behind the SOM-QE approach is that through use of images, determination of a scene's current status is performed and from subsequent images of the same scene, changes that have occurred in time within the scene can be analysed. In this chapter, an overview of the use of artificial intelligence systems to process images and in particular, to detect changes through images is given. The objectives of the research and the specific area of study are also spelt out to give a perspective of the thesis.

## **1.1 Application of Artificial Intelligence on Images**

An image refers to a 2D light intensity function  $f(x,y)$ , where  $(x,y)$  denote spatial coordinates and the value of  $f$  at any point  $(x,y)$  is proportional to the brightness or gray levels of the image at that point. Cameras can capture objects into digital images, providing an avenue for manipulation and study of objects in a computer since the image,  $f(x,y)$ , has been discretized both in spatial coordinates and brightness. Images are widely used to represent real objects, for example in medical field, images are used to study state of internal body organs. Thus, images provide a ready chance to process a scene data for autonomous machine perception. There exist advance procedures for extracting information from images in a form suitable for computer processing. When in the computer, mostly in form

of arrays, the information can be processed and be put to use in areas such as in character recognition, industrial machine vision for product assembly and inspection, military recognizance, automatic recognition of fingerprints and such similar applications.

Major procedures involved in image processing include

1. image acquisition – the capturing or collection of images,
2. image preprocessing – improving the image in ways that increase the chances of success of next processes,
3. image representation – to convert the input data to a form suitable for computer processing,
4. image description – to extract features that result in some quantitative information of interest or features that are basic for differentiating one class of objects from another and
5. image interpretation which is assigning meaning to an ensemble of recognized objects.

Thus, images provide a route for real objects to be analysed and studied in the field of artificial intelligence (AI). The images provide alternatives to other methods of learning the objects like directly measuring quantities/elements in the object – such as temperature of a patient, carbon dioxide concentration in air, composition of soil, among others.

A common technique used to formulate AI systems is the use of artificial neural networks (ANNs). An ANN is made up of several nodes, linked together and whose functioning imitate that of biological neurons of human brain. A node takes input data, performs simple operations on the data and passes the results to other nodes, hence forming a network system of processing nodes. The output at each node, called its activation or node value, can be altered through weight values associated with the link between nodes, a process called learning. During learning, weight values in the nodes are compared to the input value and together with a predetermined learning parameter the amount of change to be effected is calculated. Thus, as P. R. Oliveira and R. F. Romero [1996] puts it, ANN models are specified by the network topology, node characteristics and training or learning rules. The learning rules specify an initial set of weights and indicate how weights should be adapted during training to improve performance. An important property of an ANN is the ability to learn from its environment and to improve its performance through learning. ANN learns about its environment through an iterative process of adjustments applied to its synaptic weights.

There are two major learning strategies that can be employed by an ANN: the supervised learning and the unsupervised learning. In supervised learning, the results given by an ANN are compared with the expected results and the network makes adjustments based on the errors determined. The goal is to approximate a mapping function of the input to the output so that when new input data is provided, its corresponding output can be predicted. This is the case, for instance, in

pattern recognition. In unsupervised learning, the ANN is provided with the input data and not the expected output. It aims at modelling the underlying structure or distribution of data in order to learn more about the data. In this regard, an ANN algorithm is set up, provided with input data and left on its own to discover and present the interesting structure in the data. Among the techniques in this category of ANN is the K-means clustering algorithm and the focus of this thesis: the SOM algorithm.

Back in 1993, Pal and Pal [1993] predicted that ANNs would become widely applied in image processing and according to Egmont-Petersen et al. [2002], this prediction turned out to be right. ANN applications have been developed to solve different problems in image processing, with strengths and weaknesses being observed on each application. These applications have been deployed to solve various problems as categorized in Egmont-Petersen et al. [2002]. For example, in image reconstruction problems, quite complex computations are required and a unique approach is needed for each application. In Adler and Guardo [1994], an ADALINE (an early single-layer artificial neural network and the name of the physical device that implemented this network) network is trained to perform an electrical impedance tomography (EIT) reconstruction. In image restoration problems one wants to derive an image that is not distorted by the (physical) measurement system. The system might introduce noise, motion blur, out-of-focus blur, distortion caused by low resolution, among other distortions. Restoration can employ all information about the nature of the distortions introduced by the

system, for example, the point spread function.

Another category of image processing is the image enhancement problems, where the goal of the ANN is to amplify specific features, with most applications being based on regression ANNs. A well known enhancement problem is edge detection. A straightforward application of regression feed-forward ANNs, trained to behave like edge detection, was reported by Griffiths [1988].

In data reduction problems, ANNs are applied in image compression and feature extraction. ANN approaches have to compete with well-established compression techniques such as JPEG, a standard reference in this domain P. R. Oliveira and R. F. Romero [1996]. The major advantage of ANNs over JPEG is that their parameters are adaptable, which may give better compression rates when trained for specific image material. For instance, P. R. Oliveira and R. F. Romero [1996] performed a comparative study and confirmed the performance of the PCA ANN as superior to the JPEG for all the compression ratios used to compress the images in their experiments.

In image segmentation, the image is partitioned into parts that are coherent according to some criterion. This may be applied as a classification task where labels are assigned to individual pixels or voxels.

In object recognition, locating the positions, possible orientations and scales of instances of objects in an image are done. Egmont-Petersen et al. [2002], has reported several pixel-based and feature-based object recognition applications of

ANNs. Another area in image processing that ANNs are applied is image understanding which combines techniques from segmentation or object recognition with knowledge of the expected image content. This can then be applied, for instance, to classify objects such as chromosomes from extracted structures or to classify ships recognized from pixel data, Egmont-Petersen et al. [2002].

More recently, D. Jiang [2013] has applied a SOM based procedure for MRI image processing. They noted that MRI images are usually corrupted by Rician noise that is generated during the image formation. Rician is a non-additive, signal dependent and highly non-linear noise that is difficult to separate from the signal. The SOM algorithm was applied, taking the Rician noise into consideration, to de-noise and segment an MRI image. In image segmentation, an ensemble - a learning paradigm where multiple neural networks are jointly used to solve a problem - of SOMs, Jiang and Zhou [2004], is used to perform segmentation. In, Chen et al. [2017], a SOM is used to develop a crack recognition model for bridge inspection.

## **1.2 Review of change detection work**

Change detection is an important domain in computer vision with applications ranging from video surveillance and medical imaging to remote sensing in urban and environmental change detection. Before changes can be detected, images are typically preprocessed to register them geometrically and correct for any radio-



metric variation Radke et al. [2005a]. In remote sensing, where the goal is to detect urban changes such as the extent of urbanization from a series of 2D map built from satellite images, parallax effects are negligible and synthetic aperture radar is frequently used to lessen the effect of atmospheric and lighting change across time. However, medical images require pixel-accurate registration as a starting point since the situations of their capture are different from that of the satellite images.

Change detection methods can be classified into several categories depending on type of scene, changes to detect, methods, and available information, Sakurada and Okatani [2015]. In 2D image domain, which according to Radke et al. [2005a], forms a majority of the work they surveyed, a typical approach involve identifying a scene, the region of interest (ROI), capture a set of its images at different times, and train an ANN to determine changes between the images. Then a newly captured query image can be run on the ANN to detect changes. A concern in this type of studies is dealing with irrelevant changes such as difference in illumination. It usually requires the images to be captured from the same viewpoint, and thus cannot deal with query images captured from different viewpoints. SOM-QE falls under this category and it requires the query image to be brought into similar conditions as those of the training image through appropriate preprocessing procedures.

Image science has proposed methods for the automated processing of medical images, which involve various image processing techniques to identify specific

diagnostic ROI and features, such as lesions. Challenges still abound and advance techniques are required to tackle them. For instance, a simple difference map of two longitudinal co-registered MRI volumes fails to detect specific tumour evolution, due to non-linear contrast change between the two data sets, according to Angelini et al. [2007]. They proposed a computational framework to enable comparison of MRI volumes based on gray-scale normalization to determine quantitative tumour growth between successive time intervals. Angelini et al. [2010] proposed three tumour growth indices, namely; volume, maximum radius and spherical radius. The approach, however, requires an initial manual segmentation of images, which can be a time-consuming task. In Konukoglu et al. [2008], they first semi-automatically segmented a tumour in an initial patient scan and then aligned the successive scans using a hierarchical registration scheme to measure growth or shrinkage from the images. This method relies on accurate segmentation and requires manual supervision, in order to detect changes of up to a few voxels in the pathology. Pohl et al. [2011a] describe a procedure aimed for difficult-to-detect brain tumour changes. The approach combines input from a medical expert with a computational technique. In this thesis, a new technique is proposed based on self-organized mapping that considers the whole medical image, as opposed to an image segment, as a ROI. This excludes manual benchmarking tasks designed to eliminate inclusion of structures with similarity to tumour pathology. The basic principle behind direct image analysis is that there exists an intrinsic relationship between medical images and their clinical measurements, which can be exploited to eliminate intermediate procedures in image analysis. Compared to traditional

methods, direct methods have more clinical significance by targeting the final outcome. Thus, direct methods not only reduce high computational costs, but also avoid errors induced by any intermediate operations. Direct methods also serve as a bridge between emerging machine learning algorithms and clinical image measurements.

As observed in Radke et al. [2005a], the goal of change detection is to identify the set of pixels that are significantly different between the last image in a sequence and the previous images. But significantly different may vary from application to another, making it difficult to compare results. SOM-QE technique takes each input feature vector from the image, labels it, and then uses the label to monitor changes that have occurred within the same vector with time. By detecting difference at the input sample level, the technique is able to tell when changes have occurred or not occurred in parts of the image and by extension, changes within regions and sub-regions of an area can be quantified.

Image pairs taken at different times may have temporal differences in illumination and photographing conditions. In Sakurada and Okatani [2015], they had to cope with visual difference in camera viewpoints for the two images as they were captured from a vehicle, although running on the same street and had been matched using GPS data.

To cope with these issues, some of the previous studies consider the problem in the 3D domain. In this domain, Crispell et al. [2012], Huertas and Nevatla [1998], Eden and Cooper [2008], and Taneja et al. [2011], a model of the target scene is

built to a ‘steady state,’ and used to compare a query image against it to detect changes. The 3D model of the scene is created using a 3D sensor. In Huertas and Nevatla [1998], to estimate the existence of a building, the edges extracted from its aerial images are matched with the projection of its 3D model to detect change. Schindler and Dellaert [2010] proposed using a large number of images of a city taken over several decades. Their method performs several types of temporal inferences, such as estimating the time when each building was constructed. More recently Matzen and Snavely [2014] did similar work only that their method uses Internet photo collections to detect 2D changes of a scene, such as changes of advertisements’ billboards and painting on a building’s wall. Work in this domain assume that a 3D model of a scene is given beforehand or can be created from images, and that the input images can be registered to the model with pixel-level accuracy Matzen and Snavely [2014], Schindler and Dellaert [2010] and Taneja et al. [2013]. However, a 3D model is not always available for every city. Besides, it is sometimes hard to perform precise image registration, due to lack of sufficient visual features. These are particularly the case when the scene undergoes enormous amount of changes. Working in 3D domain tends to require large computational cost, which can be another difficulty when detection of changes for a large city is required. In the present SOM-QE idea, satellite images, captured from a fixed position, are used and hence avoid the visual problem. In Sakurada and Okatani [2015], they used a method that uses features of convolution neural network (CNN) in combination with super-pixel segmentation. They observed that though CNN features detect the occurrence of scene changes, it did not pro-

vide precise segmentation boundaries of the changes, hence the application of super-pixel segmentation. Therefore, despite having reasonable performance, the method relies on super-pixel regularization and sky/ground segmentation to delineate changes accurately.

The work by Sakurada et al. [2013] defines a probabilistic framework in which changes over all possible disparities are evaluated and integrated for each re-projected ray. While this avoids the need for explicit modelling and additional information or sensors, their framework makes the assumption of per-pixel independence in order to be tractable but still remains computationally expensive. SOM-QE is a computationally efficient approach which works from image data to determine variability in the image irrespective of the structure of objects in the image. After the image sequences have been aligned through registration and normalized when need be, a similarity measure, the QE, is calculated and employed to determine changes of interest between the data while ignoring other nuisance changes. The definition of what constitutes a change of interest or a nuisance change varies depending on the task. Changes of interest may be purely geometric, such as the appearance or disappearance of urban structures Sakurada et al. [2013], Taneja et al. [2011] and Taneja et al. [2013], or textural, such as changes in billboards or shop-fronts Matzen and Snavely [2014] or surface defects Stent [2015]. Nuisance changes may include lighting effects, for example, cast shadows. Stent [2015] proposes training change detection networks from scratch on image patches to classify changes for industrial inspection. In contrast to these

prior works, SOM-QE adopts the self-organizing network approach, first used in Kohonen [1981a] , and demonstrate its ability to learn appropriate, spatially and precise differences between images.

In their review of change detection algorithms, Skifstad and Jain [1989] reported that besides the specific technique used for measuring changes, the change detection process employed in the works they reviewed was generally the same. The input images are first divided up into defined regions. In SOM-QE technique proposed here, the image is considered as a whole. This avoids segmentation which can be computationally expensive, depends on some human operator decisions, or is not suitable to some type of land shapes. As pointed out in Palanivel and Duraisamy [2012], uncertain nature is present in the image segmentation process. SOM-QE method assigns a QE value to each input feature vector of an image based on a trained SOM, providing a clear indication on how far the best matching unit is from the input vector it won during the learning process.

Most existing change detection methods require a decision as to where to place threshold boundaries in order to separate areas of change from those of no change, Singh [1989]. The threshold value is supplied empirically or statistically by the analyst, rendering the results obtained to be subjective. However, with SOM-QE technique, no thresholding value is required and input feature vectors are treated equally and with the same weight to arrive at the final decision.

Another approach to determining the changes that have taken place between images involve determining changes in land-use zones' size within cities over time.

Major land uses in a city - built-up, agricultural, water body, undeveloped land, among others are identified. By use of satellite images of the city, plus information from local city authorities, and/or collecting locally relevant data, the size of each land-use zone is determined. This size is compared for a series of images taken from the ROI over time to determine the change, given as percentage occupation of each land-use item. Conclusions are then derived on changes that have occurred, and the land-use zone that has 'encroached' on the other within the specified period is shown, as in Hegazy and Kaloop [2015], Kayet and Pathak [2015] among others.

But there are other causes of changes in cities. Changes in city growth are not limited to the changing size occupied by land-use zones. For example, a new house built within a land-use zone does not cause change in the size of the area, and hence such change will not be captured by the method. Besides, it has been shown that, within a particular land-use zone, features of the other land-use zones occupy substantial land. As determined in Angel et al. [2016], the share of built-up area occupied by roads and avenues was on average at  $20 \pm 2$  in 38 cities across the world, as at the year 2015. Thus, SOM-QE method suggested here is able to sense small changes, caused by other factors in addition to those caused by the changing occupational size of a land-use zone. This is done fast enough and can be appropriate for use in an ideal application scenario. It took less than 3 minutes to determine changes between images in a series of 25 images covering the 25 years studied for a ROI in Las Vegas city, USA.

### **1.3 Motivation for this work**

Guthmann et al. [2005] established that shorter return visit interval (RVI) for patient has a positive correlation with percentage change in blood pressure and that RVI may be a tool in the management of hypertension. Schectman et al. [2005] concurs that prolonging the RVI may affect quality of care when prevention measures and chronic disease management receive less attention as clinic visits become less frequent.

Schwartz et al. [1999] noted that physicians lengthened revisit intervals for routine visits and shortened them when the visit required a change in the disease management. On the other hand, changes that have occurred between shortened RVI may be too small to be detected by human observers. There is therefore, a need to have a tool that will enable the automatic detection of subtle but significant changes in time series of images likely to reflect growing or receding lesions.

Likewise, from satellite images, comparing the status of two cities requires the capture of minute details in each, which SOM-QE does effectively. The motivation behind this study is to develop a change detection method that can be used for visualization of healing or worsening disease condition as captured by medical images or city urbanization or environmental changes as captured through satellite images, as well as for the purpose of quantifying the change occurring within time.



## 1.4 Objectives of the study

The goals of this thesis are threefold:

1. To develop a platform for
  - (a) determining the variation status of an object through studying the object's image at a particular time.
  - (b) tracking changes taking place in the object over time through images taken from the same object at different times.
2. The platform should be fast enough and appropriate for use in an ideal application scenario, for example, during a patient's clinical visit at the hospital.
3. To develop a new method for calculating quantization error in a time series image dataset that is more accurate than the existing method.

The goals are attained by accomplishing the following specific objectives:

1. Analyse objects through their images taken for medical diagnosis, environmental monitoring or for city development purposes
2. Assign unique labels to objects through their images based on the object's contents
3. Differentiate the content of an object at different times based on the object's SOM-QE values at the different times

4. Detect changes in an object given its series of images taken at different times.
5. Quantify change and give direction of change within an object over time.
6. Quantify variation within an object through studying its images.
7. Develop a robust and fast application for change detection.
8. Provide data for use in change prediction for a region.

## **1.5 Statement of the problem**

Cancer patients require that their condition be monitored seamlessly, with accuracy, and that they be aware and be informed of the outcomes and their status promptly at every clinical visit. City residents and administrators expect equal development and distributions of city resources within the city, easy status comparison with peer cities and monitoring of the environment for example, for harmful gases, and that they instantly be made aware whenever slight positive or negative changes occur.

Today there is too many late diagnoses of cancer and other chronic diseases that results in too many deaths. There is uneven city development and increase in environmental degradation that has seen the weather pattern changed with unfair and negative consequence for life. If these problems are ignored; deaths will

increase and resources to handle the cascading problems will need to be increased too, the cities may end up being unevenly and skewed developed which could result in feelings of inequality, discrimination, lawsuits and further damage to the leadership ability to guide growths within cities.

SOM-QE is designed to detect small changes that have occurred within a patient, thus reducing periods between clinical visits, senses regional development status and detect minute environmental changes from the relevant images to improve on monitoring of patients and city's status, and thus solve the problem.

In SOM-QE, a clear path to change detection is set: SOM learns the image to provide its ideal pixel values. Then QE provides the difference between the real and the ideal values, which for different images within a series can tell when changes have occurred in the organ or in the city with time.

## **1.6 Scope**

SOM-QE relies on information it gleans from medical and satellite images individually or/and in the time series image dataset to determine variability and changes in objects as portrayed through their input features. The learning process of SOM determines the set of vectors that acts as the platform on which input vectors are referenced to determine their QE values. Hence, the accuracy of the QE value returned relies on this set of vectors. SOM-QE works better when the input

vectors have values of between 0 and 1. It should be noted that manual inspection of scenes can pick up other changes that the current SOM-QE system cannot detect, such as lesions occluded behind internal body parts or a new construction appearing just outside of an existing building that obscures its view. In its present state, SOM-QE takes 2D images as input. 3D images are outside its scope.

## **1.7 Assumptions**

For images to be compared in the proposed SOM-QE algorithm, they must have been captured under similar lighting, colour and orientation conditions. Medical images, satellite images and Urban Atlas maps are assumed to be preprocessed accordingly for effective determination of their SOM-QE values.

## **1.8 Limitations**

SOM-QE uses medical images as provided by radiologist and spatial images from the available satellites. Though sufficient preprocessing procedures are carried out on the images, it is beyond SOM-QE algorithm's mandate to capture the image in the desired quality. The findings in this research are still valid and useful despite this limitation.

## 1.9 Thesis organization

After a general overview of SOM, its functional principles and the derivation of QE, the thesis sets out to explain the details behind the SOM-QE concept and states the hypothesis in chapter 2. In chapter 3, a series of application scenarios are described before giving an in-depth description of experiments conducted with human observers on detection of change within images in a "man versus machine" style. Then, discussion on SOM-QE's performance on real medical and satellite images is presented. Later, it is shown that SOM-QE values from a time series set of images, can be used to generate predictions on changes in the ROI. The technique is then evaluated, before a new method of determining QE is introduced. In chapter 4, the results of SOM-QE performance in various change detection applications are discussed. Finally, in chapter 5, conclusions on the major findings of the research are presented and their contribution to knowledge is highlighted.

In this chapter, the use of images in computer systems to analyse objects is discussed. Details on the analysis of change that has occurred in an object between two times are provided as they exist in literature, alongside those of the proposed method. In the next chapter, the structure and the working of the new method are explained and demonstrated.

## **Chapter 2**

# **Self-Organizing Map and the Quantization Error (SOM-QE)**

The new measure of image variation and change detection proposed in this thesis and referred to as SOM-QE, is discussed in details in this chapter. It involves two concepts; the self-organizing map (SOM) and the quantization error (QE). QE is obtained when the final weights of SOM are subtracted from the original input vectors of the image, effectively telling how close the SOM is to the image. To fully comprehend the idea behind SOM and hence SOM-QE, it is important to trace its origin, which is the working of the human brain. This also justifies the choice of SOM over other ANNs in solving the problem of determining variation within objects through their images. Then, details on the design of SOM-QE algorithm are presented. Later, the SOM-QE idea is analysed using two basic images

and validated separately using two commonly used dataset content measures – the variance and the histogram. The chapter ends by stating the hypothesis that guides the remaining chapters of the thesis.

## **2.1 Brain maps and vector quantization**

According to Kohonen [2013], for many years it had been known that various cortical areas of the brain are specialized to process different modalities of cognitive functions. This was confirmed when Mountcastle [1957] and Hubel and Wiesel [1962] discovered that indeed certain single neural cells in the brain respond selectively to some specific sensory stimuli. These cells, called brain maps, often form local assemblies, in which their topographic location corresponds to some feature value of a specific stimulus in an orderly fashion.

Since the brain is an efficient processor of information, it is worth imitating it for an ANN to post reliable results. Image scene, like the ones in medical or satellite images, are composed of various objects which require to be processed separately, or locally, as the brain maps do. For instance, within a lung image there may be a lesion or a water dam in a city map, each of which is processed by a suitable brain map. ANN units can be set to process data in a near-similar manner to the brain maps.

Initially, the believe was that brain maps are determined genetically. Later, the

brain maps, at least their fine structures and feature scales, were found to depend on sensory experiences and other occurrences. Studies of brain maps that are strongly modified by experiences were reported by Merzenich et al. [1983], among others. In the 1970s, Grossberg [1976], Nass and Cooper [1975] and Perez et al. [1975] investigated whether feature-sensitive cells could be formed automatically in artificial systems through learning.

These works were among the first to succeed in showing that input-driven self-organization was possible. Feature-sensitive units were implemented through competitive learning ANNs. In general, the ANNs had subsets of their units adapt to different input signals during the training process.

However, these early biologically-inspired brain maps were not suitable for practical data analysis. First, they produced partitioned maps after the learning process. The maps were made up of small patches, and there was no global order over the whole map. But, in particular, Suga and O'Neill [1979], TUNTURI [1950]-Tunturi [1952] and Zeki [1980] have shown that brain maps of tonotopic maps, the colour maps and the sonar-echo maps respectively are globally organized, confirming the first failure of the early brain maps. The second shortcoming of these models was lack of ability to scale up as they could not be used for large networks and high signal dimensionality, even with increased computing power, Kohonen [2013].

SOM introduced a control factor whose amount depends on local signal activity, but which does not contribute to the signals. The control factor plays the role



of determining how much the signal can modify the selected subsets of neural connections in the network. This allows the ANN to work up to the capacity limit of the modern computers.

Then to follow up on improvement of the brain maps, optimally tuned feature-sensitive filters that employed competitive learning, called vector quantization (VQ), were implemented by LLOYD [1982] and Forgy, E.W. [1965] in scalar and vector forms respectively. VQ is currently a standard technology in digital signal processing.

In VQ, feature vectors are partitioned into a finite number of contiguous regions, each represented by one unit vector, called codebook vector. ‘The codebook vectors are constructed such that the mean distance, measured in some metric, of an input data item from the best-matching codebook vector, called the winner, is minimized. That is, the mean quantization error is minimized.’,Kohonen [2013].

For simplicity, the VQ is illustrated using the Euclidean distance metric only. Let the input data items constitute n-dimensional Euclidean vectors, denoted by  $x$ . Let the codebook vectors be denoted by  $m_i$ , and  $m_c$  be a particular codebook vector called the winner as it has the smallest Euclidean distance from  $x$ :

$$m_c = \underset{i}{\operatorname{argmin}} \|x - m_i\| \quad (2.1)$$

If  $p(x)$  is the probability density of  $x$ , the mean quantization error  $E$  is defined as:

$$E = \int_v ||x - m_i||^2 P(x) dV \quad (2.2)$$

where  $dV$  is a two-dimensional differential of the data space  $V$ . The objective function  $E$ , being an energy function, can be minimized by a gradient-descent procedure.

When input data items are finite, batch computation VQ can be implemented in what is sometimes called Lloyd-Forgy, after LLOYD [1982] and Forgy, E.W. [1965], and commonly called the k-means clustering.

## 2.2 SOM

SOM is an ANN that is a non-linear mapping and which is similar to the VQ, except that its processing units become spatially and globally ordered Kohonen [1982]. SOM units are associated with the nodes of a regular, usually 2D grid as shown in Figure 2.1.

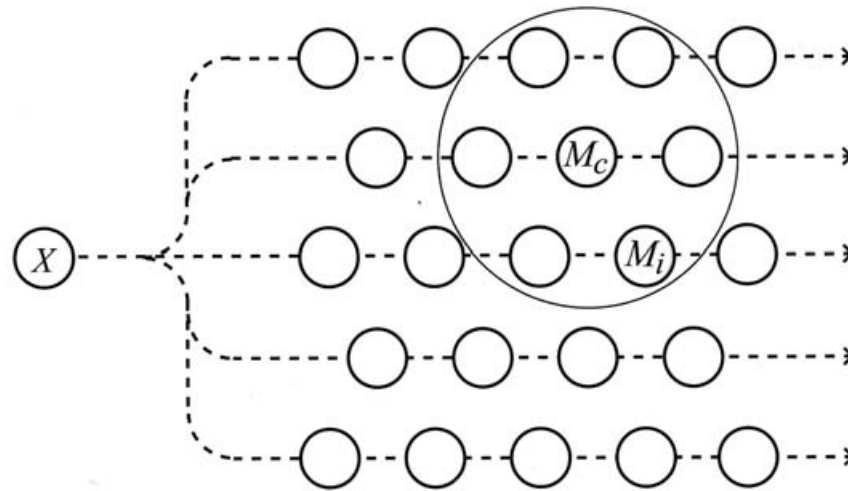


Figure 2.1: An illustration of a Self-Organizing Map. An input data item  $X$  is broadcast to a set of models  $M_i$ , of which  $M_c$  matches best with  $X$ . All models that lie in the neighbourhood (larger circle) of  $M_c$  in the array will be updated together in a training step to make them match better with  $X$  than with the rest at the end of the step. Figure courtesy of Kohonen [2014b]

According to SOM founder in Kohonen [2013], the learning principles and mathematics of SOM are based on a central idea, that; every input data item selects a unit from the map that it matches best. Then, the selected unit and a subset of its spatial neighbours in the map, are modified to match the input vector better.

In effect, SOM learns from a given dataset to produce results that:

1. place similar data samples together.
2. as much as possible, maintains the location of each sample in relation to its

neighbours in the original dataset, that is, topology preserving.

This explains the main reason for the choice of SOM for the task of this research, that: unlike in most biologically inspired ANNs, the topographic order in the SOM can always be materialized globally over the whole map. Thus, when a trained SOM is given a new and previously unknown input vector, this input is identified with the best-matching unit in SOM and hence it is classified with the particular unit.

During the learning process, matching by similarity is done between the input data and the initial unit values in SOM. Both the input data and the SOM unit values are expressed as real vectors, consisting of numerical results. The vectors are placed on the same scale, through normalization of both scales, in this case by having their maximum and minimum become the same. After that, the standard Euclidean measure is used to determine the level of similarity between the input vector and the map unit vector. SOM has been known to work with even complex interdependencies of variables and return results by using Euclidean distance with normalization, Kohonen [2013]. Another consideration made is the presentation of an image as an input vector. Images have natural variations caused by translations, rotations, differences in size or in lighting conditions. To minimize the effect of these variation, image registration and normalization are done. Red-green-blue, (RGB), colour as a characteristic feature of the image, is extracted and presented as input vector of the image. This enables the input object to be a restricted set of invariant features, which drastically reduce the computing load,

Kohonen [2013].

The ANN's learning procedure is unsupervised with specific self-organizing dynamics that do not require error correction as do supervised learning algorithms. SOM produces a lower-dimension representation of the input space and for each input vector, a competitive winner-take-all learning algorithm Kohonen [1981a] achieves the lower-dimension visualization of the input data. SOMs are typically applied as feature clustering of input data starting from an initially random feature map. The input data are recursively fed into the learning procedure to optimize the final map into a stable representation of features and ROI. Each region of the map can be considered in terms of a specific feature class of the input space. Whenever the synaptic weights associated with a node of the map match the input vector, that specific map area is selectively optimized, bringing it closer in resemblance to the data of the class the input vector belongs to. From an initial distribution of random weights and over thousands of iterations, SOM progressively sets up a map of stable representations of image regions or ROI. Each corresponding region of the final map is a feature cluster and the graphical output is a certain type of feature map of the input space.

The map structure obtained from the learning process leads to SOM being viewed as a topology preserving transformation from high dimensional space to a low dimensional space Kohonen [1995]. This low dimensional space is usually a 2D or 1D grid. From this point of view SOM can be compared to other dimensionality reduction and data unfolding methods, Moosavi [2014]. Among the meth-

ods, which are rooted in Topological Data Analysis (TDA), Zomorodian [2011], are; Multidimensional Scaling (MDS), Kruskal [1964], Locally Linear Embedding (LLE) Roweis and Saul [2000], ISOMAP Tenenbaum [2000], and Mapper Singh et al. [2007]. But SOM goes beyond this. Besides the transformation of data, SOM discovers ‘the shape of data’ in terms of topology and geometry, which leads to successful methods in visualization and exploratory data analysis tasks. In this view of SOM, regardless of the global dimensionality of the observed data set, given a similarity measure among individual data points, a self-referential coordinate system can be constructed, by which each instance of the observation becomes a dimension for itself compared to all the other points, Moosavi [2014].

Topology preservation implies that vectors that are close in the high-dimensional space end up being mapped to nodes that are close in the 2D space. For example, lesions in a lung will occupy the same relative position in the trained dataset as they did in the original image, or that a particular building in the city maintains its location relative to other buildings in the original image.

Topological preservation is attained when the BMU and its neighbours ‘learn’, which is accomplished through adjusting their weights to fit more closely to values of an input vector. The ‘learning’ is more for the BMU and decreases as the distance of a neighbouring unit from BMU increases, as explained in details in section 2.4.

These two facts, grouping input samples and topology preservation, makes SOM a good fit for the goal of this thesis. Data is learned and grouped based on its

similarity while considering their current location. This means that each data item makes contribution to the variation in the image from its local location, making the SOM-QE value to be a more reliable and accurate measure of variation.

### **2.3 SOM learning: winner-takes-all**

The vector space of the SOM is Euclidean Kohonen [1981a], and the central idea behind the principles of self-organized mapping is that every input data item is matched to the closest fitting neuron unit of the neural map, the winner. The winning neurons for the corresponding regions are progressively modified on that principle until they optimally match the entire data set. The learning procedure follows the neural-biological principles of lateral inhibition and the general rule of Hebbian synaptic learning Hartline et al. [1956]. On the other hand, since the spatial neighbourhood around the winners in the map are continuously modified during learning, a degree of local and differential ordering of the map is mathematically applied in the smoothing process. The resulting local ordering effect will gradually be propagated across the entire SOM. The parameters in SOM model can be variable and depend on the type of input data being implemented. The goal of this winner-take-all learning is to ensure that the final map stably represents critical similarities in the input data.

In general two operations take place in the SOM learning: first, there is the spatial clustering of activity into one centre of high activity, the location of which is a

function of the input pattern. This location becomes the winner. Secondly, there is the adaptive modification of the interconnections in the local area around the winner such that all neural functions in this area are tuned better to the prevailing input activity and will respond stronger to it. This local area imitates the brain map, as explained in section 2.1.

Thus, for different inputs, different local areas will be modified, and in the long run different areas of the ‘map’ will become selectively tuned to different domains of the input in an ordered and almost optimal fashion.

Figure 2.1, adapted from Kohonen [2013] , shows the effect of input data to the map.

Only a subset of the map units is able to learn the present input vector and even within the subset the amount of learning is varied – strength of learning decreases as the distance to the unit from the BMU increases. Figure 2.2 is a synonymous illustration with the real feeling on human skin. The sensing of the sharp object pressed on the skin is more at the point of touch and reduces outwards from this point. On SOM, the ‘point of touch’ is the BMU while the rest of the region on the skin that will feel the touch by the sharp object corresponds to the BMU’s ‘neighbourhood’.





Figure 2.2: The spatially diffusive local sensitivity of a single touch receptor may be used to illustrate the functional model underlying SOM. On pressing the skin surface with a pointed object, the feeling is more intense at the point of touch and reduces as distance from the point increases outwards.

## 2.4 Network architecture

A 2D organization of the map units was adapted in this work since it is usually effective for approximation of similarity relations of high-dimensional data, as is the case with images, Kohonen [2013]. Since it is not possible to guess or estimate the exact size of the SOM map beforehand, it was determined by the trial-and-error method after seeing the quality of the first guess, Kohonen [1981b]. For most of the images encountered in this work, a 4 by 4 map, giving 16 processing units, was found to be the optimal size.

The map is connected to the input layer, which can be an n-dimensional vector to

form the network.

In the detailed implementation of the original SOM algorithm provided in Buckland [2005] , each learning unit occupies a specific topological position - an x-y coordinate on the map - and contains a vector of weights of the same dimension as the input vectors. In most of the cases in this thesis, RGB values of the image are extracted and used as input vectors to the map, hence the units are set to have three weights, one for each element of the input vector: red, green and blue.

The adaptation of the synaptic vectors in the models is done as proposed by Kohonen in Kohonen [1981b] and Kohonen [2014a]:

1. Determine the best-matching unit for the current input vector.
2. Make the best-matching unit and its topologically nearest neighbours more similar to the input vector.

To attain this, SOM does not need a target output to be specified, instead, where the model weights match the input vector, that area of the map is selectively changed through the learning process to improve its resemblance to the data in the input vector. From an initial distribution of random weights in the units, and after several iterations, the SOM eventually settles into a map of stable zones. Each zone is effectively a feature classifier, such that the graphical output represents feature map of the input space, Figure 2.3. At the end of the training process, if any new, previously unseen input vector is presented to the network, it will stimulate units in the zone with whose weight vectors are more similar to its values

than the other zones. This effectively, clusters the new input as a member of the zone it stimulates.

The region around the BMU where units are adjusted at every iteration is identified by the neighbourhood radius. This is a value that starts large, typically set to the 'radius' of the map, but diminishes at each time-step. This radius, together with the learning rate, determine the amount of learning to be effected on the units.

As illustrated in Buckland [2005], the training steps involved in the SOM algorithm are:

1. Each unit's weights are initialized using vector values picked randomly from the image.
2. A vector is chosen at random from the set of RGB features extracted from the image data and presented to the map.
3. Every map unit is evaluated to determine the amount of difference between its weights' values and the input vector's values. The unit with the smallest difference 'wins' the input vector to become its BMU.
4. The radius of the neighbourhood of the BMU is calculated. Any unit found within this radius from the BMU is deemed to be inside the BMU's neighbourhood.
5. Weights of units within the BMU's neighbourhood are adjusted to reduce their difference with the input vector. The closer a unit is to the BMU, the

more its weights are altered, making it ‘learn’ more than the units that are far.

6. steps 2 to 5 are repeated for a specified number of iterations, N.

To know the BMU for the input vector, all the units are iterated as their Euclidean distance with the current input vector is calculated. The Euclidean distance,  $d$ , is calculated as:

$$d = \sqrt{\sum_{i=0}^{i=n} (V_i - W_i)^2} \quad (2.3)$$

where  $V$  is the current input vector and  $W$  is the unit’s weight vector. The unit with the lowest distance becomes the BMU for the input vector.

During each iteration and after the BMU has been determined, units within the BMU’s neighbourhood are identified. These units – they form a local region for the input vector - will have their weight vectors altered in the next step. This optimizing of the region for the input vector, sets SOM aside from other ANNs. To attain this creation of local regions, first the radius of the neighbourhood is calculated then, with the BMU as the centre, the radius is used to cover a circular area around the BMU. This becomes the neighbourhood region. At the beginning of the training, this radius is set at half the map width as in Kohonen [2013].

During learning, the neighbourhood reduces in size over time, effected by the exponential decay function:

$$\sigma(t) = \sigma_0 \exp\left(\frac{-t}{\lambda}\right) \quad t = 1, 2, 3\dots \quad (2.4)$$

where  $\sigma_0$  denotes the width of the map at time  $t_0$  and  $\lambda$  denotes a time constant.  $t$  is the current iteration of the loop. The value of  $\lambda$  depends on  $\sigma$  and on the number of iterations the algorithm is set to execute:

$$\lambda = \frac{N}{\log \sigma_0} \quad (2.5)$$

$N$ , the number of iterations to be done by the learning algorithm is set by the user at the beginning.

In practice, BMU's location can be anywhere in the map, depending on the input being processed by the network. With time, the neighbourhood reduces to the size of one unit, the BMU.

With a known radius, all the units are iterated, determining if they are within the radius or not. When a unit is within the neighbourhood, its weight vector is adjusted as follows:

$$W(t+1) = W(t) + \Theta(t)L(t)(V(t) - W(t)) \quad (2.6)$$

This is SOM's learning method, where  $t$  is the time step and  $L$  is a small variable called the learning rate, which decreases with time. From this equation, the new

adjusted weight for the unit is equal to the old weight ( $W$ ), plus a fraction of the difference, ( $L$  and  $\theta$ ), between the old weight and the input vector ( $V$ ).

The decay of the learning rate is calculated at each iteration using the equation:

$$L(t) = L_0 \exp\left(\frac{-t}{\lambda}\right) \quad t = 1, 2, 3... \quad (2.7)$$

just like in equation 4, except this time it is the learning rate that decays.

The learning rate at the start of training is set by the user. It then gradually decays over time so that during the last few iterations it is close to zero.

Equation 2.6 incorporates the learning rate decay over time and the learning strength that is proportional to the distance a unit is from the BMU. At the edges of the BMUs neighbourhood, the learning process has very little effect.

Ideally, the amount of learning should fade over time following a Gaussian decay. In equation 2.6,  $\theta$  represent the amount of influence of a unit's distance from the BMU on its learning, and is given by:

$$\Theta(t) = \exp\left(\frac{-d^2}{2\sigma^2(t)}\right) \quad t = 1, 2, 3... \quad (2.8)$$

where  $d$  is the distance a unit is from the BMU and  $\sigma$  is the width of the neighbourhood function as calculated in equation 4.  $\theta$  also decays with time.

Although colour is rendered by the computer using values from 0 to 255 for each

component - red, green and blue, the input vectors are normalized, so that each component has a value between 0 and 1. This is to match the range of the values used for the units' weights.

SOMs are commonly used in data clustering, abstraction and as visualization aids. They make it easy for humans to see relationships between the vast amounts of data carried in images. In this thesis, a new use of SOM is suggested; that the QE that is derived from SOM can make it easy for humans to see the variations in the vast data within an image.

## **2.5 The trained SOM: final synaptic weights**

Another view of SOM is that of a statistical method of data analysis using an unsupervised learning algorithm whose goal is to determine relevant properties of input data without explicit feedback from expected results. Originally inspired by feature maps in sensory systems as explained earlier, it has greatly contributed to our understanding of principles of self-organization in the brain and the development of feature maps as observed in Martin and Obermayer [2009]. Kohonen [1996] points out that although the brain mechanisms are extremely complex and contain many details, the theory of their cognitive abilities must be based on much fewer general principles. This is in line with SOM's ability to reduce multi-dimensional data to lower-dimension data. Traditionally it has been held that 'intelligent' information processing takes place from signal processing in adaptive

network structures. With a degree of adaptation that is made controllable, SOM is a successful implementation of this principle and can be viewed on different levels of abstraction: as a physiological model, or a simplified numerical algorithm.

Through an interplay of neural principles of lateral inhibition and Hebbian synaptic learning within a localized region of the one-layered neural network, the SOM acquires a low-dimensional representation of high-dimensional input features that respects topological relationships of the input space. This is progressively achieved through the updating of the initial synaptic weights, using equation 2.6. At the end of learning, when all neurons optimally match the data from the input data set, SOM acquires the matrix of the final synaptic weights. Thus, for different inputs, different local areas will be modified, and in the long run, different areas of the 'map' will become selectively tuned to different domains of the input in an ordered and almost optimal fashion, Martin and Obermayer [2009].

The final weights of SOM are the BMUs, each being associated to the input vectors it won. A BMU acts like the centroid in VQ to this category of vectors which are more similar to each other than to those associated to a different BMU. Figure 2.3 shows a trained SOM, with input vectors distributed to the 30 units using the criteria explained in the previous section.



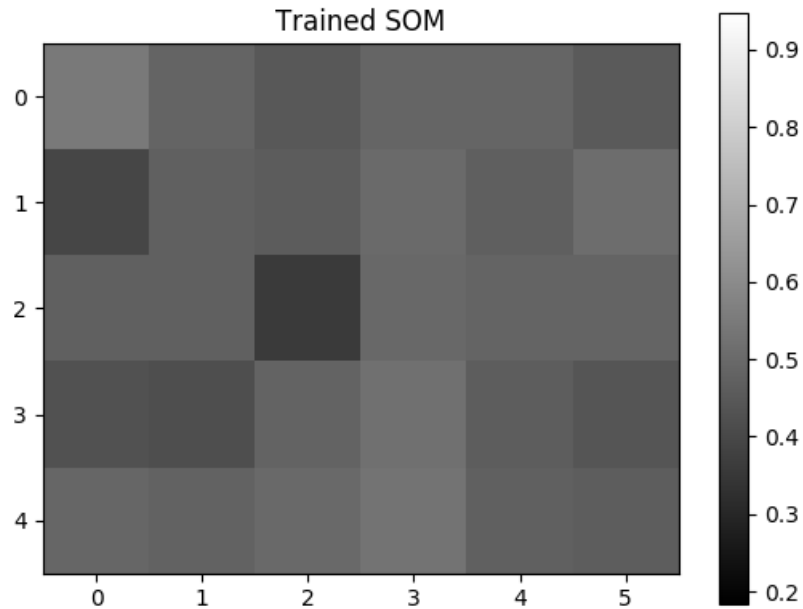


Figure 2.3: An example of a trained SOM. Each BMU is represented by a rectangular cell on the display. In this particular case, the SOM was a 5 by 6, and it considered four features, the RGBA, from an Urban Atlas map. It was trained for 10 000 iterations at a learning rate of 0.2 and a neighbourhood distance of 0.1. The colour distribution here shows how the samples from the atlas were mapped into the 30 units of the SOM after the training.

Using the colour bar provided in the figure, one can compare the number of input data samples won by each SOM unit. The input samples are made members of the local region with the BMU as their centroid. Effectively, the BMU becomes

the representative of all the samples it won, drastically reducing the dimension of the original data.

The task of SOM in SOM-QE is to create a standard platform on which QE is determined. This standard is composed of a set of 2D vectors, the BMUs, that has been generated through the competitive process described in sections 2.3 and 2.4 above.

Just like in other standards that provide a scale, for instance, to ensure uniformity in the results they post, this set of BMUs ensures that variation within images of a time series is measured and based on a uniform criteria that is capable of being replicated.

In section 3.7, a new method of calculating the QE is suggested that utilizes a fixed BMU for each input sample throughout a time series of images.

## **2.6 The quantization error (QE)**

QE of an image dataset address the question; how well does each BMU fit each of the samples it won? In this section, this question is addressed, taking into consideration QE's contribution in determining the variation within an image.

The task of finding a suitable subset that describes and represents a larger set of data vectors is called vector quantization, Gray [1984]. SOM quantize data since at the end of the learning process, each BMU has some data samples attached to it.

The BMU can be regarded as the centroid of the group of samples it won. Despite the competition among the units to win over input samples, it is likely that the unit did not become an exact match of the sample. Therefore, even a BMU for an input may still have some differences with the input from the image despite winning it, expressed as:

$$QE = x - BMU \quad (2.9)$$

where the  $BMU$  is taken from the set of final weights attained by the trained SOM, and  $x$  is an input sample it won. QE tells how far the BMU is from the input vector it won during the learning process.

This difference is the core idea that is applied to attain the objectives of this thesis. Equation 2.9 is the mathematical expression of determination of QE. To be a representative of the entire image, the average QE from each of the image's input samples is calculated and used as a label for the image. Statistically, the mean of data is a preferred measure of central tendency as it takes into considerations all data points. The mean value gives the lowest amount of error from all other values in the data set each time a measure is taken. The mean QE is given by equation 2.11. Thus, QE measures variation and when determined for each input sample in the image, it provides a measure of variations across the image.

Since each QE value is determined from the final weights of the same trained SOM, the QE values for different images or input vectors can be compared to each other to determine change between them.

The change between input feature vector or images from different times is given through QE:

$$D(I_1, I_2) = QE_1 - QE_2 \quad (2.10)$$

where  $D(I_1, I_2)$  is the difference metric and  $QE_i$  is the metric computed for a particular image space across moments in time. The function is a measure of change between the two images or corresponding input samples and can either be designed using domain knowledge or learned from a given dataset. The definition of change is always problem-specific; this thesis deals with local changes in the state of a patient, in a city or in the environment such as receding lesions in the lung, construction of new building or increase in carbon gas concentration in air respectively.

Most existing change detection methods require a decision as to where to place threshold boundaries in order to separate areas of change from those of no change, Jiang and Zhou [2004]. The threshold value is supplied empirically or statistically by the analyst, rendering the results obtained to be subjective. In SOM-QE technique, no thresholding value is required and input feature vectors are treated equally and with the same weight to arrive at the final decision.

## 2.7 The SOM-QE concept

To demonstrate this new concept, two artificial images are used. These are basically simple images meant to ease the understanding of the idea. The first is an RGB image of shape 1 by 4 by 3, with equal pixels for the three channels; red, green and blue as shown below:

```
array([[[[0.57735027, 0.57735027, 0.57735027]],  
[[0.57735027, 0.57735027, 0.57735027]],  
[[0.57735027, 0.57735027, 0.57735027]],  
[[0.57735027, 0.57735027, 0.57735027]]])
```

This is a single row array with four input vectors each consisting of three values. A second image, same in size and in shape as the first, was created by altering the values of the second and the fourth input vectors of the first image as shown below:

```
array([[[[0.57735027, 0.57735027, 0.57735027]],  
[[1. , 1. , 1. ]],  
[[0.57735027, 0.57735027, 0.57735027]],  
[[0.7 , 0.7 , 0.7 ]]])
```

Thus, the RGB values in the second and fourth pixels were changed to 1 and 0.7

respectively. All other aspects of the image were maintained constant as they were in the first image. Any change between the two images can then be attributed to difference caused by the alteration of the two input vectors. No prediction about localisation of this change is made. With such basic images it becomes possible to visualize their content and to follow up any changes that occur between them. Thus, humans can easily monitor changes between these two images and have the opportunity to compare their results with those returned by SOM-QE. The knowledge gained from the conclusion is then used to generalize the working of SOM-QE when applied to real images, as is done with medical and satellite images in a later chapter.

To understand these images better, their histograms are used to show the difference between them, Figure 2.4:

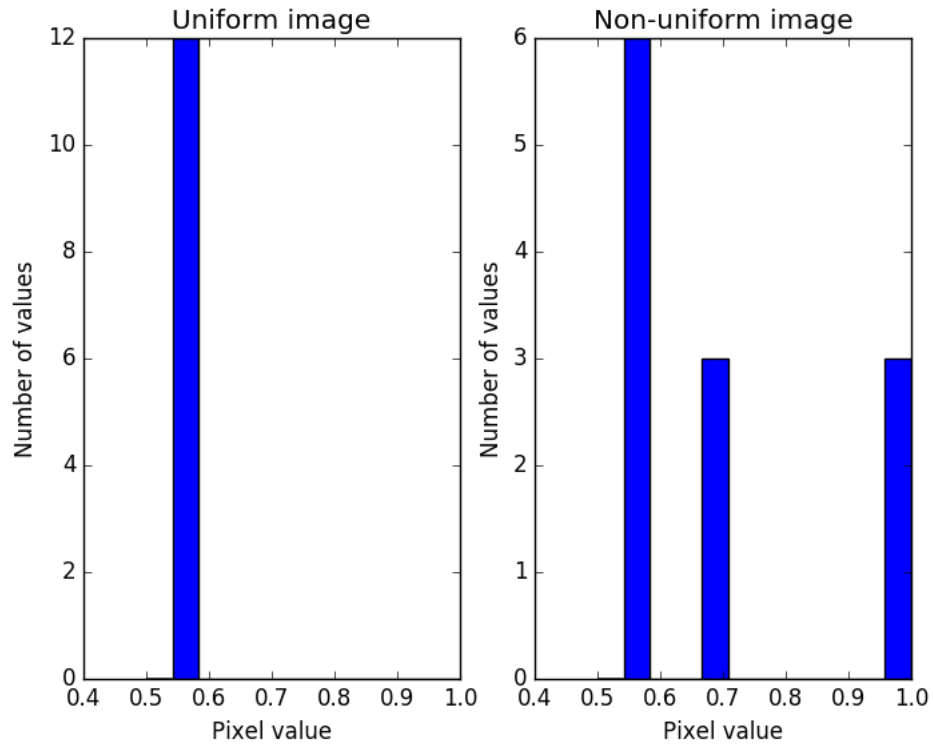


Figure 2.4: Histogram of the two basic images. On the left, all 12 values are shown to belong to one category since they are equal in the uniform image. To the right, the values are placed in three categories of 6 , 3 , and 3, confirming the variation that exist in the non-uniform image. Note that an input vector has 3 values.

One bin accommodates all the 12 values in the first image since its values are equal and hence uniform. Three bins are required for the second image, one for the 6 values in the first and third input vectors since they are equal, and one each

for the values in second and fourth input vectors since each is unique on its own.

Figure 2.4 depicts the differences in the composition of the two images. Both images have four input vectors, those of the first image being equal making it a uniform image. On the other hand, two input vectors are equal in the second image while the other two are different, making the image to have three distinct regions.

Further, the difference between the two images can be quantified by determining the variation within each. One way to attain this is to calculate the image variance. The image array is a dataset, hence its variance can be computed, giving a measure of the spread of the distribution. For the two images, their variance is:

uniform image: 0.0000

non-uniform image: 0.0298

This shows there exist difference between the two images, with the non-uniform image having more variations within it than the uniform image. The variance is the average of the squared deviations from the mean.

Then, SOM-QE is applied on the two images to detect their differences. After training a SOM using a different input image, the following QE values are obtained:

uniform image: 0.0000

non-uniform image: 0.2361



Just like the two methods above, SOM-QE reveals the existence of differences between the two images. The non-uniform image has varied components, and a SOM-QE score of 0.2361, while the uniform image has no variations within its components with SOM-QE score of 0.000. This is depicted in Figure 2.5.

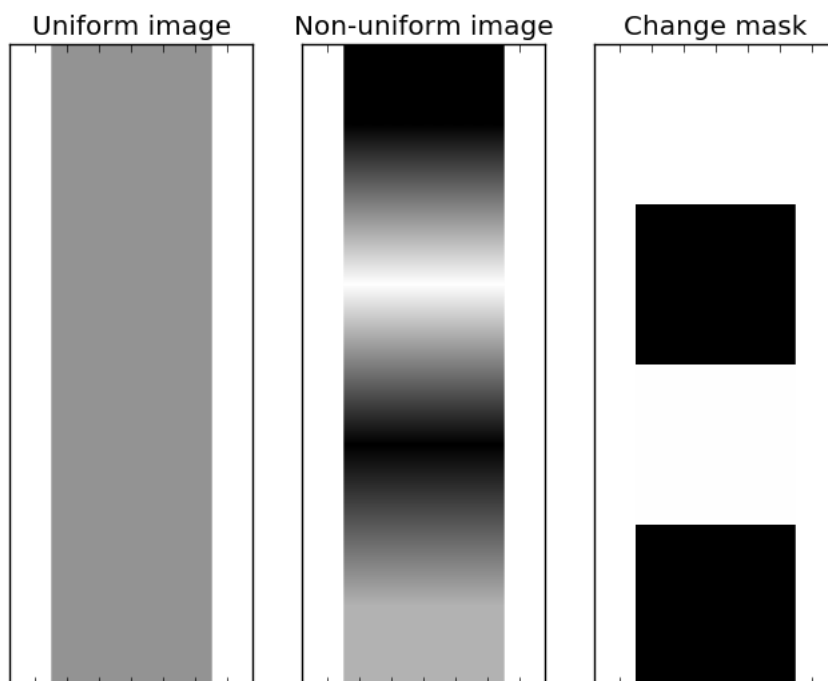


Figure 2.5: Difference between the two basic images. The change mask is a binary image showing local regions represented by each of the four input vectors and whether it changed (white) or did not change (black) between the images.

The code used to produce the results is included in the supplementary material, appendix B.

SOM-QE calculates the QE of each input vector in the image, using equation 9 , which was 0.0 throughout the uniform image and 0.0, 0.7321, 0.000 and 0.2124 for the first, second, third and fourth input vectors respectively for the non-uniform image. The QE of each input vector is compared in the two images to determine if there was a change, using equation 2.10. Where the input vector has different QE values in the two images, the corresponding zone has been marked white, otherwise the zone is black as shown in Figure 2.5.

SOM-QE gives further details about the changes that occurred between the two images. In the uniform image, all the four input vectors were won by the same SOM unit, that is, they have the same BMU. This confirms the image to be a one-zoned image. The non-uniform image, on the other hand is a two-zoned image according to SOM-QE. Two input vectors - [1., 1., 1.] and [0.7, 0.7, 0.7] - were won by one SOM unit with an average QE of 0.4722, while the other two – [0.57735027, 0.57735027, 0.57735027] and [0.57735027, 0.57735027, 0.57735027] - were won by another SOM unit with an average QE of 0.000.

Thus, SOM-QE is a measure of variation within an image as well as a change detector between images. This is confirmed when its results are compared to those posted by the histogram and the variance calculation – two measures used by the scientific community to determine the distribution of content in a dataset.

The process of determining the difference between the two images, took SOM-QE 0.87 second, making it appropriate and convenient for an image series pre-analysis task. This involved training the SOM, calculating QE for the two images, comparing the QE for differences, creating the change mask image and displaying the results. See Figure 2.6 for a schematic representation of the SOM-QE process.

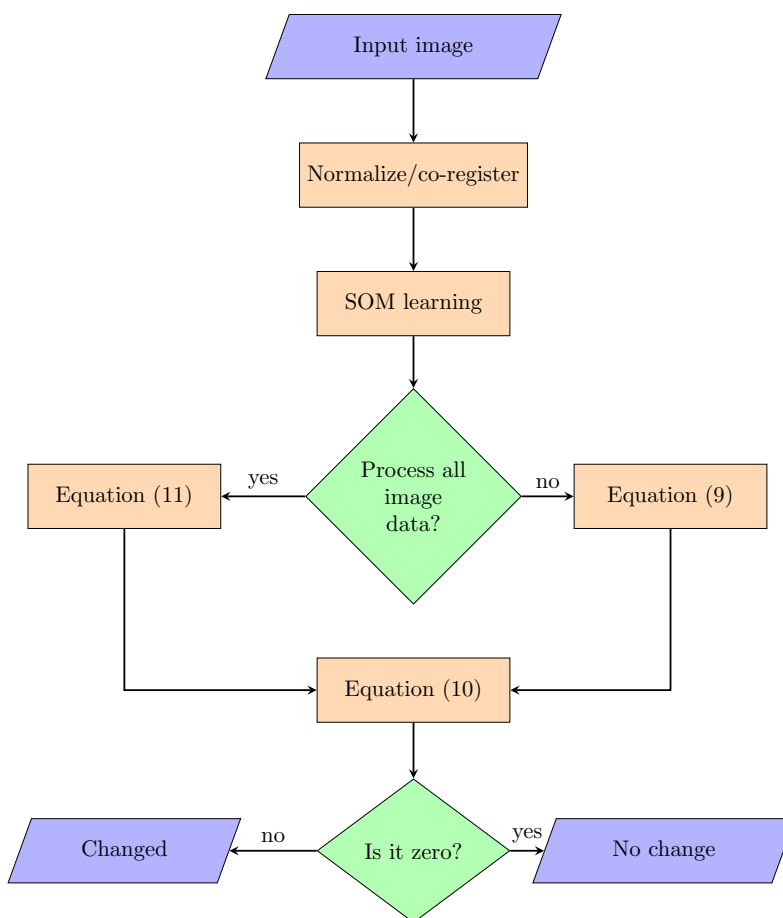


Figure 2.6: The SOM-QE set-up as used to determine changes between two images, using equation 2.11, or between the input vector of the same position within the two images using equation 2.9.

SOM-QE value obtained per input vector depends on SOM final weights and the input vector pixel values. SOM's final weights constitute the set of vectors from which a potential BMU is drawn from. The set is a function of the image values and is created as a result of learning the dataset. This effectively makes SOM the platform on which QE for the various input vectors is determined. The more the input vector is from the its BMU, the bigger its QE value.

When the object changes over time, its pixel values increase or decrease accordingly to reflect its new status. When the new input vectors are subjected to SOM for reference, the change is noticed through increased or decreased QE value between the two times. The QE is zero when the input vector equals its BMU, and it increases when the input vector becomes bigger or smaller than the BMU. Only the magnitude of QE is important at this level. However, when comparing an input vector at two different instances, the QE value at the first instant is subtracted from that at the second instant, equation 2.10. In this case, a positive QE value will indicate an increase in variation while a negative QE value will indicate a decrease in variation. A zero will mean there was no change in variation for the input vector. This new observation can be stated as: QE increases with the increase in local or global variability within the image.

The same SOM settings were used to process the two images, which have same properties except their distribution of the colour intensity. Due to lack of variation within it, the first image returned a single cluster, meaning that all vectors within it were similar. Its QE value is 0 indicating the uniformity – input vectors were

equal - within the content of the image. But for the second image with varied colour intensity, the QE value increased reflecting the increased variation of pixel intensity within the image.

Thus, SOM-QE managed to identify variations created in the second image.

These are two simple images whose status and differences is known and can be tracked manually. SOM-QE has been used to confirm these differences in the image status. In the next chapter, the use of SOM-QE on real images – medical and satellite images - is discussed and demonstrated.

QE has traditionally been used to evaluate the quality of SOMs, or to benchmark a series of SOMs with different parameters trained on the same dataset Kohonen [2014a], Gray [1984] and Pözlbauer [2004]. Thus, QE is a quality measure for SOM and it is used to determine how good a SOM set-up performs. SOM with different parameters - map size, learning rate, neighbourhood distance - are run on a given dataset. On each run, QE is determined. The combination of the parameters producing the lowest QE value is taken to be the optimal setting for the SOM. In this thesis, QE is exploited on a different and entirely novel perspective. The goal here is to benchmark a series of datasets using the same SOM, that is, a SOM trained under the same parameters. The same SOM - same map size, feature size, learning rate and neighbourhood radius – is used to analyse series of image datasets with clinical significance, or glean information from the satellite images. When, the image data is altered and the SOM parameters are not altered, changes in the QE can reasonably be attributed to the developments taking place in the

object whose image is under study. This is why SOM-QE is proposed as, for example, a clinical determinant of the progression or remission of lesions through medical images. The QE is the norm of the difference of an input vector  $x$ , and the vector's best-matching unit. The BMU of  $x$  is the final synaptic weight in SOM that won  $x$ . Thus, the QE reflects the average distance between each data vector and its corresponding BMU:

$$QE = 1/N \sum_{i=1}^N ||x_i - (BMU_i)|| \quad (2.11)$$

where  $N$  is the number of input sample vectors  $x$  in the input data and BMU is the final weight that won  $x$  among the final weights of SOM.

The QE becomes a statistical measure of variance associated with the final synaptic weights of the SOM. It disregards map topology and alignment Pözlbauer [2004] and its calculation, like that of the final synaptic weights, results directly from the unsupervised learning procedure. On this basis, it is postulated that the QE reflects critical variations in the map-to-data matching process in a similar way as the statistical variance around a mean reflects the dispersion of the raw data around that mean. Just like there can be one mean value for differently dispersed raw data, we can have differently dispersed QE for one final synaptic weight, the BMU.

## **2.8 Hypothesis: SOM-QE value reflects critical variations in image content and it predicts future image status.**

In an image, such as a lung image, the variation of the content is captured by SOM-QE through equation 2.11. When the same is applied to a local region, the status of the region within the image becomes known. This enables the differentiation of objects within the image and can be used to identify abnormalities in a scene, such as lesions in a lung. In a set of time series images from the same scene, variations in the SOM-QE value could be due to small local differences in the content across the images. This possibility has not been explored before, yet, it opens new direction for fast automatic processing of a series of image data for which a quick decision about change or no change needs to be made. In particular, it is postulated that SOM-QE value:

1. is as a measure of small variations within an image,
2. becomes the image label to be used in tracking changes within the image,
3. determines minute changes that occur within an object through its images taken at different times.

In this chapter, the fundamental principles of SOM-QE and how they can be exploited are discussed. The chapter ends by stating the hypothesis that guides the

rest of the thesis.

In the next chapter, this postulate is tested and validated using a series of simulations on time series images, both computer generated and real.



# Chapter 3

## Experimental Methodology

Differences between images of the same scene may be caused by the motion in the field of view, the addition or removal of an object from the scene, changes in illumination, or noise from digitization process, Skifstad and Jain [1989]. The changes due to addition or removal of an object to or from a scene, corresponding to, for example, a growing or receding lesion (object) in a lung (image scene) is of importance in the medical field.

In this chapter, determination of such changes is considered and in the process, the hypothesis postulated in chapter 2 is confirmed.

SOM-QE technique considers the fact that some changes occurring between images can be unimportant or nuisance. These include changes induced by camera motion, sensor noise, illumination variation or atmospheric absorption among

others. Hence, as a necessary preprocessing step for all change detection algorithms Radke et al. [2005b], image registration - which aligns several images into the same coordinate frame is performed. Intensity variations in images caused by changes in the strength or position of light sources in the scene are also considered unimportant, hence each image is normalized before processing.

These pre-processing procedure, together with SOM-QE's style of working at pixel level and employing brain-like analysis technique makes it superior to other change detection methods.

The general SOM-QE application is as follows. Image series of a scene of interest are obtained. Using one of the images, a SOM is trained and then the QE value of the rest of the images is determined. Comparing the QE of a pair of images provides the difference and hence the change between them. Figure 2.6 provides details of the technique. To evaluate SOM-QE, its performance is compared to real measurements that correspond to a dataset of images and also with the results of 14 other methods reported in Wang et al. [2014].

This chapter starts by demonstrating five example scenarios where SOM-QE can be used, section 3.1. In section 3.2, it is shown that the changes detected by SOM-QE are too small for human experts to see. It then shows the application and the working of SOM-QE on real images drawn from the medical field and the satellite images, sections 3.3 and 3.4. Then, a demonstration on use of SOM-QE values to predict future changes is done in section 3.5, before evaluating the technique's performance in section 3.6. In the last section of the chapter, section 3.7, a new

method of calculating QE is proposed.

### **3.1 Change detection problems detectable by SOM-QE**

The goal of this section is to demonstrate that SOM-QE value for a series of images varies consistently, reliably, and predictably with local variations in spatially distributed contrast signals in random-dot images, and in image series with regularly distributed spatial contrasts in their geometric configurations. Five scenarios are considered, each being a representative of possible situations in real life where changes of interest occur and which require accurate monitoring for various reasons. For instance, city administrators may want to know when a new building comes up in the city. Such can enable them realize when an illegal building is being erected. In the image, this means a new object appears in a scene it never existed.

The scenarios describe here are by no means the only situations that SOM-QE can be applied. These are just examples of the kind of change problems that generally occur in a scene and which require accurate and fast determination.

Use of artificial images is preferred in this section since their content and composition is known and hence allows comparison with the SOM-QE results.

On the grounds of these systematic variations, it will be shown that SOM-QE is a highly sensitive and reliable indicator of local and global image homogeneity: as images from a time series become more heterogeneous in spatial contents, their SOM-QE value increases; conversely, as images from a time series become more homogeneous in spatial contents, their SOM-QE value consistently decreases, provided that other factors that may alter the image content are kept constant across images of a given series.

The artificial images in this section are created in a way to ensure that only the intended change exists between them. This is achieved by including only the required content in each image. For the real medical and satellite images, nuisance causes of change are minimized through use of appropriate image pre-processing procedures.

Through the simulations in this section, the hypothesis postulated in section 2.8 is confirmed and proved.

### **3.1.1 Materials and methods**

Time series of images with variable amount of black and white pixel contents, and of size 792 by 777 pixels, were generated. Content of each image was manipulated in such a way that the resulting series of images would lead to conclusion that confirm or contradict the set hypothesis.

### 3.1.1.1. Randomly distributed spatial contrast with increasing white pixel contents

Six images were created to form a series dataset, Figure 3.1.

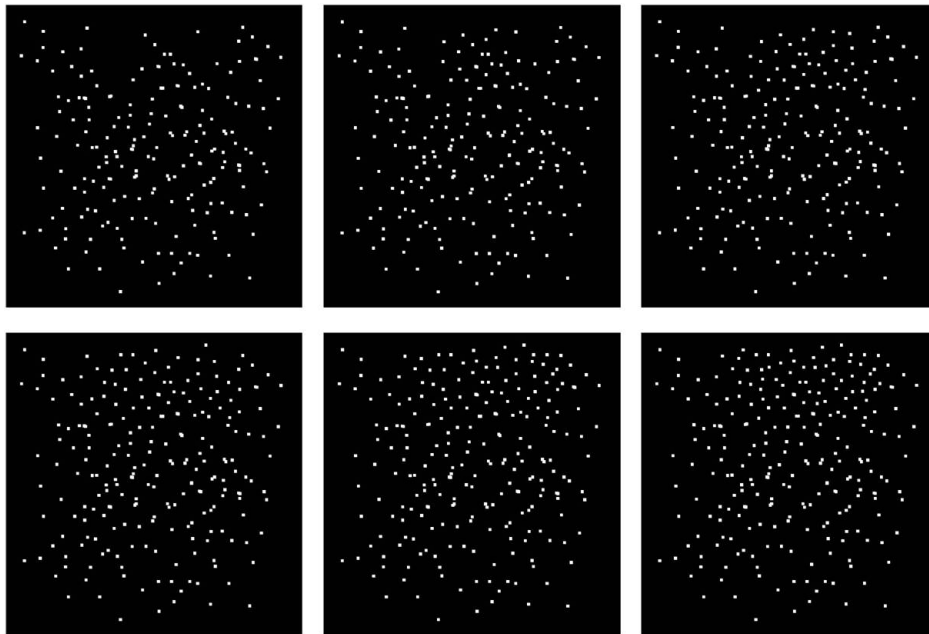


Figure 3.1: Adding local contrast to a scene. The number of the white dots progressively increases between the first and last image in the series. When a dot represent an object (like a building) in an image (like a city), then consecutive changes that occur from one image (like at the beginning of a period) to another (like at the end of the period) can be quantified and monitored using SOM-QE status value.

The percentage of the randomly distributed white pixel content was increased

from +10% in the second image to +60% in the last image of the series. The first, the original image, is used as the reference for the others in the series. The luminance intensity of white and black image contents was measured with a standard photosensitive lens, and was constant at  $60 \text{ cd/m}^2$  and at  $2 \text{ cd/m}^2$  for white and black pixel respectively across all images. Only the spatial extent of local contrast was varied in this set-up.

### **3.1.1.2 Spatially increasing extent of geometrically distributed contrast**

In the second time series of images, nine images were created, Figure 3.2.

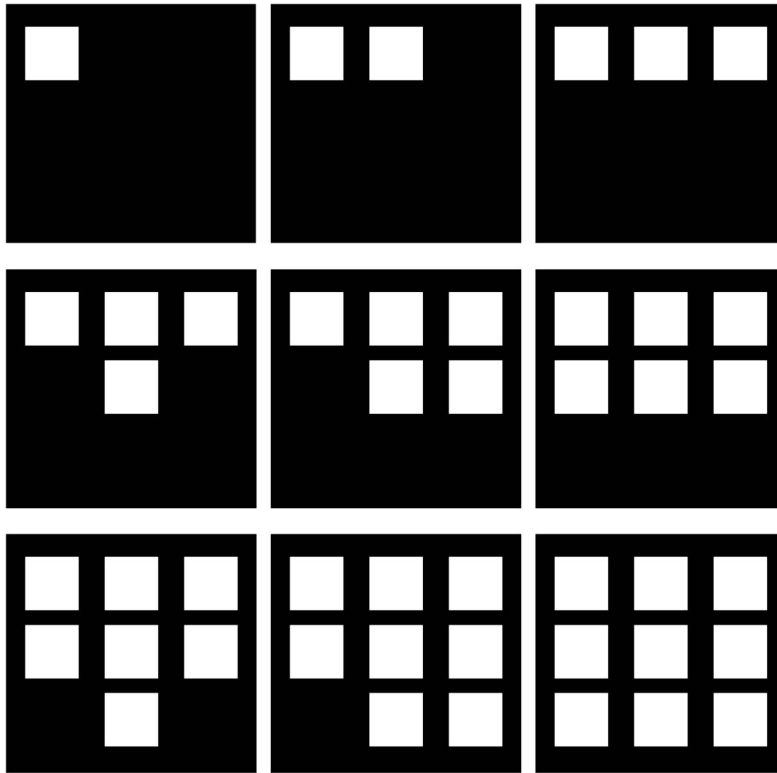


Figure 3.2: Adding an object at every time instant, to form ‘checkerboard 1’. The object added is the same at every time instant. The percentage of systematically spaced white pixel content progressively increases between the first and last image of this series, producing the ‘checkerboard’ patterns.

The percentage of systematically distributed white pixel content in the images increases gradually from 8% in the first image to 72% in the ninth image of the series.

### 3.1.1.3 Increasing local content of geometrically distributed spatial contrast

In this time series of nine images, Figure 3.3, the size of systematically spaced white pixel content in the images increases gradually from 2% in the first image to 18% in the last image of the series.

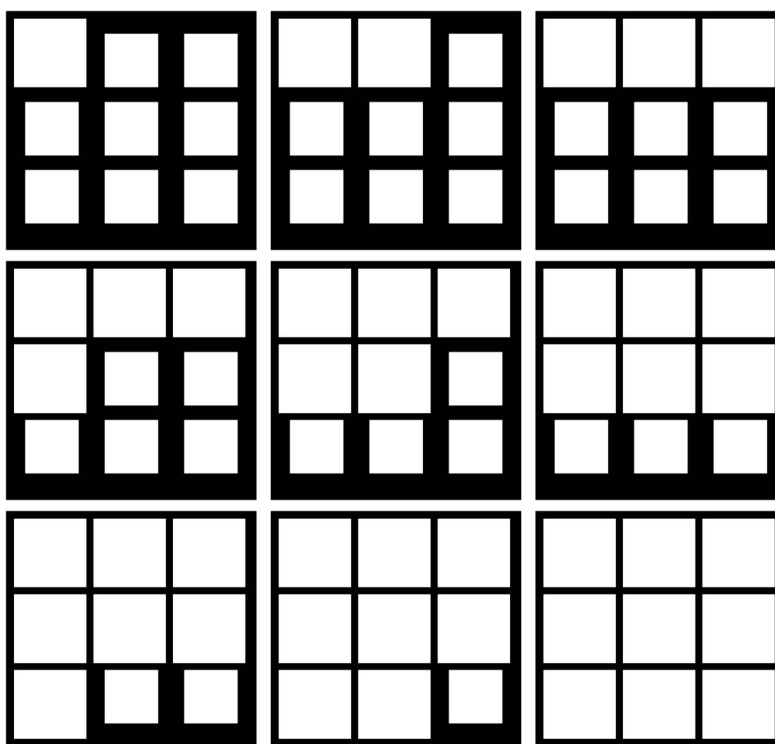


Figure 3.3: Objects increase in size, one at a time, to form 'checkerboard 2'. The percentage of systematically spaced white pixel content progressively increases between the first and last image, producing the systematic increase in single element size of the "checkerboard" patterns.



#### **3.1.1.4 Spatial contrast pattern with increasing contrast area at the centre**

In the fourth time series with six images, Figure 3.4, the size of a centrally located white square increases in the images. From occupying 1% of the image in the first image, the white pixel occupies 32% in the sixth image.

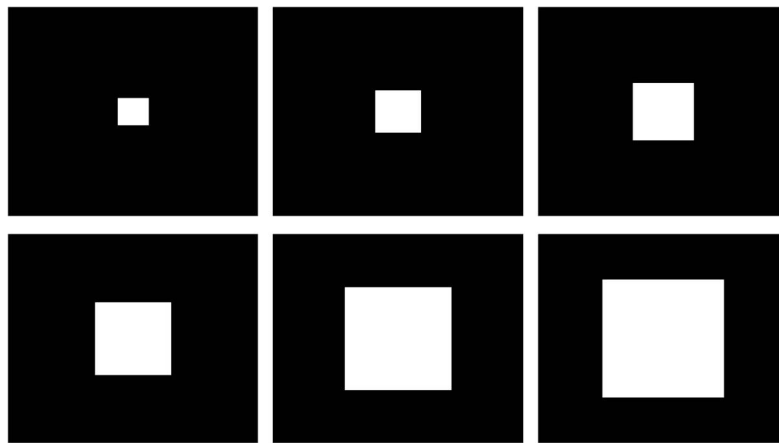


Figure 3.4: Growing object within a scene. The size of the object increases proportionally from the centre. The percentage of the centrally placed white pixel contents progressively increases between the first and the last image in this series.

#### **3.1.1.5 Spatial contrast pattern with constant contrast area of varying intensity**

Identically sized images with gradually varying contrast intensity of a central region with constant spatial extent across images were generated for this time series, Figure 3.5.

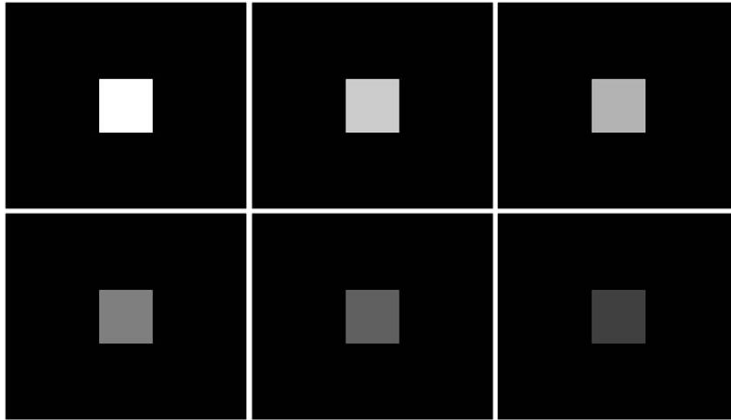


Figure 3.5: Fixed-size object with varying light intensity over time in a scene. It demonstrate a changing object – local zone – that does not involve change in size of the object. This type of change is typically missed when determination of change is done based on changing area occupied by a zone, like when the built-up zone encroaches the agricultural zone during the city growth.

### 3.1.1.6. SOM set-up

Before running the images in SOM-QE, each image was normalized to put them on a single scale. This was done using the relation:

$$I_{new} = \left( \frac{I - I_{min}}{I_{max} - I_{min}} \right) \times 255 \quad (3.1)$$

where  $I$  is the current image value,  $I_{min}$ ,  $I_{max}$  and  $I_{new}$  are the minimum, maximum and the normalized image values respectively. This normalizes the values

within the 0 to 255 range. In some cases, the normalization of the values is done within the 0 to 10 range.

Then, a four-by-four SOM, resulting in sixteen artificial units, was implemented with an initial neighbourhood radius of 1.2 and a learning rate of 0.2. SOM learning was performed on the last image of each time series. The neural network was set to learn for 10,000 iterations and its final weight vectors used to determine the QE value for each image.

Images in section 3.1.1.5 were not normalized to allow SOM-QE capture the changes caused by the varying intensity of the central region, which is the aim of the section. When normalized, the images had no change between them, confirming their uniformity and that changes occurred between them only due to the intensity variation. Figure 3.10 shows both results.

Linear regression analyses were performed to test the statistical significance of the SOM-QE values as a function of the variations in the images. Determining that SOM-QE values are a function of the variation within images, confirms SOM-QE as a measure of variation within the images.

### **3.1.2 Results**

SOM-QE value from each image was plotted as a function of the increase (%) in spatial pixel content in each of the time series dataset. The results are shown in Figure 3.6, Figure 3.7, Figure 3.8, Figure 3.9 and Figure 3.10 for the five example

applications of SOM-QE.

As a given extent of spatially distributed contrast increases across images of a given time series, the QE from the SOM output also increases. The results from linear regression analysis show excellent goodness of the linear fits, as revealed by the linear regression coefficients  $R^2$ , with statistically significant trends as revealed by the  $t$  values from the corresponding Student distributions.  $R^2$ ,  $t$ , and the probability limits  $p$  of statistical significance are given in the legend of each Figure.

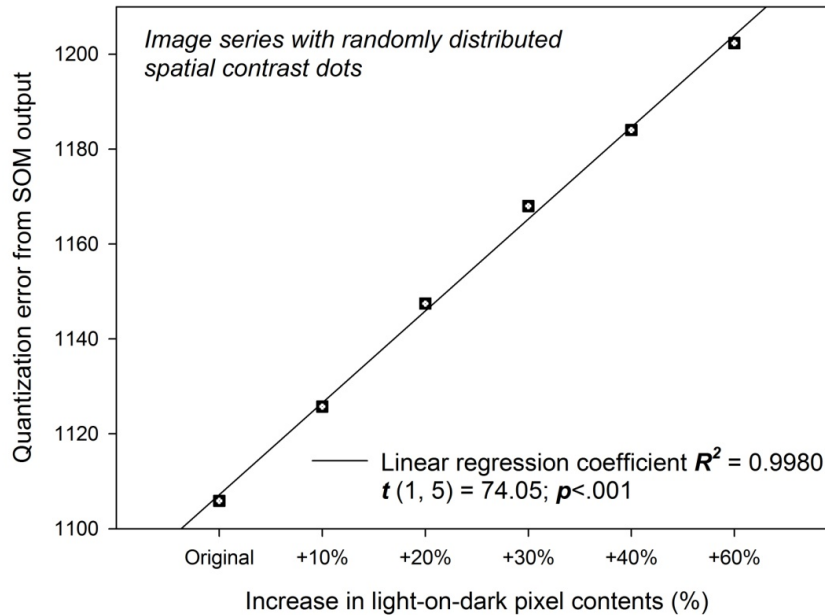


Figure 3.6: SOM-QE output as a function of spatial extent of contrast due to varying number of randomly distributed white dots on the black image background. When the intensity of contrast is constant across images, as is the case here, the QE is shown to increase linearly with the increase in spatial extent of contrast expressed in percentage of the total image area. This increase is statistically significant as shown by the  $t$  value from the Student distribution of the raw data and the associated probability limits ( $p$ ). The phenomenon is accounted for by an almost perfect linear fit (model), as shown by an  $R^2$  value  $> .99$  (almost 1).

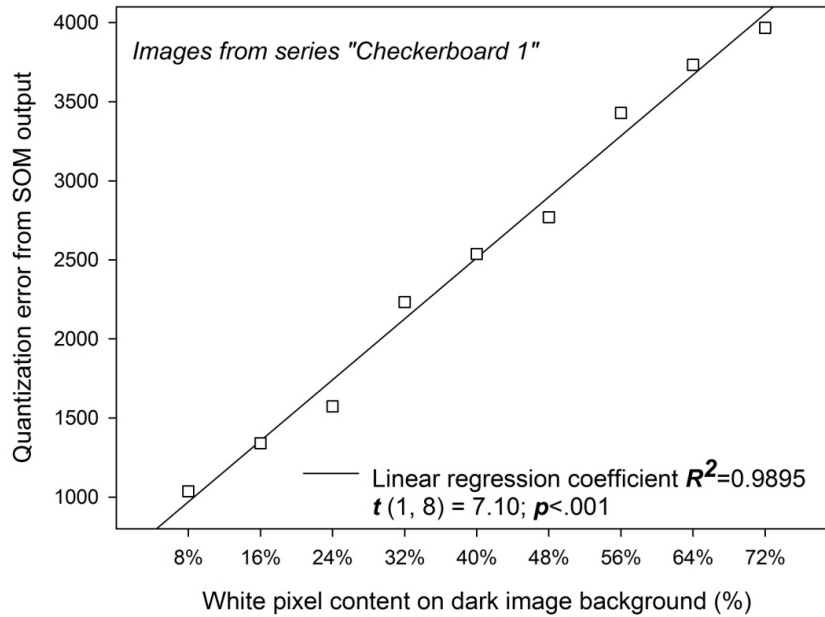


Figure 3.7: Variations in QE output plotted as a function of spatial extent of contrast in terms of number of geometrically distributed white squares on the black image background. The QE is shown to increase linearly with the increase in spatial extent of contrast expressed in % of the total image area. The linear trend is statistically significant as shown by the  $t$  value from the Student distribution of the raw data and the associated probability limits ( $p$ ).

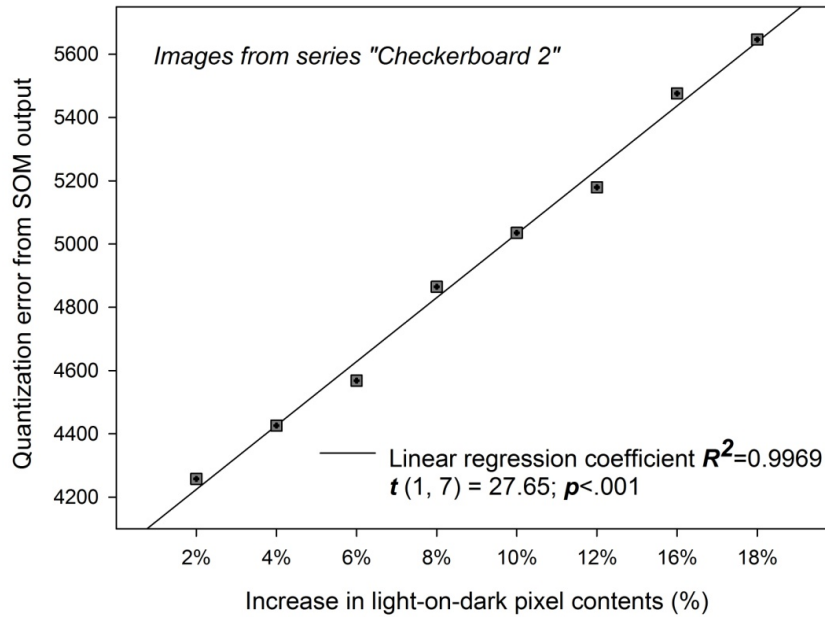


Figure 3.8: SOM-QE value as a function of locally increasing size of geometrically distributed white squares on the black image background of the "checkerboard 2" series.

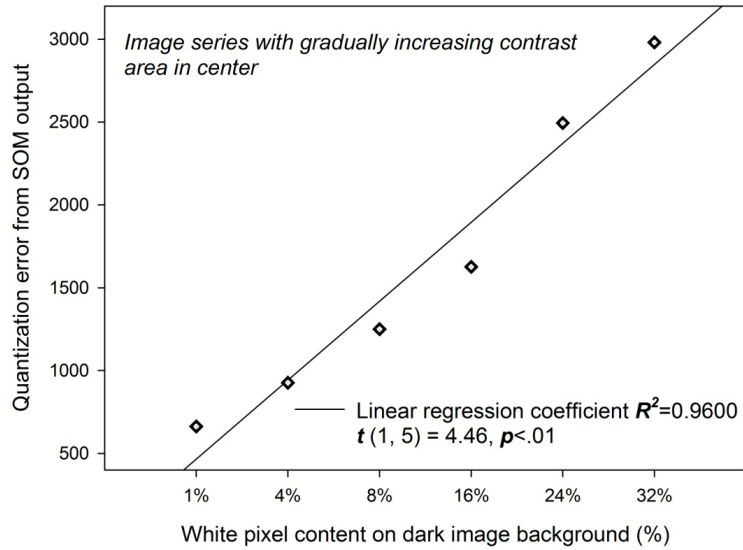


Figure 3.9: Variations in SOM-QE output plotted as a function of increasing contrast area at the centre of the black image background. As in the previous cases, SOM-QE is shown to increase linearly and significantly with the increase in spatial extent of contrast.



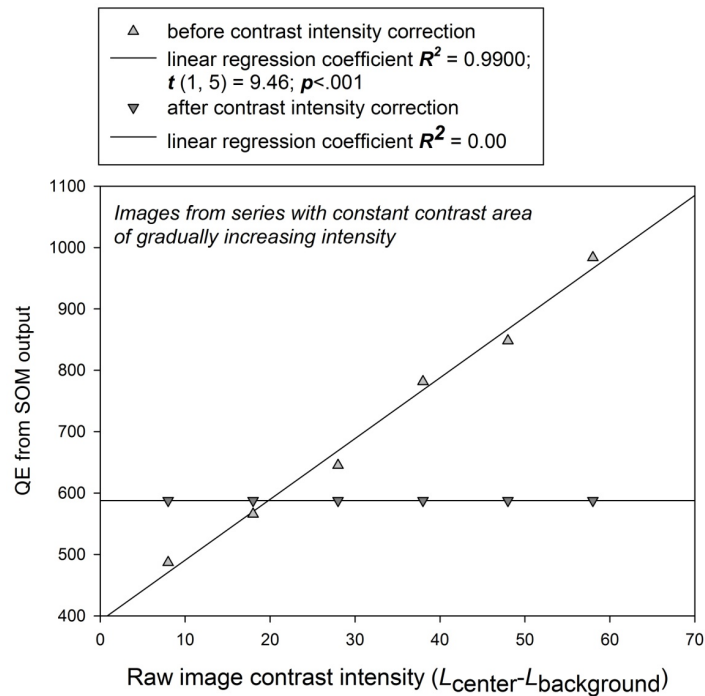


Figure 3.10: Significantly increasing SOM-QE output as a function of increasing contrast intensity of the area at the centre of the black image background when the spatial extent of that area is kept constant across images. The SOM-QE is shown to increase linearly and significantly with the increase in contrast intensity across the images. After contrast intensity correction of the images from this series using the transform given in equation 3.1, the SOM-QE value is shown to remain constant, as shown by the horizontal line in this graph

A common observation in the five cases was that as the spatially distributed contrast increased, the SOM-QE value also increased. Linear regression analysis showed excellent goodness of the linear fits, as revealed by the linear regression

coefficients  $R^2$ , with statistically significant trends as revealed by the  $t$  values from the corresponding Student's  $t$  distributions.  $R^2$ ,  $t$ , and the probability limits  $p$  of statistical significance are given in the legend of each figure.

The five scenarios provide typical examples of situations where changes can occur and be captured by SOM-QE algorithm. Each of the type of change can be of importance in the medical fraternity or in the planning and management of cities.

The simulations suggest that SOM-QE values from a series of images is a statistically reliable indicator of spatial changes in image regions when the intensity of contrast is constant across images of a given series.

On the basis of these results, it is important that image datasets are of constant contrast intensities, and where necessary be preprocessed using the contrast intensity correction transform given by equation 3.1.

The results in this section serve to partly confirm the hypothesis put forward in section 2.8, that SOM-QE can detect changes within images. The next aspect of the hypothesis - that even small changes are detectable by SOM-QE – is proven in the following section.

Hence, in the light of these results, SOM-QE capability to reliably detect small changes in spatial contents across images was put to test. To determine how small the changes captured by SOM-QE can be, psychophysical detection experiment were set up with human observers, as explained in the next section.

The simulations shown above provide substantial proof of concept beyond any reasonable doubt that the QE from the SOM output is a statistically reliable indicator of spatial changes in image regions under the condition that the intensity of contrast is constant across images of a given series. On the basis of these results, it will be made sure that all further analyses of image time series presented here are run on series of images with constant contrast intensities, if necessary pre-processed using the contrast intensity correction transform given above to ensure this condition holds for any given image series. This opens perspectives for the fast automatic pre-analysis of large bodies of images. In the medical fields these could be scans or MRI images taken over time from one and the same patient with a given critical condition the evolution of which is slow and progressive and hard to detect in the medical images, for example. The algorithm for SOM learning is easy to implement and the computational times for whole set of analyses are of a few seconds, bearing in mind that SOM performs a global analysis of the entire image. This opens new doors for complex problems such as the monitoring cancer progression/remission, which is often performed via manual segmentation of several images in an MRI sequence, which is prohibitively time consuming, or via automatic segmentation, a challenging and computationally expensive task that may result in high estimation errors Rey et al. [2002a]. The QE allows to almost instantly get some idea of the likelihood of change in terms of progression or remission, in real-time, directly from image statistics using the self-organizing machine learning technique. Moreover, the QE value of the output of these analyses detects even the smallest changes in potentially relevant local image contents that

are impossible for humans to see, even when they are expert radiologists Wandeto et al. [2017]. In the next section, we will compare the QE distributions from SOM run on time series of original imaging data from a patient before and after blunt force traumatic injury to test whether the QE consistently and reliably detects the change in the medical images across time. In a further step, artificial lesion-like content is added to medical images and SOM analyses are run on these modified images. This is similar to what was done in previous work Pohl et al. [2011b] prior to further computational analyses using a metric of visual classification by an expert.

## **3.2 How sensitive is SOM-QE? Comparing SOM-QE to human detection**

To answer this question, ground truth data was collected in a series of experiments involving human observers.

Computer generated random-dot images with different sizes of one of the dots were used. The changing dot reflects a local zone in an image whose size increases by 5%, 10 and 30% in three images. The resulting images were identical in size and spatial configuration. In the experiment, they were paired with the original image where all dots were of equal size.

In the psychophysical experiments, human observers had to judge whether a given

image pair appeared the ‘same’ or ‘different’. The decision by the observer was recorded down for each observation. This same-different paradigm was adopted for the experimental design from David M. Green [1966] and Dresch et al. [2002]. Then, SOM-QE values from these images were compared to the psychophysical data and analysed following the principles of signal detection theory in Roweis and Saul [2000].

### **3.2.1 Subjects**

32 healthy, young novices, 26 male and 6 female, all volunteers aged between 19 and 34 years of age and 3 expert radiologists, 2 male and 1 female, participated in the studies. Experiments were conducted in conformity with the Helsinki Declaration relative to experimental investigations on human subjects. All subjects had normal visual acuity and gave written informed consent to participate.

### **3.2.2 Materials and methods**

Four computer generated random-dot images of identical size, identical contrast and spatial contrast distribution were created using Adobe RGB in Photoshop. In three of these four images, a dot’s diameter was increased, to yield images with a 5%, 10% and 30% local dot size increase. The adjusted dot was at exactly the same location in the images. Thus, a dataset of 4 images was formed consisting

of an original random-dot image, and three other images created from it with the various enlarged sizes of one of their dots.

Each of these three images was paired with the original ‘no change’ image by randomly placing it to its left and to its right, see Figure 3.11.

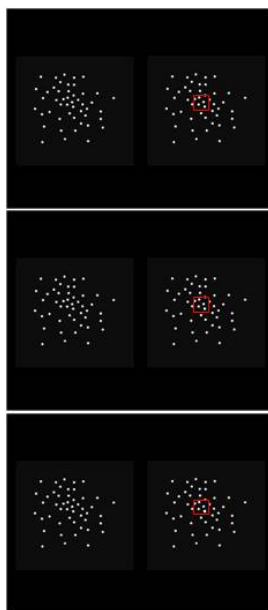


Figure 3.11: Three random dot-image pairs. In one of the images of a pair, there is an increase in the size of a single dot by 5 %, 10 % or 30 %. The affected dot is shown in the right image of each pair, highlighted by the red square. The images are paired with the original image where no such local change was added, shown on the left of a pair. Right and left images in a pair varied between presentations, in random order. Pairs of identical images (not shown here) were also presented in a task sequence to measure false alert rates, the ‘guess rates’.

Pairs of identical images were also presented in a task sequence to measure false alert rate, the 'guess rate'. This determined the subjects' tendency to over-diagnose through the false positive detections. The exposure duration of the image pairs was varied to test whether the visual processing time affects detection.

The subject was seated at a distance of about 75 centimetres from the computer screen in a semi-dark room. The image pairs were presented in a random sequence and each pair was followed by a blank screen presentation of five seconds to avoid visual after-image, which could have interfered with the task. In one session, the exposure duration for each image pair was five seconds, in another session, the exposure duration was observer controlled. This means that the subject could look at a pair for as long as he deemed necessary to reach a decision, then pressed a key to get the five-second blank screen before the next pair was displayed. The task instruction was to 'decide as swiftly and accurately as possible whether the two images in a pair appear to be the same or different.' The number of 'same' and 'different' judgements in response to a given image pair was recorded into an individual file, for each subject and session. 16 of the 32 subjects started with the five second exposure duration session followed by the session with the observer controlled exposure duration. The other 16 performed the task sessions in the reversed order to counterbalance possible sequential timing effects.

Any detection of a difference, called correct positive or 'hit', could only be due to detection of the artificially induced local difference in one of the two images in the pair, as all other image parameters (contrast intensity, contrast sign, spatial

distribution of contrasts, relative size) were identical in all images used in the experiments.

### **3.2.3 Results**

The total number of ‘same’ and ‘different’ responses for each type of image pair was divided by the total number of presentations of that pair for a given subject and experimental session. These response frequencies were then multiplied by 100 to produce percentages of correct negatives (CN), reflecting the percentage of ‘same’ responses to pairs of the same image, false negatives (FN) reflecting the percentage of ‘same’ responses to pairs of different images, false positives (FP) reflecting the percentage of ‘different’ responses to pairs of the same image, and correct positives (CP) reflecting the percentage of ‘different’ responses to pairs of different images.

#### **3.2.3.1. Performance of the novice observers**

The distributions of responses by the novice population are shown in Table 3.1, Table 3.2, and Table 3.3 as a function of the change in local image contents, with 5 %, 10% and 30% local increase in single dot size respectively, and as a function of the exposure duration of the image pairs; a) and b).

It was checked to confirm that the position of an image in a pair, left or right, had



		SAME	DIFFERENT	
<b>R</b>	"same"	88.7 (CN)	91.4 (FN)	[a) 5 seconds exposure
	"different"	11.3 (FP)	8.6 (CP)	

		SAME	DIFFERENT	
<b>R</b>	"same"	86.5 (CN)	91.4 (FN)	(b) observer controlled
	"different"	13.5 (FP)	8.6 (CP)	

Table 3.1: Conditional response rates expressed in percent (%) for the ‘no-change’ image paired with the ‘5% local change’ image under conditions of five seconds exposure duration (a), and observer controlled exposure duration (b). Correct positive (CP), often also called ‘hits’, correct negative (CN), false positive (FP), and false negative (FN) response rates are shown.

		SAME	DIFFERENT	
<b>R</b>	"same"	87.5 (CN)	82.0 (FN)	(a) 5 seconds exposure
	"different"	12.5 (FP)	18.0 (CP)	

		SAME	DIFFERENT	
<b>R</b>	"same"	87.0 (CN)	77.4 (FN)	(a) observer controlled
	"different"	13.0 (FP)	22.6 (CP)	

Table 3.2: Conditional response rates for the ‘no-change’ image paired with the ‘10% local change’ image under conditions of five seconds exposure duration (a), and observer controlled exposure duration (b).

no effect on the responses. That is, there was no positional bias. Therefore, the average response frequencies for images positioned on left and on right are used. Comparing the results in a) and b) of Table 3.1, Table 3.2 and Table 3.3, it is clear that the percentage of FP, the ‘guess rate’, does not vary much with the exposure duration of the image pairs, whereas the percentage of CP, the ‘hit rate’, increases markedly when the exposure duration is observer controlled. Given the constant FP, the subjects consistently used the same decision criterion across sessions, otherwise, the FP would also have varied with the image exposure duration.

		SAME	DIFFERENT	
<b>R</b>	"same"	85.5 (CN)	66.4 (FN)	(a) 5 seconds exposure
	"different"	14.5 (FP)	33.6 (CP)	

		SAME	DIFFERENT	
<b>R</b>	"same"	86.5 (CN)	60.9 (FN)	(b) observer controlled
	"different"	13.5 (FP)	39.1 (CP)	

Table 3.3: Conditional response rates for the ‘no-change’ image paired with the ‘30% change’ image under conditions of five seconds exposure duration (a), and observer controlled exposure duration (b) for each image pair.

Limiting the image exposure time negatively affects the CP. Also, when comparing between Table 3.1, Table 3.2 and Table 3.3, it is clearly seen that the (CP) increases as local dot size increases. In pairs where one of the images has a 5% local dot size increase Table 3.1, the CP is smaller than the FP, which indicates that the subjects are basically guessing and are unable to detect the local difference in image contents. In pairs where one of the images has the 10% or the 30% local dot size increase, the CP is twice, Table 3.2, to three times, Table 3.3, the FP, which shows that the local difference in the image content is beginning to be detected. In pairs with observer controlled exposure duration where one image has the 30% local increase in dot size, the CP is the highest at 40%.

Next, the average CP were submitted to a two-way ANOVA for the three levels of the ‘lesion’ (the growth in dot size) factor L3 and the two levels of the exposure duration factor E2 to assess the statistical significance of the effects. It is observed that there is a statistically significant result for the effect of ‘lesion’ on the average ‘hit rate’, with  $F(2, 23) = 38.04$ ;  $p < .001$ , and a significant effect of exposure

duration, with  $F(1, 23) = 8.13$ ;  $p < .05$ . The effect's sizes in terms of means and standard errors (SEM) are represented in Figure 3.12.

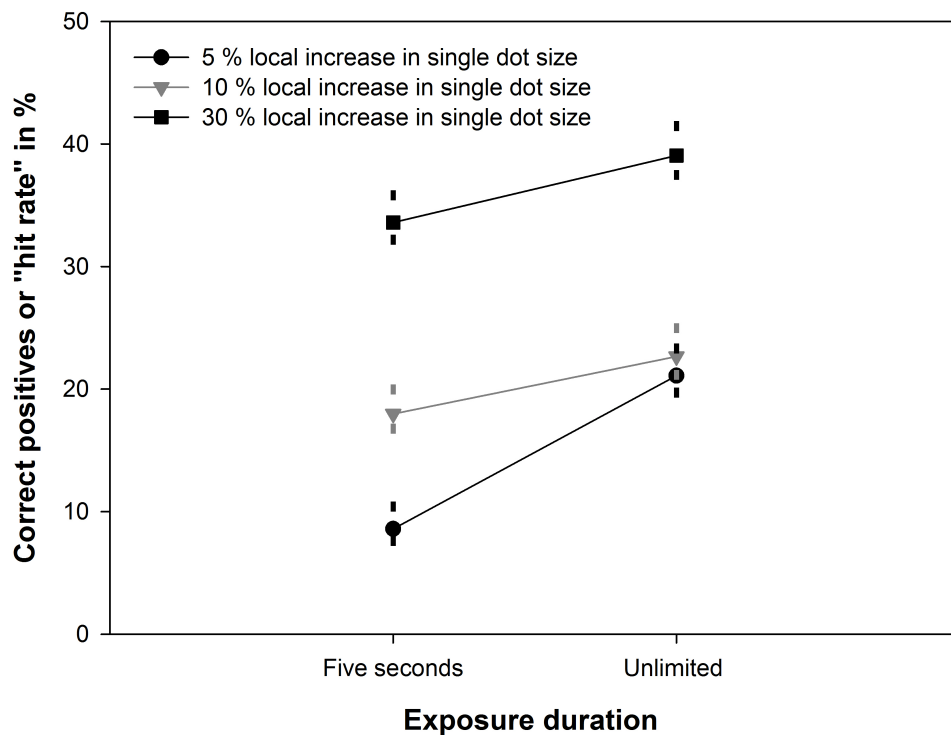


Figure 3.12: Average hit rates (CP) and their standard errors as a function of local dot-size increase in % and the image exposure duration.

### 3.2.3.2 Performance of the expert radiologists

With a 5% local dot size increase, Table 3.4, there is no detection even by the expert radiologists who are experienced in visually scanning complex images for

		SAME	DIFFERENT	
<b>R</b>	"same"	41.7 (CN)	58.3 (FN)	(a) 5 seconds exposure
	"different"	58.3 (FP)	41.7 (CP)	

		SAME	DIFFERENT	
<b>R</b>	"same"	41.7 (CN)	41.7 (FN)	(b) observer controlled
	"different"	58.3 (FP)	58.3 (CP)	

Table 3.4: The conditional detection rates of the experts for random-dot images with a 5% increase in local size of a single dot in the image. There is no detection of this change by the experts, they are basically guessing. Note that the guess rate (FP rate) of the three experts here is noticeably higher than that of the novices. Expert radiologists thus, seem to have a stronger tendency to produce false positives, the ‘better safe than sorry’ strategy.

changes in fine detail.

Here, the experts are basically guessing as can be seen from their CP rate after subtraction of the FP. Note that the guess rate of the three experts is noticeably higher than that of the novices. Expert radiologists seem to have a stronger tendency to produce false positives, the ‘better safe than sorry’ strategy. With a 10% local dot size increase, Table 3.5, the experts are still basically guessing, but beginning to detect the difference in the two images when they can control the exposure duration - the guess rate is no longer zero.

With a 30% local dot size increase, Table 3.6, the experts, just like the novices detect the difference between the two images better when they control exposure duration.

Given the higher guess rates of the experts, who tend to respond ‘different’ when

		SAME	DIFFERENT	
<b>R</b>	"same"	41.7 (CN)	50.0 (FN)	(a) 5 seconds exposure
	"different"	58.3 (FP)	50.0 (CP)	

		SAME	DIFFERENT	
<b>R</b>	"same"	41.7 (CN)	16.6 (FN)	(b) observer controlled
	"different"	58.3 (FP)	83.4 (CP)	

Table 3.5: The conditional detection rates of the experts for random-dot images with a 10% increase in local size of a single dot in the image. There is no detection of this change by the experts, they are still basically guessing. Note the high FP rates.

		SAME	DIFFERENT	
<b>R</b>	"same"	41.7 (CN)	16.6 (FN)	(a) 5 seconds exposure
	"different"	58.3 (FP)	83.4 (CP)	

		SAME	DIFFERENT	
<b>R</b>	"same"	41.7 (CN)	8.4 (FN)	(b) observer controlled
	"different"	58.3 (FP)	91.6 (CP)	

Table 3.6: Conditional detection rates of the experts for random-dot images with a 30% local dot size increase. The experts, like the novices, detect a 30% difference in local dot size between the two images better when they can control exposure duration. In whole, the FP or guess rates are still too high to conclude that the experts reliably detect the local change in the images.

the two images are the same to a greater extent than the novices, it cannot be concluded that the experts more reliably detect the 30% increase in local dot size. Their correct positive rate after subtraction of the false negative rate is still well below a psychophysical threshold of 75% correct. To arrive at detection rate, the false positives are subtracted from the correct positives as in David M. Green [1966]. In this case: CP rate – FP rate (guess rate) is no longer zero, but about 25. The best attained detection rate is 33.3%.

To compare with the human detection performances, the SOM-QE values obtained from the same random-dot image dataset were plotted as a function of image type, Figure 3.13.

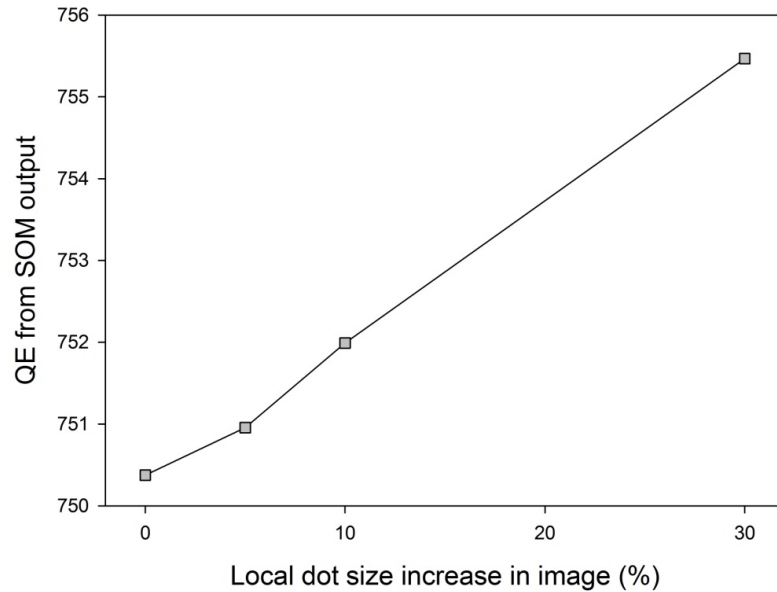


Figure 3.13: SOM-QE output as a function of local dot size increase in images. The change is reliably detected as shown by the consistently increasing SOM-QE value.

These data show clearly that SOM-QE reliably detects the small local changes in the random dot images, as reflected by a steadily increasing QE as the size of a single dot in the image increases.

Here the task of SOM-QE is to determine and assign each image a unique label. The value of the label is based on the image content. Hence, when the image content changes, the label changes too, making this label unique for the image within the dataset. From the label, the difference between images is made clear.

This can go a long way in assisting the radiologist to minimize guessing in their image analysis tasks. SOM-QE gives a clear difference between images, pointing the radiologist to the right direction in the diagnosis process.

### **3.2.3.3 Evaluating SOM-QE in light of some other approaches**

Pohl et al. [2011a] describe a semi-automatic procedure targeted toward identifying difficult-to-detect changes in brain tumour imaging. They synthetically grew the pathology by simulating tumour growth. They recorded tumour growth percentages of 1% (9 mm cubic ), 3%, 5%, 11%, 16%, and 22% (195 mm cubic ).

They noted that ‘visually detecting growths of 1% and 5% is extremely difficult.’ On performance of their own suggested technique, they observed: ‘The metric was generally a conservative estimate of change for all cases with growth larger than 1%.’ Sample images from the dataset they used in their work is shown in Figure 3.14, adapted from Pohl et al. [2011a].



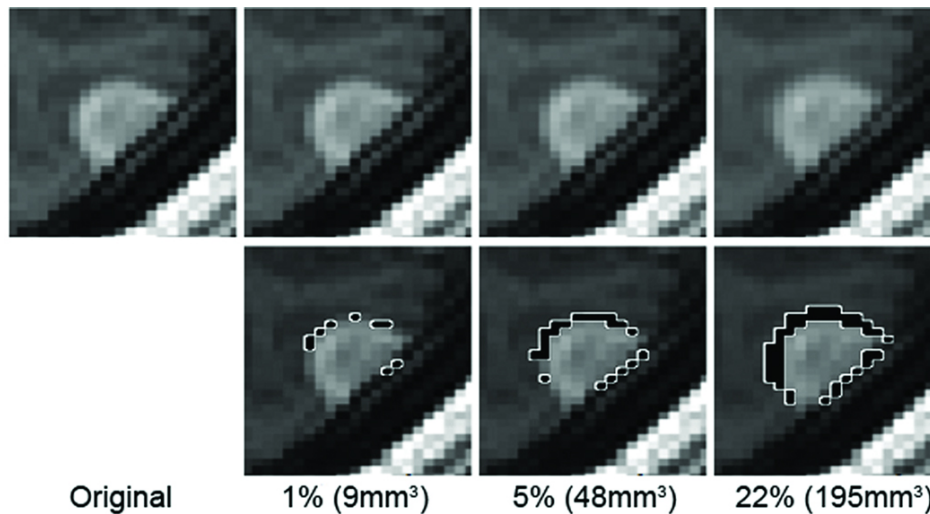


Figure 3.14: Part of the image dataset used in another approach reported in literature to detect changes caused by the growing lesion. SOM-QE was also applied on this dataset and found to detect smaller growth than the other technique.

SOM-QE was run on this dataset in order to compare its performance with this other approach, Table 3.7.

%lesion growth	SOM-QE value	Magnitude change
0	142.1839	
1	142.0677	0.1162
5	143.5304	1.3465
22	146.0702	3.8863

Table 3.7: SOM-QE performance on a dataset with lesion growth in brain images. SOM-QE outperformed the other method especially on the identification of smaller growth.

Note that from the original image to the 1% lesion image the change is detected as a drop of the SOM-QE value. This implies that the addition of ‘lesion’ reduced

variation within the image. The changes in the other levels of lesion-growth increased the variations within the image.

Using SOM-QE method, lesion growth was detected even at early stages (lower percent volumes) - unlike in the case of depending on visual recognition and other techniques in literature.

This confirms the second aspect of the hypothesis in section 2.8, that the changes sensed by SOM-QE can be very small.

### **3.2.4 Discussion**

The experiments with human observers confirm that small local changes in images are hard to detect for humans, while they are reliably captured by the SOM-QE algorithm used in this work. This work is important as it introduces a new way of looking at automatic change detection when dealing with the small local changes. This opens perspectives for the fast automatic pre-analysis of large bodies of images. In the medical field these could be scans or MRI images taken over time from the same patient with a given critical condition, the evolution of which is slow and progressive and hard to detect, for example. The algorithm for SOM learning is easy to implement and the computational times for the whole set of analyses are of a few seconds, bearing in mind that SOM-QE performs a global analysis of the entire image. This opens new doors for complex problems such as the monitoring of cancer progression/remission, which is often performed via

manual segmentation of several images in an MRI sequence, is prohibitively time consuming, or via automatic segmentation, which is a challenging and computationally expensive task that may result in high estimation errors Rey et al. [2002b]. In SOM-QE, an idea that almost instantly enables the determination of the likelihood of change in terms of progression or remission, a contribution in solving the change detection problem is made. It works in real-time, directly utilizing statistics from the image collected using the SOM machine learning technique. Moreover, the SOM-QE value detects even the small changes in potentially relevant local image contents that are impossible for humans to see, even when they are expert radiologists.

In the next section, SOM-QE is applied on time series of original imaging data from a patient with an injured knee. Then, artificial lesion-like content is added to the medical images and SOM-QE is run on the modified images too.

### **3.3 Change detection in time series of medical images**

In this section, SOM-QE is applied to track clinical information through medical images.

In medicine, the annotation of image data is subject to considerable differences between individuals, even when they are highly specialized experts such as radi-

ologists van Riel, S.J; et al. [2015]. Therefore, the analysis of medical images through computer techniques can be of assistance to the human expert in clinical diagnosis. Radiologists have to assess the progression of patients' conditions on the basis of often hardly detectable, local changes in medical images. These are captured through various imaging techniques, such as magnetic resonance imaging (MRI), computerized tomography (CT), and positron emission tomography (PET), providing the radiologist with visual information about the state or progression of a given condition and helping to determine the course of treatment.

Traditional methods for handling medical images involve direct visual inspection, which is by its nature subjective. Image science therefore, has proposed methods for reducing subjectivity by introducing automated procedures. This involves various image processing techniques aimed at identifying specific diagnostic regions and specific features representing tumours and lesions. For example, to avoid time-consuming voxel-by-voxel comparison for detecting changes between two images, the images can be aligned and displacement fields may be computed for recovering apparent motion by using a non-rigid registration algorithm van Riel, S.J; et al. [2015]. This and similar techniques focus on searching of ROI for tumours or evolving lesions. A computer algorithm compares multiple series of images to produce a map of the changes, and expert knowledge is then applied to that map in a series of post-processing steps in order to generate a set of metrics describing the changes occurring in the images. During this process, domain-specific knowledge need to be introduced, which attempts to reduce the impact of

subjectivity by incorporating generic information an expert might use when annotating medical images manually. This, however, does not completely eliminate subjectivity. Patriarche and Erickson [2007] and Angelini et al. [2007] provide other approaches that proposed a computational framework to enable comparison of MRI volumes based on gray-scale normalization, to determine quantitative tumour growth between successive time intervals. Specific tumour growth indices were computed, such as volume, maximum radius, and spherical radius. This approach also requires the initial manual segmentation of the images, which is a time-consuming task. Semi-automatically segmenting successive images and then aligning them on the basis of hierarchical registration schemes has also been proposed for measuring growth or shrinkage in local image details, Angelini et al. [2010]. All these methods rely on the accuracy of segmentation and require manual annotation for classifying local changes in pathology of up to a few voxels.

Other methods such as Konukoglu et al. [2008] which combine input from a medical expert with a computational technique are more specifically aimed at difficult-to-detect brain tumour changes. These methods, again, involve a subjectivity factor which is problematic given the inter-individual differences between experts Schectman et al. [2005].

The SOM-QE approach to the problem of change detection of time series of medical images considers the whole image as opposed to an image segment of a specific ROI. Such an approach of direct analysis of the medical image as a whole has the advantage of not requiring manual benchmarking. The basic idea behind direct

analysis is that there exists an intrinsic relationship between images with varying contents and their clinical significance, and that this relationship can be exploited directly without additional intermediate procedures of image processing. Compared to some of the traditional methods briefly reviewed above, SOM-QE has a deeper meaning in the sense that it is close to the most natural approach to the problem. It directly targets the final outcome of change detection like a medical expert would, and thereby bridges the gap between machine learning and the classic medical image inspection approach of the human expert. A medical expert such as a radiologist explores images in a time-series dataset as a whole, and one by one to monitor the progression of a patient's conditions. Like the SOM-QE, the expert derives diagnostic information from this 'natural' procedure to reach a decision on the likely progression or remission of a condition such as a tumour or lesion, thereby evaluating the likely progress of a patient's state or response to therapy. This classic visual method of determining differences between one series of images to another can, however, fail to detect very small differences. This can be overcome by use of SOM-QE algorithm for rapid automatic change detection in medical image data.

Here, the power of QE to capture critical local changes is tested on time series of MRI images from a patient with an injured knee. Further, simulations on MRI images to which Poisson noise as well as synthetic local lesion content were progressively added, are conducted and show that SOM-QE is fast, and consistently detects minimal changes in medical image data. It is suggested that SOM-QE al-

gorithm can be implemented to assist human experts such as radiologists in change detection decision making.

### **3.3.1 Materials and methods**

A 16 by 16 SOM with an initial neighbourhood radius of 5 and learning rate of 0.2 was set up for image learning. These initial values were obtained after testing SOMs with different numbers of neurons to make sure that the cluster structures show sufficient resolution and statistical accuracy Kohonen [2014b]. The learning process was started with vectors picked randomly from the image array to be the initial values of the SOM unit vectors. For the following three simulations, the SOMs used similar parameters.

Images datasets used in this section are provided in the supplementary material section.

#### **3.3.1.1. Original time series of MRI images**

In the first experiment, SOM was run on two sets of MRI images. The images were captured from a patient with a sprained knee during two consecutive clinical visits, courtesy of Hopital de Hautepierre, Strasbourg, France. The same acquisition parameters (machine, sequence, coil, and so on) were used to acquire each set which consisted of 20 MRI images. The images are included in the appendix

section.

SOM-QE was run on these images and posted the results shown in Figure 3.17.

### **3.3.1.2. MRI time series images with artificially added digital lesion contents**

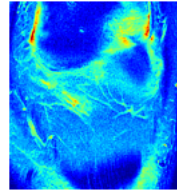
In the second experiment, artificial lesion content was added to each of the original sets of images. On the first MRI set of images, synthetic lesion was added locally to each image to form a new set of images. Since the aim was to reinforce changes within the images between time series, the new set of images retained all the characteristics of the first set, except for the additional lesion content, which was uniformly positioned in each of the 20 images of the series. Effectively, a synthetic lesion was introduced on each image in a way that ensured the differences between the original and new sets are due to the lesion, and not by external factors like location of camera, lighting, the patient's position on the MRI machine and so forth. Furthermore, the spatial extent of the introduced lesion content is known. Here, it was a 44 by 26 pixels elliptic shape at 72 by 72 dpi gray-scale resolution.

Next, on the set of images with an added lesion, a second lesion was added to form a third set of images. Thus, three sets of images were ready for simulation experiment. Each set consisted of 20 images. The first set was the original images as taken during the first clinical visit of the patient. The second and the third sets were created by adding one and two lesions respectively to the first set. The three sets of images formed a time series dataset of images. Figure 3.15 shows the first

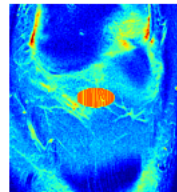


image from each of the three sets.

Original Knee - June image set



1 lesion added



2 lesions added

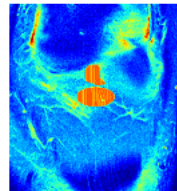


Figure 3.15: To eliminate external factors that could also contribute to change - like the patient position on MRI machine – artificial lesions were added on one set of images. To form the second set of images, one lesion was added to the first set while two lesions were added to create the third set. This figure shows the first image from each set of images.

The results of processing this time series dataset of images are shown in Figure 3.18.

In Pohl et al. [2011b], original images were also modified by adding synthetically

evolving pathological content of 1%, 5% and 22% volume growth and then used in visual recognition experiments, testing whether the artificial pathologies would be detected by medical expert. SOM-QE was applied on the same dataset and results compared as shown in Table 3.7.

### **3.3.1.3. Medical images with Poisson noise added**

In this section Poisson frequency distribution process was used to add noise on each of the two sets of knee images. Poisson noise was preferred over the other types of impurities generation because it is correlated with the intensity of each pixel in the image. The process produces a sample image from a Poisson distribution for each pixel of the original image.

The SOM-QE values obtained from each of the original sets and the corresponding noised set are shown in Figure 3.19. The same Poisson distribution parameters were applied to add the impurities in both series. By its nature, the Poisson method populates the image with impurities in proportion to existing pixels values hence the difference in what was ‘added’ to each set of images. Figure 3.16, shows sample images from this dataset.

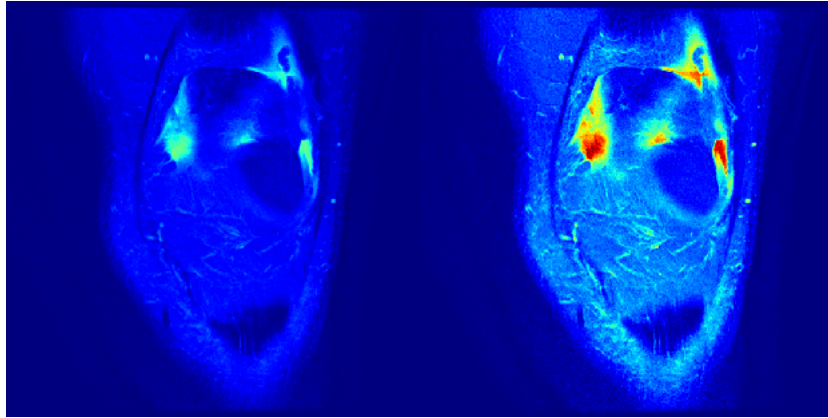


Figure 3.16: Samples of MRI images taken on the first (top left) and second (bottom left) clinical visit by the patient. On the right, the same images after adding Poisson distributed noise, which represents a way of adding lesion contents synthetically and is less arbitrary compared with adding pixels locally. The complete image dataset is provided in the supplementary material section.

### 3.3.2 Results

The SOM-QE values obtained from the two original sets of images are shown in Figure 3.17 below.

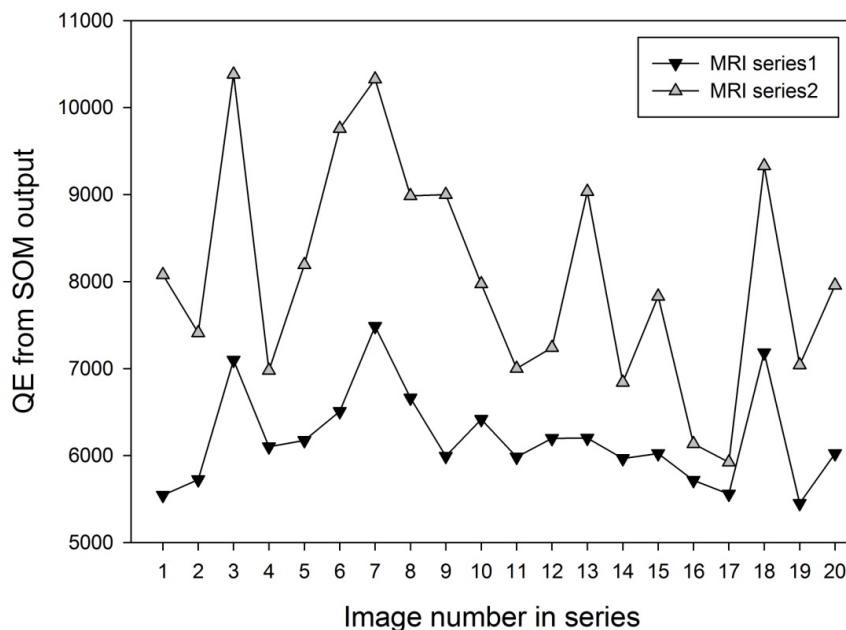


Figure 3.17: Results from SOM-QE analyses on time series of the original MRI images, taken at two different clinical visits by the patient. It is shown that the SOM-QE value increases significantly ( $t(1, 38) = 3.336; p < .01$ ) between the two times. Thus, the SOM-QE is a statistically reliable detection measure of the change between the images from the two series.

The QE distributions were submitted to one-way analysis of variance (ANOVA), which signalled that differences in SOM-QE values on the two image series is statistically significant ( $t(1, 38) = 3.336; p < .01$ ). This significant difference in the SOM-QE distributions directly reflects the clinical significance of the image differences between the first and the second visit.

The results from SOM-QE on the image series with added artificial lesion content, Figure 3.18, similarly produced systematic increase in the QE between original image series and the image series with added ‘lesion’. These SOM-QE results were also submitted to one-way analysis of variance (ANOVA). The differences between the SOM-QE distributions for the two series are also statistically significant ( $t(1, 38) = 5.61; p < .01$  and  $t(1, 38) = 2.18; p < .05$  respectively).

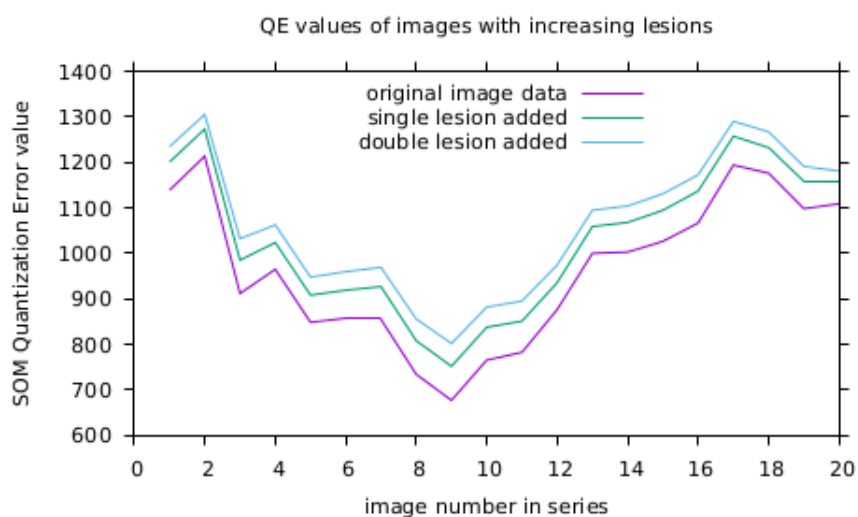


Figure 3.18: Local ‘lesions’ added. Differences between SOM-QE values for original image and ‘2 lesions added’ image series were statistically significant: ( $t(1, 38)=2.055, p < .05$ ).

The results of SOM-QE run on the original MRI image series with and without Poisson noise are shown in Figure 3.19.

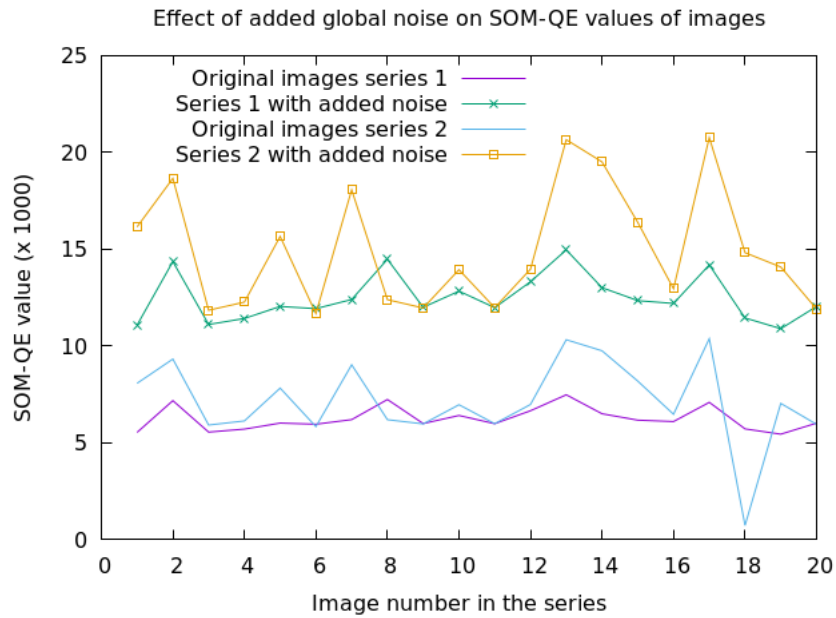


Figure 3.19: Global ‘lesions’ added on images. The dots, considered here to be the ‘lesions’, were added to each image based on Poisson distribution frequency. SOM-QE output increases significantly ( $t(1, 38)=3336$ ;  $p < .01$ ) between the image series. In the original images series 1, small synthetic lesion was added, while in original images series 2, a larger synthetic lesion was added. For each manipulation, the difference in the SOM-QE outputs is statistically significant, that is,  $t(1, 38)=3337$ ;  $p < .01$  for series 1 and  $t(1, 38)=3336$ ;  $p < .01$  for series 2.

Adding Poisson noise to the original MRI images produces differences in the SOM-QE distributions that are, again, statistically significant ( $t(1, 38) = 20.76$ ;  $p < .001$  and  $t(1, 38) = 9.68$ ;  $p < .01$  for series 1 and 2 and their modified versions, respectively). It is thus shown that adding Poisson frequency distribution

noise to the original MRI images has increased the SOM-QE values of the images proportionally.

### **3.3.3 Discussion**

Biomedical signal and image processing focuses on different goals in the educational and research fields of biomedical engineering, Kaçar and Sakoğlu [2016] among others. With growing physiological knowledge, a wider range of innovative research on clinical methods makes use of such processing in medical applications, and many advanced algorithms in the signal and image processing field rely on time frequency representation approaches, especially in the field of neural-sciences Mavratzakis et al. [2016], and in functional imaging of the cardiovascular system.

Imaging modalities are now widely accessible and can deal with the analysis of disease progression to provide diagnostic information. They, however, involve multiple steps of computational analysis and processing and does not enable straightforward and instant decision making. It is important to point out that a deeper analysis of all these different approaches would be beyond the scope of this thesis, which is aimed at testing a simple method of fast and almost instant change detection that can be applied to images generated by the different biomedical imaging approaches. By this virtue, the method described here has the potential to aid human observing performance to help improve decision making

of the medical experts.

The results from the series of simulations described in this chapter suggest that SOM-QE analysis is well-tailored for fast change detection through large bodies of medical images. It allows the automatic detection of subtle but significant changes in time series of images likely to reflect growing or receding lesions. In clinical practice, finding evidence for subtle growth through visual inspection of serial imaging can be very difficult. This is especially true for scans taken at relatively short intervals (less than a year). Visual inspection often misses the slow evolution because the change may be obscured by variations in body position, slice position, or intensity profile between scans. In some cases, the change can be too small to be noticed. Surgeons and oncologists frequently compute the change in tumour volume by comparing the measurements from consecutive scans. When the change in tumour volume is too small and hence difficult to detect between two sequential scans, radiologists tend to compare the most recent scan with the earliest available image to find any visible evidence for an evolution of the tumour.

The resulting analysis does, however, not reflect the current development of the tumour but rather a retrospective perspective of tumour evolution, as pointed out earlier. This study addresses this problem, as the fast SOM-QE can easily be implemented to aid clinicians in deciding on the treatment. The process of executing the code to determine the QE distribution for a series of twenty images takes about 40 seconds. This involves reading the DICOM images from a folder, running the SOM and determining the QE for each image, displaying the image



on the screen and saving the QE value in a text file. In summary, whenever the SOM-QE value on a patient's medical images taken at consecutive times rises, it is a potential indication that lesions or other pathological changes of the organ under study may be developing, while a decrease of the SOM-QE value may indicate that a pathology is receding. To the best of our knowledge, this approach is the first to automatically detect potentially critical local changes in a patient by comparing images taken from subsequent clinical visits without relying on visual inspection or manual annotations.

The SOM-QE method detects these changes rapidly with a minimal computation time using consecutive images of an organ without having to rely on derived image qualities as is the case for image subtraction methods. The SOM-QE method also represents a clear advantage compared with monitoring a condition, for example cancer progression or remission, using manual segmentation techniques on each image from an MRI sequence, which is prohibitively time consuming.

In the human and environmental sciences, time-series of satellite images may reveal important data about changes in environmental conditions and natural or urban landscape structures that are of potential interest to citizens, historians, or policy makers. The next section gives details of SOM-QE results from extracts of satellite images for specific geographic regions of interest.

### **3.4 Change detection in time series of satellite images**

In this section, SOM-QE is applied to detect changes given satellite images of specific geographic ROI. It is also used to determine urban growth variability through Atlas maps and to detect changes in carbon dioxide gas concentration in air.

The detection and characterization of critical changes in public spaces of the natural or the built environment reflected by changes in image time series such as photographs or remotely sensed image data may be of considerable importance for risk mitigation policies and public awareness. This places a premium on techniques for discriminating between changed and unchanged contents in large time series of images. Hence, various computational methods of change detection in image data including remotely sensed data, exploiting different types of transforms and algorithms, have been developed to meet this challenge. Existing methods have been reviewed previously in excellent papers, for example by Singh [1989] and by Rosin and Ioannidis [2003]. Known computations include Otsu's algorithm OTSU [1979], Kapur's algorithm Kapur et al. [1985], and various other procedures such as pixel-based change detection, image differencing, automated thresholding, image rationing, regression analysis on image data, the least-square method for change detection, change vector analysis, median filtering, background filtering, and fuzzy logic algorithms Devore [2004], Griffiths

[1988], among others. The scope of any of these methods is limited by the specific goal pursued.

As pointed out earlier, image change detection involves being able to reveal critical changes through analysis of discrete data sets drawn from image time series. One of the major the major sources of such images is the remotely sensed data obtained from Earth-orbiting satellites. It provides image time series through repetitive coverage at short intervals with consistent image quality Singh [1989].

We use statistical trend analysis to prove that:

1. the QE distributions from the SOM on the different images corresponding to the geographical ROI under study reliably reflect these critical changes across the years
2. the QE output is significantly correlated with the most relevant demographic data for the same reference time period.

### **3.4.1 Determining urban growth variability through Atlas maps**

In this section, SOM-QE is used to show the status of cities at two different times. Using satellite-based Atlas images, the status of Berlin and Strasbourg in year 2006 and in year 2012 is determined and compared. To attain this, images of each city taken at the two times were processed through SOM-QE. The Urban Atlas maps used are from Copernicus - 'the European Programme for the establishment

of a European capacity for Earth Observation’.

The results obtained are shown in Table 3.8.

City	SOM-QE value		Change
	Year 2006	Year 2012	
Berlin	0.7210	0.6589	decrease
Strasbourg	0.8175	0.8246	increase

Table 3.8: SOM-QE values for satellite images taken of Berlin decrease as a function of time, while SOM-QE values for images taken of Strasbourg, during the same reference period, increase. These trends reflect the evolution in these two different urban landscapes across the reference time period.

From the SOM-QE values between the two years, the level of uniformity increased in Berlin, that is, sections within the city changed to resemble or match each other more in the period between 2006 to 2012. On the other hand, the uniformity within Strasbourg reduced between the same period. The implication is that some sections of Strasbourg were developed at the expense of others. This is vital information for the mayors of the two cities or other concerned authorities. The information was processed by SOM-QE in under 1 minute.

### **3.4.2 Regions in Las Vegas**

The satellite image extracts used in this section correspond to three distinct geographical ROI referred here as: Las Vegas City Center, Lake Mead and its close surroundings, and the Residential North of Las Vegas. Statistical trend analysis is used to evaluate the SOM-QE performance on visualizing structural change across

time in the regions, highlighting significantly correlated demographic data for the specific time period. The statistics is utilized to prove that:

1. the SOM-QE values from the different images corresponding to each ROI under study reliably reflect these critical changes across the years
2. the SOM-QE output is significantly correlated with the relevant demographic data for the same reference time period.

Samples from the datasets of images are shown in Figure 3.20. The samples are the first and the last image from each of the three geographic ROI.

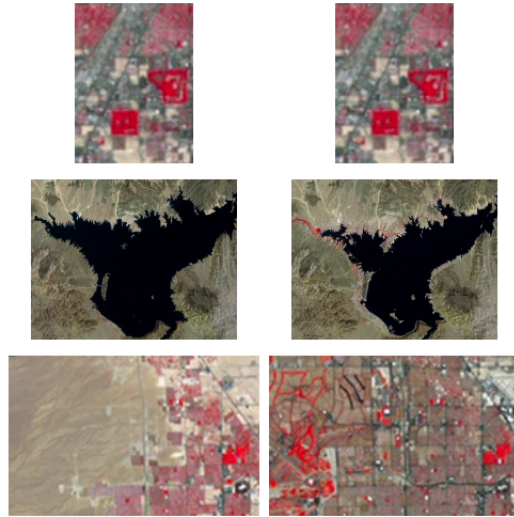


Figure 3.20: The two images on each row from left to right are the first and the last in their respective series, captured in year 1984 and year 2008 respectively. On the top is a section from the residential North of Las Vegas, in the middle is Lake Mead and its immediate surroundings and at the bottom is a section of Las Vegas City centre. Complete image datasets for each ROI are provided in the supplementary material section.

After preprocessing to ensure equivalence in scale, contrast intensity and alignment of the extracted images, the image input is exploited directly without additional or intermediate procedural analysis. To control for differences in intensity across images of a given time series, a transform as defined by equation 3.1 is applied. The images in each set were also co-registered by applying the method in,

Thévenaz et al. [1998], matching them to one image to minimize changes caused by misalignment.

#### **3.4.2.1 Materials and methods**

The images were extracted from a time-lapse animation of the western half of the city of Las Vegas, Nevada, from 1972-2013, as captured by Landsat sensors. The animation portrays the outward expansion of the city as made of data from all the Landsat satellites, Jentoft-Nilsen et al. [2012]. The images are false-colour, showing healthy vegetation in red.

The large red areas are actually green space, mostly golf courses and city parks. According to Jentoft-Nilsen et al. [2012], the images became a lot sharper around 1984, when new instrument designs improved the ability to resolve smaller parcels of land. Consequently, the dataset considered here is for the 25 years between year 1984 and year 2008, with one image per year. Besides, during this period, major structural changes in the urban landscape of Las Vegas City and the Residential North, and the gradual dwindling of the nearby Lake Mead's water levels due to the effects of global climate change was witnessed. It is these changes that SOM-QE aims to portray.

From the extracted images, each of the three ROI was cropped out from every year's image to form three datasets. Each dataset consists of 25 images, one for every year between 1984 to 2008.

The cropping was done in such a way to ensure that the same scene was covered from each image per dataset. Then, each year's image was registered with year 2013's image, for the Residential North dataset and year 2011's image for the City Centre and Lake Mead datasets. The choice of these later images as the base image is motivated by fact that with increasing improving Landsat instruments over the years, the images were bound to have their scan planes in better location than the others. Then, the same images were used to train a 4 by 4 SOM for each dataset using a neighbourhood distance of 1.2 and at a learning rate of 0.2 for 10,000 iterations.

Since the original images used colour to emphasize different areas on the maps, pixel-based RGB values are used as input features to the SOM. This ensures a pixel-by-pixel capture of detail and avoids errors due to inaccurate feature calculation which often occur with complex images Suzuki [2012]. With the trained SOM, QE values were determined for each of the 25 images of each dataset.

Images datasets used in this section are provided in the supplementary material section.

### **Las Vegas City Centre ROI**

The City Centre image dataset consist of images of size 72 by 98 pixels. It provides a special challenge in change detection analysis since few and small changes were bound to occur in the period of study. The ROI was already built-up by 1984 leaving little room for new constructions, for example. As pointed out in Guest



and Nelson [1978], it is the suburban that gains in status while the centres of the oldest metropolitan areas presumably were unattractive to higher status persons, and the development of the auto-mobile permitted them to leave. This is also evident from Figure 3.20, top row, where a challenge to tell the difference between the image on the right and the one to the left will be a difficult one for a visual observer despite the images having been captured 25 years apart. Such a challenge was the subject of section 3.2, where the human observer was found to perform dismally in recognition of small differences between two images. Through this ROI, SOM-QE is used to show that city centres are characterized by a relative centralization, or at least no decentralization, as reported in Guest and Nelson [1978].

The income and poverty charts for Las Vegas show how its suburbs still have the economic advantage as reported in Juday [2015].

The QE values were fed into linear regression analysis, Figure 3.22. To relate the development captured by SOM-QE figures on the number of visitors to the region during the period are shown in Figure 3.23 and the population growth is shown in Figure 3.24. Figure 3.25 and Figure 3.26 relates the SOM-QE values to the number of visitors and population trends respectively.

### **Lake Mead ROI**

Lake Mead dataset has images covering 430 by 366 pixels. It is an artificial lake situated lake in the Nevada Desert.

SOM-QE results from this dataset are shown in Figure 3.27. Figure 3.28 shows the water level trends during the period while Figure 3.29 is a comparison of the falling water levels with SOM-QE values.

### **Residential North**

This geographic ROI is a section situated on the North of Las Vegas City, USA. It corresponds to an image of size 186 by 119 pixels. The selected area encloses Sun City and North Las Vegas Airport to the top left and right respectively. At the bottom are the Suncoast Hotel and Casino, to the left, and the Spring Preserve to the right.

SOM-QE results from this dataset are shown in Figure 3.30. Figure 3.31 shows the population trend during the period while Figure 3.32 is the relationship between the population growth and the SOM-QE values.

#### **3.4.2.2 SOM-QE on objects within a ROI**

In the next step, changes that occurred in specific areas within the Residential North ROI are quantified. The SOM-QE for each input vector is determined using equation 9 and the difference with the corresponding vector in subsequent year(s) is calculated using equation 10 to give the change. See sample results in Table 3.9. An input feature vector represents an object within the ROI, enabling changes on each object within the scene to be monitored. See Figure 3.33.

### 3.4.2.3 Results

SOM-QE results from the three ROI are shown and discussed in the light of their statistical significance from linear trend analysis. Pearson's correlation method is used to link the QE to a set of highly relevant demographic data from the same reference time period. Images from the three datasets are provided in the Supplementary Materials section.

#### Las Vegas City Centre

During the reference time period, significant but small changes in building density across the whole of Las Vegas City was witnessed. Photographic snapshots taken on parts of the 'Strip', the central artery of Las Vegas, where most attractions are located, illustrate some of these changes, Figure 3.21.



Figure 3.21: Photographic snapshots of parts of 'The Strip' across the years 1982-2010. From left to right, the photos were taken in 1984, 1995, 2005 and 2008 respectively. They give some idea of the structural changes that took place in Las Vegas City during the reference time period of this study, for which the satellite images generated by NASA were retrieved.

However, the changes in the small ROI used for this study were not as elaborate and clear for the human observer as those in the photographs. As Figure 3.22 illustrates the SOM-QE value ranged from 0.2404 in 1984 to a high of 0.3143 in 2008. This translates to an increase of 0.039, or 30.74%, during the 25 years.

Results in terms of QE output of the SOMs for the 25 image extracts corresponding to the ROI Las Vegas City are shown below, Figure 3.22 as a function of the year in which an image was taken. The variations in the QE shown reflect varying spatial contrast distribution in the images across time. These are indicative of the major structural changes in the urban landscape during the reference time period. Trend analysis (linear regression analysis) on these data reveals a trend towards increase in QE as a function of time expressed in terms of the progression in years of the reference period 1984-2008, with a linear regression coefficient  $R^2 = .48$ , and a  $t(1, 24) = 2.13$ ,  $p < .05$  indicating that the trend towards increase in QE with time is statistically significant. Contrast intensity across images of a time series for a given ROI being controlled for by preprocessing, the significant increase in QE from SOM output reliably signals a significant increase in spatial extent of contrast regions in the images with time. Trend analysis on related demographic data for Las Vegas City show that both the number of visitors in millions and the estimated total population in thousands have increased significantly over the reference time period.

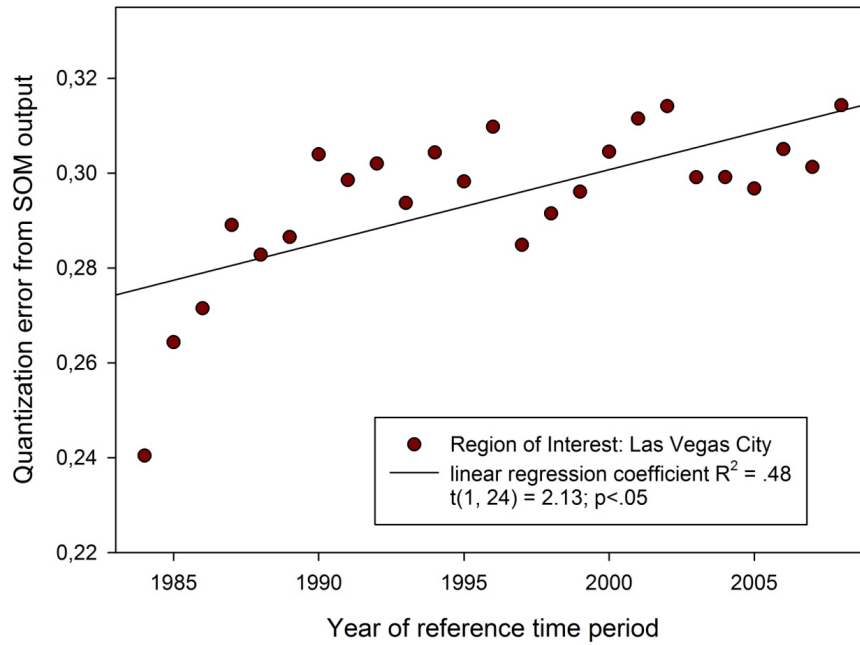


Figure 3.22: Variations in SOM-QE output plotted as a function of time. SOM-QE values were found to change in a statistically significant manner in the geographic ROI 'Las Vegas City'.

From section 3.2, even expert observers could not clearly tell such difference between images! On average, the ROI grew by about 1.22% per year, which is out of the ability of visual human observers and other computational approaches discussed in literature. Yet, SOM-QE performed this, leaving no doubt as to existence of difference between any two of the images, at a time of 7.1 seconds only. The variations in the QE shown reflect varying spatial contrast distribution in the images across time. These are indicative of the major structural changes in the

urban landscape during the reference time period. Linear regression analysis on these data reveals a trend towards increase in SOM-QE value as a function of time during the study period. The one-sample statistic,  $t(1, 24) = 2.13$ ,  $p < .05$  indicates that this trend over time is statistically significant. It confirms SOM-QE output as reliable indicator of the significant increase in spatial extent of contrast regions in the images with time. Trend analysis on related demographic data for Las Vegas City show that both the number of visitors and the estimated total population have increased significantly over the reference time period, Figure 3.23 and Figure 3.24 respectively.

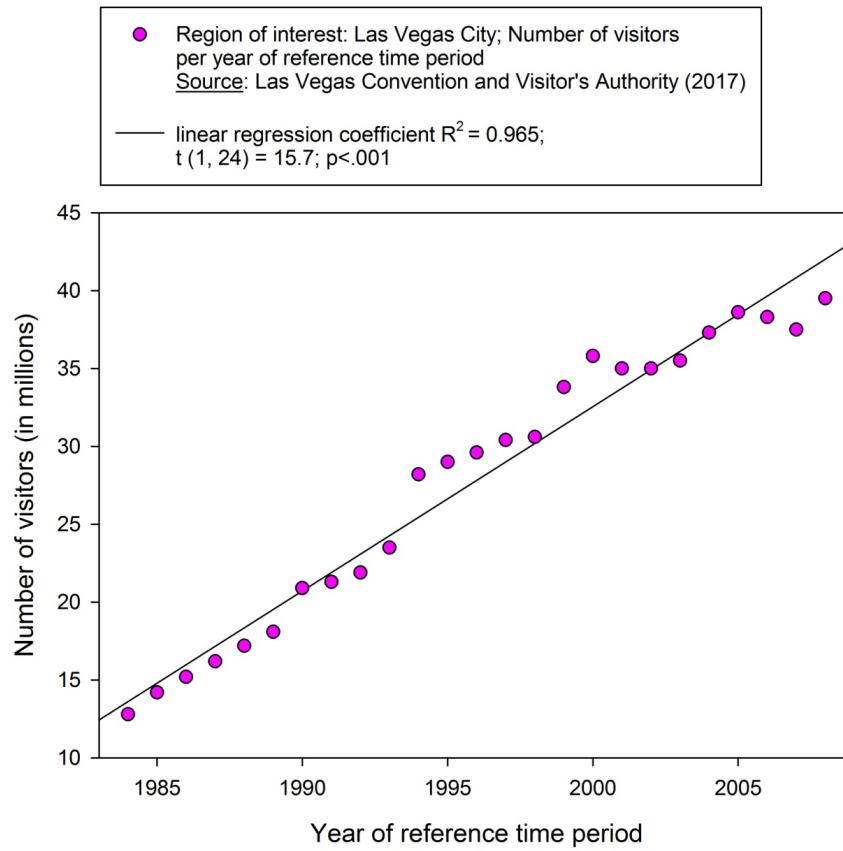


Figure 3.23: Number of visitors of Las Vegas City as a function of time. The linear trend yields a significant regression coefficient  $R^2 = .965$ . The increase with time is statistically significant, with  $t(1, 24) = 15.7$ ,  $p < .001$ .

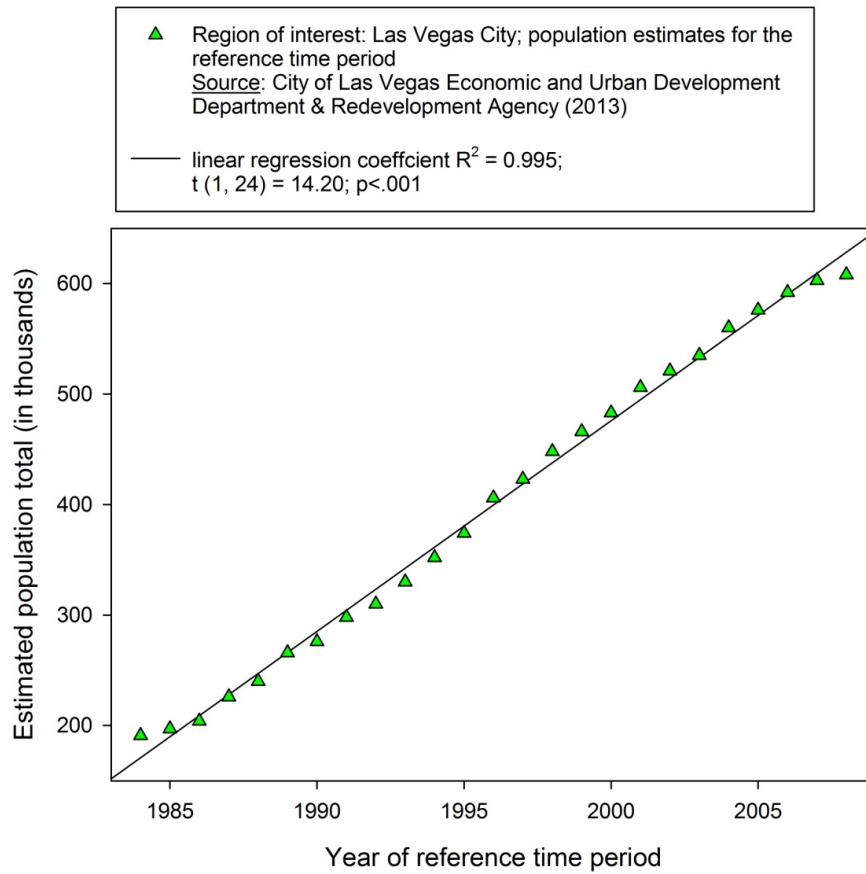


Figure 3.24: Estimated population total for Las Vegas as a function of time. The linear trend yields a significant regression coefficient  $R^2 = .995$ . The increase with time is statistically significant, with  $t(1, 24) = 14.2$ ,  $p < .001$ .

To assess the statistical correlation between the QE and other relevant demographic variables from the reference time period, Pearson’s correlation coefficient was computed on the distributions for QE against number of visitors and QE against the estimated population total.



The results of these analyses are shown in Figure 3.25 and Figure 3.26. Pearson's correlation coefficient  $R$  gives an estimate of the statistical relationship, or association, between two independent continuous phenomena, or variables based on the mathematical concept of covariance.  $R$  is associated with a probability  $p$  and carries information about the magnitude of the association, or correlation, as well as the direction of the relationship. Pearson's correlation statistic computed on the paired distributions signals statistically significant correlations between the QE and the number of visitors and between the QE and the population totals for the period of study on the Las Vegas City ROI.

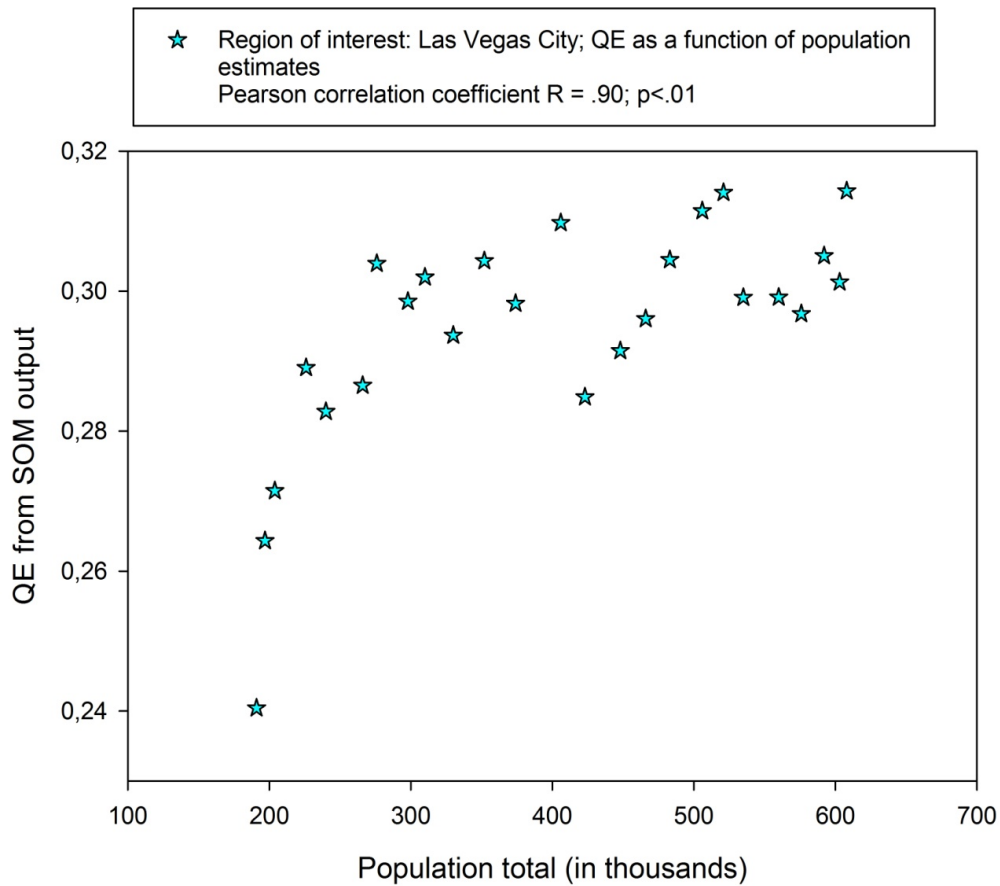


Figure 3.25: Variations in QE output plotted as a function of the number of visitors of Las Vegas City during the reference time period. Pearson's correlation statistic computed on paired distributions gives a statistically significant correlation with  $R = .75$ ,  $p < .05$ .

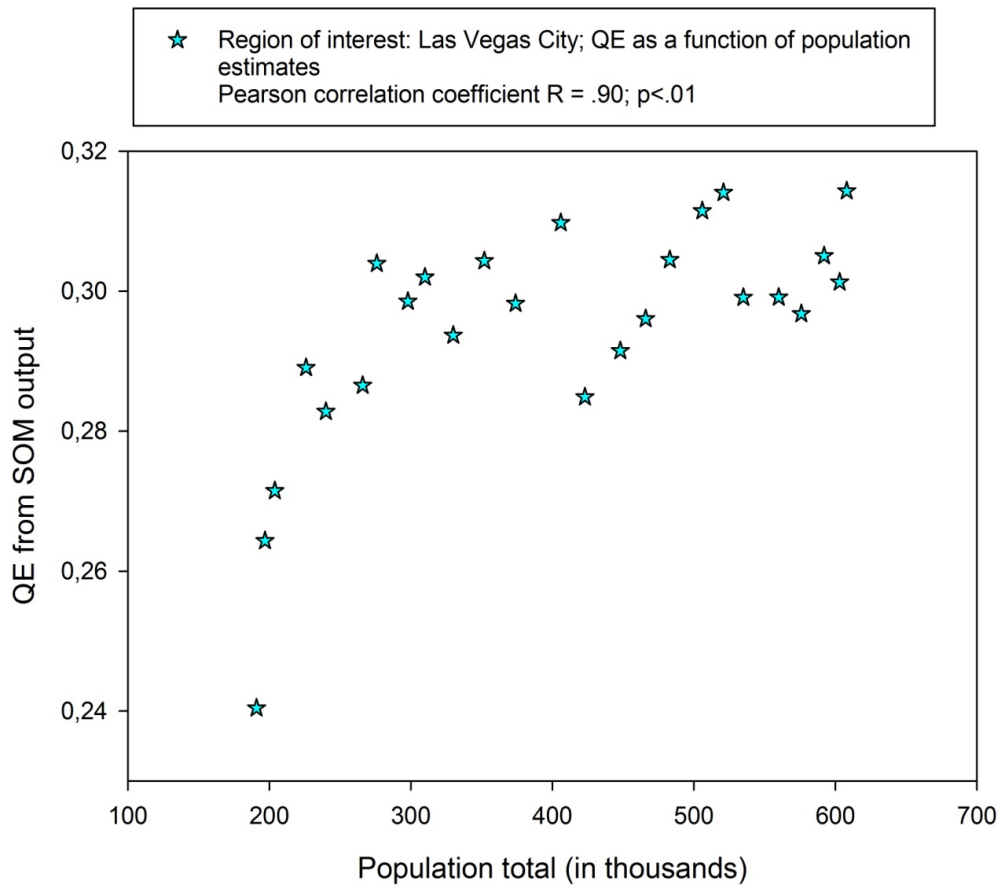


Figure 3.26: SOM-QE output plotted as a function of the number of estimated population total for each year of the reference period. Pearson’s correlation statistic computed on the paired distributions gives a statistically significant correlation with  $R = .90$ ,  $p < .01$ .

### Lake Mead Reservoir

During the reference time period, Lake Mead water levels progressively dwindled

away as a consequence of global climate change. This phenomenon is captured by SOM-QE as shown in Figure 3.27.

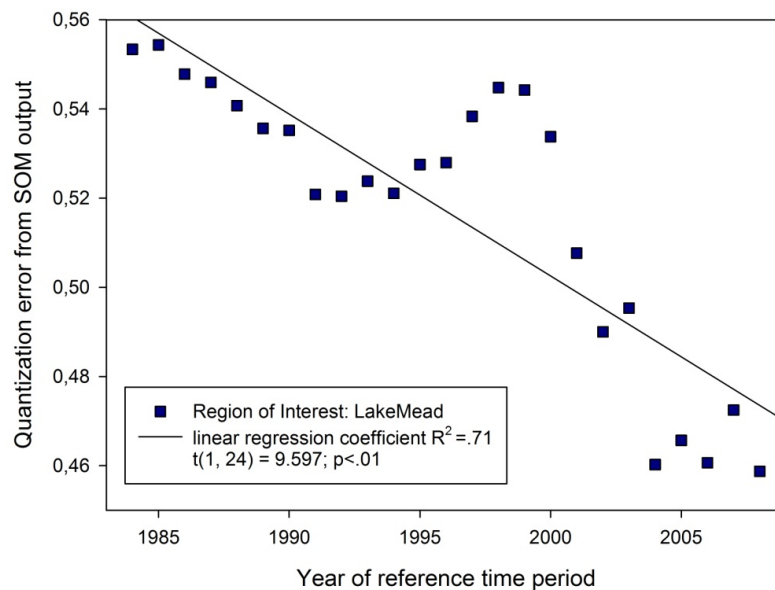


Figure 3.27: SOM-QE output plotted as a function of the time period in which the corresponding satellite images of Lake Mead were taken. The change detector (SOM-QE) is shown to decrease with time, reflecting the steady decrease in water levels of the Lake during this period (compare: Figure 3.28 and Figure 3.29). Linear regression indicates this to be statistically significant.

### Nota Bene

Here we used trend analysis by linear regression to test the direction of change of either the SOM-QE or demographic data with time. No assumption about a

linearity of this change is made. In other words, we are not making any assumption about a linear model to explain the data!

Linear regression analysis on the data reveals a trend towards decrease in SOM-QE value as a function of time, which is expressed in terms of the progression in years of the reference period. The data has a linear regression coefficient  $R^2 = .71$ , and a  $t(1, 24) = 9.597$ ,  $p < .01$  indicating that the trend towards decrease in SOM-QE with time is statistically significant.

SOM-QE output reliably signals a significant decrease in spatial extent of contrast region in the lake's images with time. This image phenomenon is directly related to the shrinking of Lake Mead, as seen in the image samples in Figure 3.20, middle row. Water level statistics for the reference time period are shown in Figure 3.28.

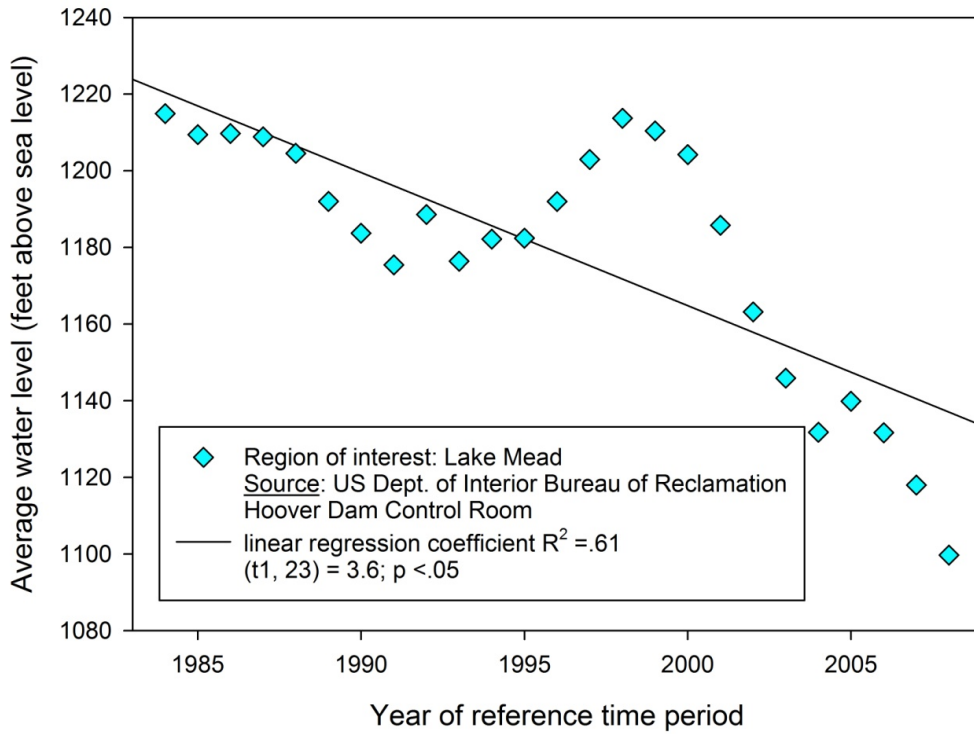


Figure 3.28: Water levels of Lake Mead as a function of time. The linear trend towards decrease yields a regression coefficient  $R^2 = .36$  and is statistically significant with  $t(1, 23) = 3.6, p < .05$ .

Pearson's correlation statistic computed on the paired distributions of QE and water levels signals a statistically significant correlation, shown in Figure 3.29, for the period under study the Lake Mead ROI.

## **Residential North**

The significant changes in building density that occurred in this geographic region of interest, turning the land from desert into a major densely built-up residential suburb of Las Vegas City, are well captured by SOM-QE values' trend, Figure 36. Linear regression analysis on the QE data returned a regression coefficient  $R^2 = .7999$ . The linear relationship between the artificial neural network (SOM) output in terms of QE and time is statistically significant with  $t(1, 24) = 33.45$ ;  $p < .001$ . This indicates that the artificial system reliably detects the critical structural changes in the images of Las Vegas North across time.

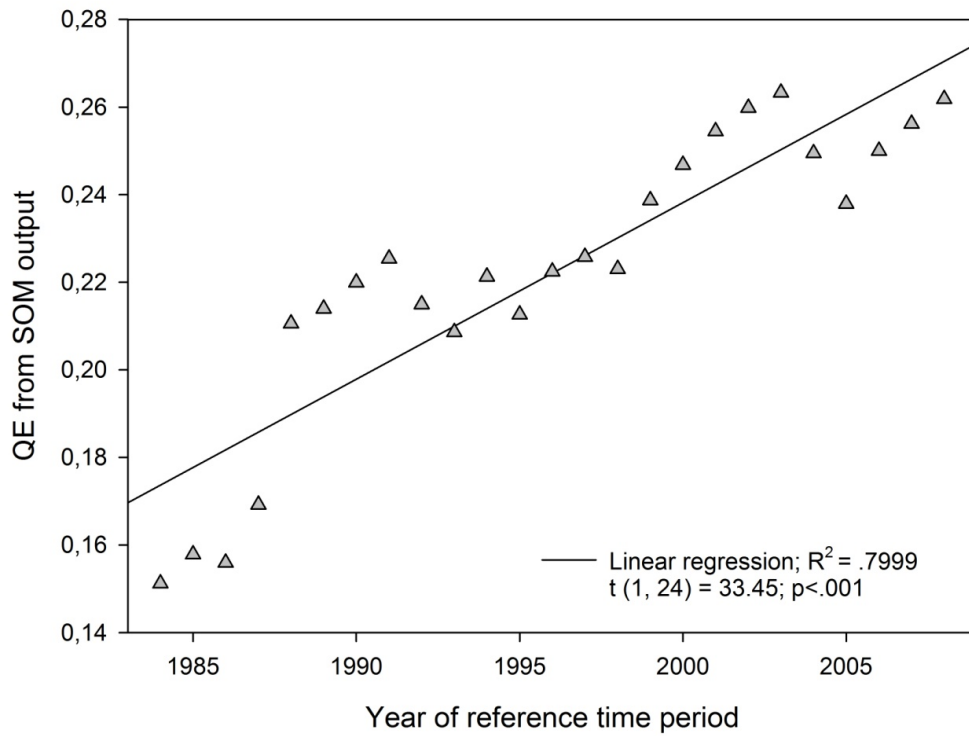


Figure 3.30: QE trend as a function of the year of the reference time period from which the input images were taken for the Residential North ROI.

The trend towards increased land cover in the North of Las Vegas is further illustrated by demographic data for that geographic ROI from the same time period, as shown in Figure 3.31.



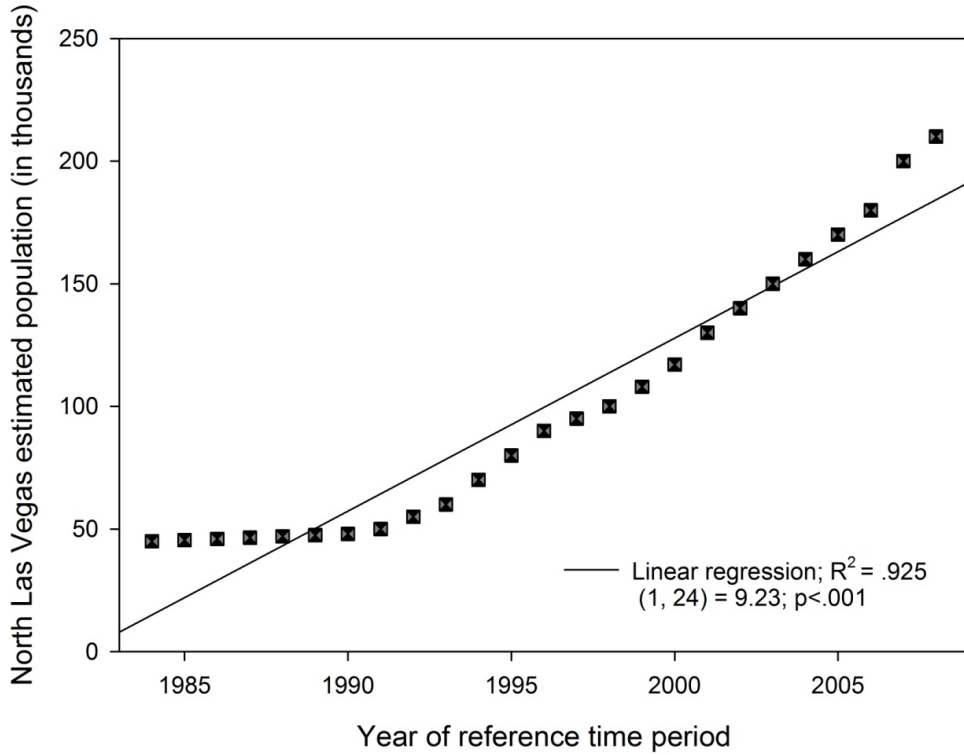


Figure 3.31: Population totals (estimates in thousands) as a function of time. This was during the reference period under study. Here, the best model to fit the demographic data is most likely a parabolic function.

Regression analysis on these data returns a regression coefficient  $R^2 = .92$ . The linear relationship between population estimates and time is statistically significant with  $t(1, 24) = 9.23, p < .001$ . Next, a plot of the SOM-QE output as a function of these population estimates is shown in Figure 3.32.

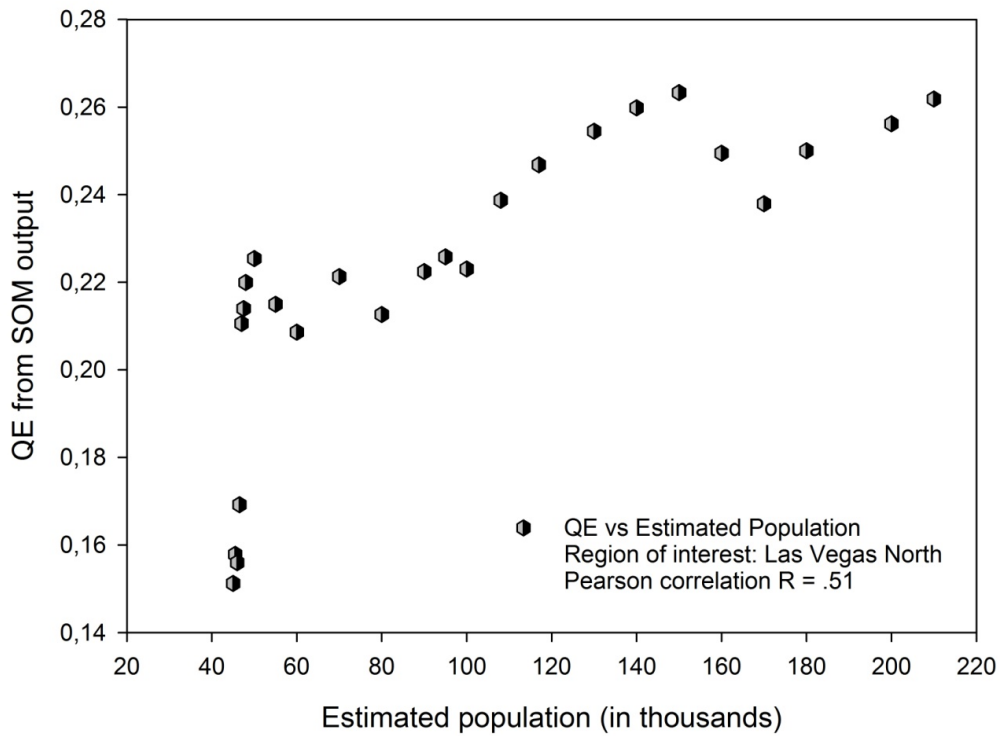


Figure 3.32: SOM-QE output from the image analyses as a function of the population estimates for the same geographic ROI Las Vegas North. The two variables are positively correlated as testified by Pearson's R.

The link between the increase in QE from the image analyses and the population estimates for the same geographic ROI Las Vegas North for the reference time period is described by a positive Pearson correlation with  $R = .51$ .

Thus, SOM-QE output from the image dataset reflects the progressive land cover

changes in this geographic ROI.

### Changes in objects within a ROI

The next results, show how SOM-QE can track changing objects within the ROI.

The QE of an input feature vector is monitored between images to determine the changes. See Table 3.9 and Figure 3.33.

Input vector position index	SOM-QE value 1984 image	SOM-QE value 1985 image	Change in QE
353	0.3316	0.3316	0
362	0.3314	0.3314	0
1284	0.2896	0.2896	0
2501	0.1551	0.1551	0
3001	0.0534	0.0566	-0.0033
3587	0.0411	0.0362	0.0049
3955	0.0711	0.0649	0.0062
7065	0.1681	0.1427	0.0254
11689	0.1287	0.1260	0.0027
17587	0.24211	0.2421	0

Table 3.9: Sampled SOM-QE values of regions within the Residential North ROI on the same position of images captured in 1984 and 1985. The last column indicates the amount and direction of change in the region as determined by SOM-QE. Note the two positions, 2501 and 17587, with SOM-QE values of 0.1551 and 0.2421 respectively and whose positions are labelled in Figure 3.33.

Some objects changed by increasing their SOM-QE values, others decreased while others did not change as shown in the last column of Table 3.9. Figure 3.33 shows the objects within the ROI, with black dots – pixels- indicating the regions that did not change between the images on each row. All other objects experienced changes.

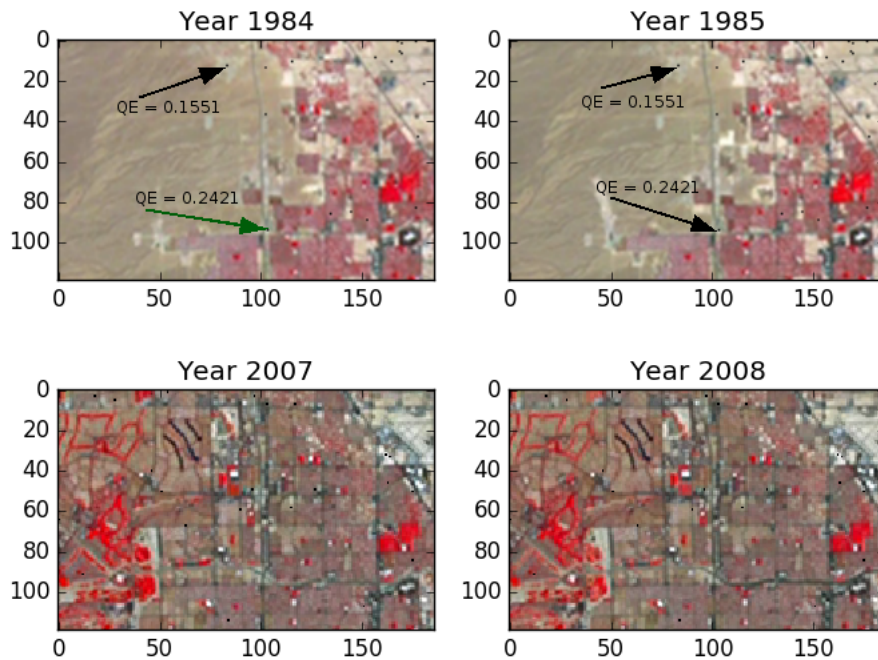


Figure 3.33: The small, black dots in each year’s image are areas that did not experience changes between the two years in each row. The rest of the image had some changes taking place. On the top row, two specific areas are shown out for illustration. One has a SOM-QE value of 0.2421, the second has SOM-QE of 0.1551 in both years, 1984 and 1985. The bottom row also shows areas of no-change between the years 2007 and 2008. It takes 7.1 seconds to detect changes and label regions between the two pairs of images, making this approach appropriate for the task.

### **3.5 Using SOM-QE to tell future occurrences**

In this section, it is shown that given a series of SOM-QE values of an object/scene, it is possible to determine future SOM-QE values and hence predict the changes that are likely to occur in the object/scene.

The dataset describes SOM-QE values of images of the City Centre of Las Vegas city, USA. The images are from the same region, each captured per year from 1984 to 2011. The SOM-QE values depict how this ROI changed during the time under consideration. The SOM-QE values were generated as described in section 3.4. There are 28 observations, having the trend shown in Figure 3.34.

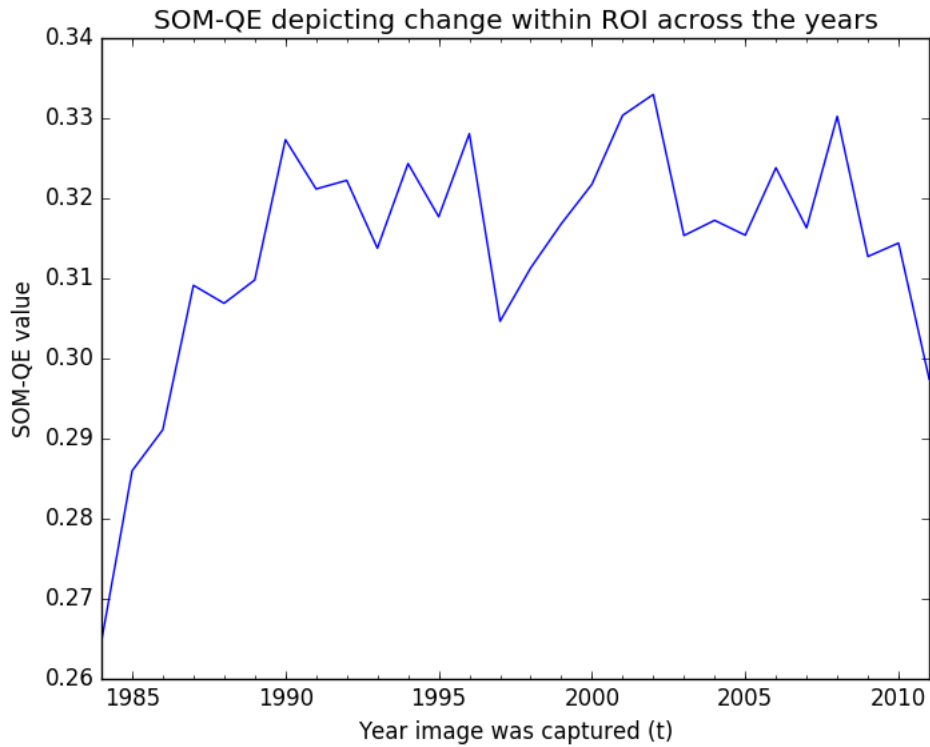


Figure 3.34: The variation of SOM-QE values of a section of the city centre of Las Vegas as a function of time, indicating when change has occurred within the region.

As shown in the plot of next time step observation ( $t + 1$ ) against the observation at the previous time step ( $t$ ) of the dataset, the observations fall along a diagonal line, Figure 3.35.

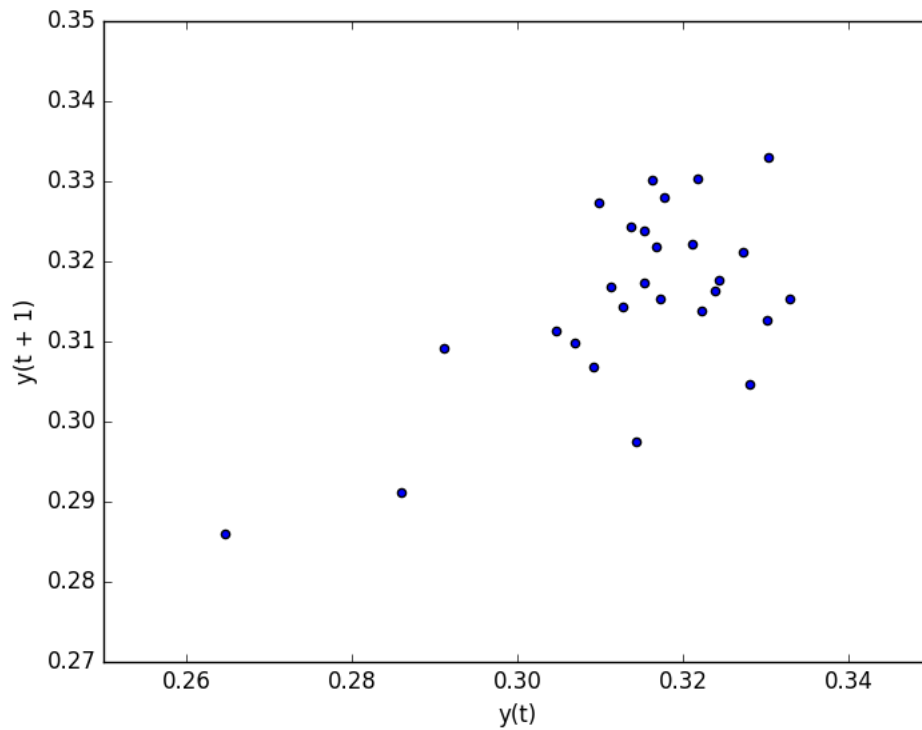


Figure 3.35: When SOM-QE is run on each of the images of ROI, a dataset of SOM-QE values is created. A plot of SOM-QE values,  $y(t + 1)$ , against their previous values,  $y(t)$ . It provides some confirmation that the SOM-QE dataset has some internal correlation, hence it can be used for prediction purposes. Thus, the new technique, SOM-QE, generates data that can be applied to determine future change, its direction and its magnitude.

This is an indication that the data points calculated over time by SOM-QE have

an internal structure that can be accounted for. Time series modelling is used here to make predictions of future SOM-QE values for the ROI.

### 3.5.1 Method

Since the aim is to predict change between consecutive images, the data is first transformed by differencing, with each observation transformed using the relation:

$$value(t) = obs(t) - obs(t - 1) \quad (3.2)$$

where  $value(t)$  is the difference between two consecutive observations. This forms the differenced dataset from the original SOM-QE values dataset.

Next, an auto-regression model with a lag of 6 was trained on the differenced dataset and used to predict SOM-QE. Auto-regression is a time series model that uses observations from previous time steps as input to a regression equation to predict the value at the next time step. 66% of the differenced data was used to train the model, while the rest was used to test the model. The regression coefficients learned by the model are used to make predictions in a rolling manner across the test dataset.

As each time step in the test dataset is executed, the prediction is derived from the coefficients and stored. The actual observation for the time step is then made available and stored to be used as a lag variable for future predictions.



Finally, the differenced dataset was transformed into the original form. This is done by keeping track of the last actual observation so as the predicted differenced value can be added to it.

This method focuses on one-step forecasts, but can work for multi-step forecasts by using the trained model repetitively and applying forecasts of previous time steps as input lag values to predict observations for subsequent time steps. Table 3.10 gives example results on this aspect.

### **3.5.2 Results**

Training and running the model first gives the Mean Squared Error (MSE) of the predictions, which is 0.0 (that is, 0 error on average, if the square root is taken to return the error score to the original units). All changes depicted by SOM-QE between images are correctly predicted by this model. The MSE tell how the model is expected to perform on average when making forecasts on new data.

Finally, a graph is created showing the actual observations in the test dataset (blue) compared to the predictions (red), shown in Figure 3.36.



Figure 3.36: The results of how predictions are derived from the differenced SOM-QE dataset. The blue plot is the actual data from the test dataset while the red plot is for the corresponding predictions.

Table 10 compares the forecasts results for the ROI for the year 2010 and 2011 with the actual observations. The change detection is seen to be on the same direction for both actual and predicted SOM-QE values in both years.

Year	Actual SOM-QE value	Predicted SOM-QE value	Actual change (current value minus previous value)	Predicted change (current value minus previous value)	Direction of change
2009	0.312736	0.317673			
2010	0.314414	0.322340	0.001678	0.004667	Positive for both
2011	0.297438	0.310476	-0.016976	-0.011864	Negative for both

Table 3.10: Predicted versus actual observation. The model was used to predict SOM-QE values for two years, 2010 and 2011. The predicted change in the two years was the same as the actual observation. Actual observation is obtained by running SOM-QE on the image captured in the year.

## 3.6 Evaluating SOM-QE performance

In this section, the performance of SOM-QE is compared with that of other methods using two image datasets. In the first case, the images are accompanied by real measurement of the amount of a gas in air providing the ground truth data to benchmark SOM-QE performance as a change detector and the use of its data in prediction. In the second case, a change detection dataset that is presented in literature as posing difficulties for change detection methods is used.

### 3.6.1 Carbon dioxide gas measurements

To determine the accuracy of using SOM-QE values as a change detector and in a prediction task, it is tested on a different dataset. This dataset provides real measurements captured by instruments which are compared with SOM-QE values

obtained from corresponding images to determine the accuracy.



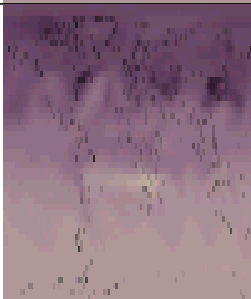
The dataset is composed of a movie showing the annual cycle of carbon dioxide gas ( $CO_2$ ) in the Northern Hemisphere. The movie captures the period from January 1 to December 31, 2012 and indicate the distinct rise and fall of carbon dioxide levels over a year's time. Along with the movie, daily average atmospheric  $CO_2$  measurements recorded at Mauna Loa Observatory, Hawaii USA, are also provided, Thoning et al. [2017].



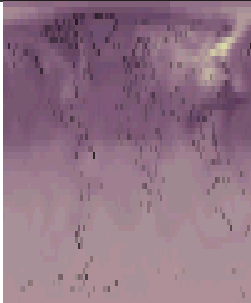

The unit used to record the gas data is parts per million (ppm), which is the number of  $CO_2$  molecules present in every million molecules of air. The annual pattern is caused by the uptake and release of  $CO_2$  from seasonal plant growth on the vast landmasses of the Northern Hemisphere. The annual maximum  $CO_2$  concentration in the Northern Hemisphere occurs around May. The spring build-up happens because decaying plants have been releasing carbon throughout the winter. The annual minimum concentration occurs around October, after new growth has withdrawn  $CO_2$  from the air during photosynthesis.





The dataset is suitable for use in this instance because, when the pollutants molecules increase the variation within the 1 million molecules of air increases too. This means for low ppm, SOM-QE should increase/reduce with increase/reduction of the amount of  $CO_2$ .

From the year 2012 movie, 203 frames were extracted to form the time series dataset of images. The images were of the same size, 2048 by 1026 pixels and

being from the same movie, they had similar properties such as alignment and brightness. A 4 by 4 SOM was set up and, using a neighbourhood radius of 1.2, a learning rate of 0.2 and 10000 iterations the SOM was trained. Then, the trained SOM was used to determine the QE value of each image, see Table 3.11.

Month	Image	$CO_2$ amount (ppm)	Change in $CO_2$	SOM-QE value	Change in SOM-QE value	Compare change in $CO_2$ and change in SOM-QE value
January		394.8		0.1673		
February		393.55	-1.25	0.1910	0.02	miss
March		394.98	1.43	0.2204	0.03	hit

<b>Month</b>	<b>Image</b>	<b><math>CO_2</math> amount (ppm)</b>	<b>Change in <math>CO_2</math></b>	<b>SOM-QE value</b>	<b>Change in SOM-QE value</b>	<b>Compare change in <math>CO_2</math> and change in SOM-QE value</b>
April		396.28	1.3	0.2465	0.03	hit
May		396.98	0.7	0.2537	0.01	hit
June		396.17	-0.81	0.1794	-0.07	hit
July		394.62	-1.55	0.1419	-0.04	hit

Month	Image	$CO_2$ amount (ppm)	Change in $CO_2$	SOM-QE value	Change in SOM-QE value	Compare change in $CO_2$ and change in SOM-QE value
August		392.34	-2.28	0.1495	0.01	miss
September		390.76	-1.58	0.1247	-0.02	hit
October		390.83	0.07	0.1075	-0.02	miss
November		393.13	2.3	0.1477	0.04	hit


Month	Image	$CO_2$ amount (ppm)	Change in $CO_2$	SOM-QE value	Change in SOM-QE value	Compare change in $CO_2$ and change in SOM-QE value
December		394.82	1.69	0.2023	0.05	hit

Table 3.11: When both changes are in the same direction, that is, both are an increase or both are a decrease, then a ‘hit’ result is obtained, while when the changes are in opposite direction, it becomes a ‘miss’ results. 8 out of 11 changes are hits, which is 72.7 % score. This is a good score and can be improved if the matching of dates of images’ capture with those of gas level measurement is improved. That is, the date of image capture should be as close as possible to the date of taking the gas measurement.

When the 203 images are evenly spread in the year, an image is picked per month of the year. Each of the 12 images can then be associated with the corresponding recorded measurement of the month, Table 3.11. The  $CO_2$  reading taken at the mid month – the 15<sup>th</sup> of every month– is used as the corresponding monthly



reading.

From the results, the performance of SOM-QE as a change detector can be calculated as:

$$\text{precision, } p = 8 \div 11 = 0.727$$

$$\text{recall, } r = 8 \div 11 = 0.727$$

$$\text{and F1 score of } (2 \times p \times r) \div (p + r) = 0.727$$

This is a better score than those reported in related literature. For instance, Sakurada and Okatani [2015], reported results posted by various 2D change detectors where their own was the best with an  $F1$  score of 0.723.

The 12 SOM-QE values obtained from the monthly images were used to train a predictor. The prediction for SOM-QE value of next image was determined as: 0.224166.

That is, January 2013 image will have a SOM-QE value of 0.2242, up from that of December 2012 image at 0.2023, a +0.0219 change. On the other hand the recorded  $CO_2$  for January 2013 is 395.5 ppm up from 394.82 ppm recorded for December 2012, a +0.68 change. This is a 'hit', meaning that SOM-QE correctly predicts that the amount of  $CO_2$  in air increased in January 2013.

### 3.6.2 Challenging change-detection image dataset

The 2014 CDnet change detection image dataset, Wang et al. [2014], incorporates challenges encountered in many surveillance settings. It provides realistic, camera-captured (without CGI), diverse set of indoor and out-door videos. The video sequences represent various challenges divided into categories. Each change detection challenge in a category is unique to that category. Such a grouping is essential for an unbiased and clear identification of the strengths and weaknesses of different change detection methods. Among the categories is the PTZ - pan-tilt-zoom camera - category which requires different type of change detection techniques in comparison to static camera videos.

In Wang et al. [2014], a total of 14 change detection methods available in literature were tested and the F-measure for each method was calculated within each category. In particular, the PTZ category showed the lowest performance, a fact attributed to its unique challenges posed by the zoomed-in/zoomed-out nature of the images involved.

Each of the 14 methods posted F1-measure scores of under 0.30. When SOM-QE was applied to this category, it scored an F1 of 0.39, clearly beating the rest which are among the best methods in literature.

In the PTZ category, any camera motion (pan, tilt or zoom) caused major false positives from each method, but SOM-QE minimized them, see Figure 3.37.



Figure 3.37: On the left and at the middle are sample input and ground truth images respectively from the 2014 CDnet dataset, PTZ category. To the right is the image produced by SOM-QE on detecting the changes between the input image and its next image frame on the video. The PTZ category of images posed unique challenges on change detection, with other methods in the literature managing F1 score of less than 0.30. SOM-QE scored an F1 score of 0.39, which is the best score in this category.

## **3.7 The SOM-QE algorithm: New method to determine QE in time series images**

### **3.7.1 Introduction**

In determination of QE, the difference between the original input vector,  $\mathbf{x}$ , and its winner, the BMU, is used, see equation 2.9. The BMU is one of the final weights in the trained SOM and is chosen to be the closest to the input vector.

For a set of time series images where change is to be detected, the winner of

vector may not be the same across the images. This is inherent from the principle of competitive learning which SOM practices. Units in the SOM map compete for the right to respond to the input data vector – the unit with the closest resemblance to wins, and becomes its BMU. Consequently, if the values in vector changed between images and it is subjected to the competition, any of the SOM units can become its BMU. Depending on the changes in , it may find itself having a new winner among the SOM weight units and this will affect results posted by equation 2.9.

In change detection, the interest is in the change that has occurred in between subsequent images in a time series dataset. This is the change that is as a result of changing status of the object whose images were acquired at different times. When the object has undergone some changes, we expect the changes to be reflected in the input vector . The set of SOM final weights, from which  $x$ 's winner is determined from, carries different values and are not necessarily equal. It therefore implies that when switches winners, it affects the results given by equation 2.9 as it include not only the change in , but also the changes due to the use of a different winner. Reporting change in this manner may be inaccurate, as it includes the results from two sources: first the actual difference between the input vector in the first dataset and that of the second dataset, and secondly the use of a different BMU to calculate the QE for the vector in the two different datasets. To maintain accuracy, this second source of change need to be eliminated.

For example, suppose we have two images with corresponding input vectors  $x_{t1}$

and  $x_{t2}$ , that is,  $x$  at time 1 and  $x$  at time 2. The two images are captured at different times and are preprocessed to ensure uniformity in alignment and lighting exposure. Input vector  $x_{t1}$  and  $x_{t2}$  are from the same position in the two images, that is, they represent the same object within the image. From a trained SOM,  $x_{t1}$  may be won by weight  $w_1$  while  $x_{t2}$  is won by weight  $w_2$ . Thus,  $w_1$  becomes the BMU for  $x_{t1}$  ( $BMU_1$ ) while  $w_2$  becomes the BMU for  $x_{t2}$  ( $BMU_2$ ). The traditional method to calculate QE is to find the the difference of the input vector and its BMU. In this case, on applying equation 9, the QE for the two instances becomes:

$$QE_1 = x_{t1} - BMU_1 \quad (3.3)$$

and,

$$QE_2 = x_{t2} - BMU_2 \quad (3.4)$$

and for the entire dataset the QE values for the object form a set:

$$QE_{object} = \{x_{t1} - BMU_1, x_{t2} - BMU_2, x_{t3} - BMU_3, \dots\} \quad (3.5)$$

that is, the object has QE values from each image in the series that is not calculated from the same BMU.

For a time series dataset this raises an issue. Input vectors  $x_{t1}$  and  $x_{t2}$  represent the

same object, only that their representation is at different times. It is therefore logical that  $QE_1$  and  $QE_2$  be determined from a common reference point (BMU) in order for them to be mathematically comparable and hence accurately determine whether change has occurred in the object or not.

### 3.7.2 Method

In this section, the change detection process is restricted to change in  $x$  between images. This is done by ensuring that input vector  $x$  is associated to the same winner across the image dataset. To attain this, the winners determined during the training phase of SOM are maintained for each  $x$ . The index of  $x$  in the training data is used to extract it on testing image and its initial winner from the training data used to determine QE.

$$QE = x - \text{original BMU of } x \quad (3.6)$$

and thus equation 3.5 becomes:

$$QE_{object} = \{x_{t1} - BMU, x_{t2} - BMU, x_{t3} - BMU, \dots\} \quad (3.7)$$

where  $BMU$  is the original BMU of  $x$ .

### 3.7.3 Results

When SOM-QE is determined using the two methods – the traditional method and the new method suggested here - the results shown in Figure 3.38 are obtained.

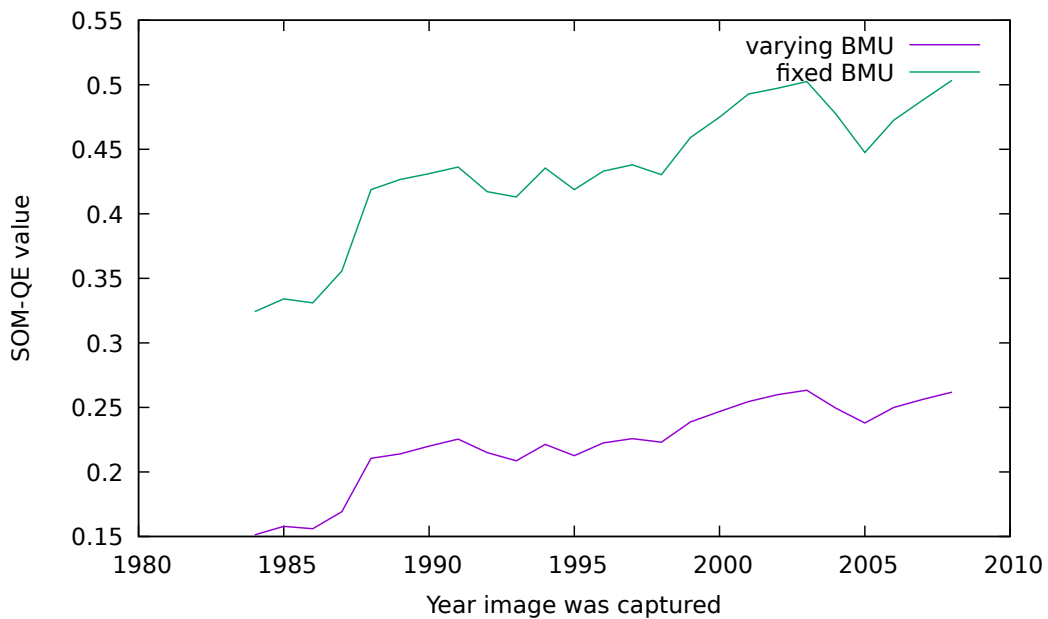


Figure 3.38: The two plots show the result of calculating SOM-QE values using the two methods. At the bottom (fixed BMU), is the result obtained by applying equation 9 where the BMU of the input vector at a particular image is used to find the QE. The plot on top (varying BMU), shows results obtained by the new method where the BMU obtained for every input vector at the end of SOM training is retained and used to determine QE for that particular vector throughout the time series, as in equation 3.6.

In both results, the trend in changing SOM-QE values is similar. But the larger SOM-QE values obtained when a fixed BMU value is applied make it more sensitive to change. The amount of change sensed by SOM-QE when a fixed BMU for an input vector is applied is bigger than when a varying BMU is used, see Figure 3.39.

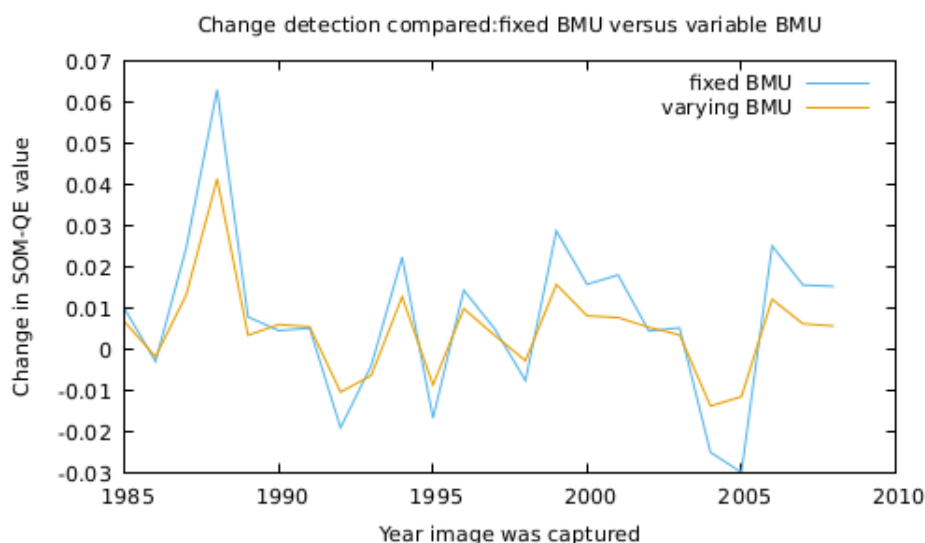


Figure 3.39: The changes that occurred in the ROI as reflected in images are shown here for the two methods of determination of SOM-QE. The fixed BMU method shows bigger change occurred between consecutive images in the series than the varying BMU method. To note change, consider the point's distance from 0 (no-change-point, on y-axis) on the two curves. For instance in year 2005, the change is 0.03 units for the new method and slightly above 0.01 units for the traditional method.



Thus, the new method provides a bigger scale of change measurement than the traditional method, and is found to be more sensitive to changes than the traditional method. This places it in a better position to detect changes, especially small changes, between images.

In this chapter, the hypothesis stated in chapter 2 is confirmed. Processing data within specialized units as is done in the human brain brings in advantages of spotting small, real changes and considerably avoids the unimportant changes. Besides, the product of SOM-QE from a time series of images is used to predict status of the ROI. It is confirmed that data generated by SOM-QE carries additional information, which can be put to some good use in change prediction. This adds and complements other prediction data available to planners, forecasting teams, among other related specialists.

In chapter 4, the results of this thesis are discussed, pin pointing how they relate to modern change application technique.

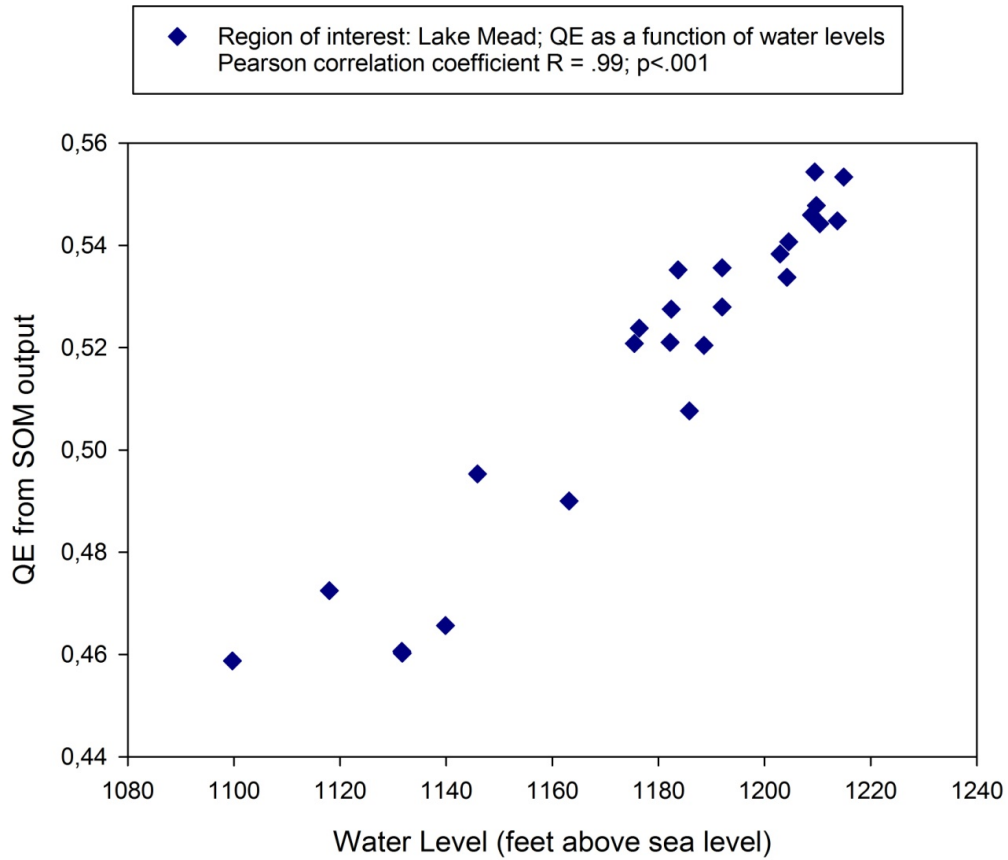


Figure 3.29: Variations in SOM-QE output plotted as a function of the water levels of Lake Mead during the reference time period. Pearson's correlation statistic computed on the paired distributions gives a statistically significant correlation with  $R = .99$ ,  $p < .001$ .

# Chapter 4

## Discussion of results

In previous chapters, the role of AI systems in processing objects through their images is discussed. In finding the differences between two images, SOM-QE is proposed and shown to detect small differences and give their location on the image within a short time. On benchmarking with other techniques, the method is found to outperform them.

Image-based change detection finds application in computer vision and robotics when identification of changed areas in a scene is required in order to fulfil some task. For example, it can improve the efficiency of 3D map maintenance by restricting updates to only the changed areas Taneja et al. [2011], Ulusoy and Mundy [2014] or allow a system to learn about the nature of objects in the environment by segmenting them as they change Finman et al. [2013].

Fast and accurate change detectors are therefore required, and in some instances are mandatory to have for some systems to deliver on their mandate. It is no longer viable to rely on manual expertise nor slow systems. Sakurada and Okatani [2015] reports that it took twenty minutes on average for an annotator to create the ground-truth map for an image pair. This demonstrates the necessity of a method for detecting scene changes automatically, accurately and fast enough. This is a role that SOM-QE can easily play, as seen when it takes 7.1 seconds to analyse the difference between a pair of satellite images and produce their change mask, section 3.4.

When, the image data is altered and the SOM parameters are not altered, changes in the QE can reasonably be attributed to the developments taking place in the scene whose image is under study. This is demonstrated using simple images, on which human can track the changes manually to confirm and evaluate SOM-QE results, in section 2.7. SOM-QE is therefore, proposed in this thesis as, for example, a clinical determinant of the progression or remission of lesions in medical images.

Further simulation of SOM-QE on real medical and satellite images confirmed that the SOM-QE values of a set of images was a function of change within the image. This was confirmed statistically through linear regression analysis and hence qualifies SOM-QE technique as a measure of variation within an image.

The hypothesis in this thesis consisted of four aspects, that; SOM-QE is a change detector, it detects small changes, it attains this relatively fast, and that it produces

data to predict status of an object. These are necessary features of a modern change detection mechanisms. The necessity sprouts from the fact that there is now lots of image data that requires to be analysed fast enough to save lives in the medical field and to attain efficient monitoring of the environment. The hypothesis was systematically proved throughout the simulations carried out in chapter three. In benchmarking with other techniques, it became clear that SOM-QE attains this hypothesis even when the changes occur in conditions where it is difficulty to tell between true and false changes.

In the SOM-QE approach, a series of 20 or more images are compared in less than three minutes, giving the changes at a glance for the whole time series dataset. There is, to my knowledge, no other method capable of providing such results.

The proof of the relative power of the SOM-QE to sense spatial extents of local image contrasts at constant intensity is given. It provides a statistically significant indicator of potentially important local changes in image contents across time which may reflect a critical evolution of man-induced and natural phenomena in these geographic regions of interest.

The sensitivity of SOM-QE was shown to be better than that of human observers. This qualifies it as a tool to accompany the radiologists in preliminary diagnosis of image data. It can give direction of change and minimize the need to rely on guess work.

SOM-QE is easy to implement too. It therefore provide instant decision about

change/no change within a series of images. It represents a promising, non-expensive technique for the automatic tracking and harvesting of landscape-change information from large bodies of image data on the basis of, in principle, ready-to-use simulations. Such information relative to critical changes in environmental conditions and natural or urban landscape structures can, as shown, be instantly correlated with other relevant demographic data which are of potential interest to citizens, historians, or policy-makers.

When changes in an object occur within difficulty-to-detect situation, as demonstrated in section 3.6.2, SOM-QE is able to detect more true changes with less nuisance changes than the other techniques reported in literature.

In section 3.5, it was shown that data generated by SOM-QE can be put to other good use – predicting the status of an image in terms of changed content, its magnitude and the direction of change.

## **Chapter 5**

### **Conclusions and Contribution**

When the first problem to be addressed is to decide whether there is a difference between two medical images, SOM-QE technique comes in handy. The difference may be clinically important, for instance, in relation to a lesion or a tumour that is likely to have changed with time, either in the direction of local increase (the patient's condition is getting worse) or in the direction of local decrease (the patient's condition is getting better). In this thesis, the problem of efficient disease diagnosis by means of structural change detection has been addressed. The solution has been shown to be cost-effective and can be adopted to assist radiologist to quickly determine presence of changes.

The detection and characterization of critical changes in objects, event scenes, or public spaces of the natural or the built environment may be of considerable

importance for swift decision making in fields such as medical, human and environmental safety, policy making for risk mitigation, or public awareness campaigns. In general terms, change detection consists of identifying differences in the state of an object or phenomenon by observing it at different times and implies being able to quantify change(s) due to the effect of time on that given object or phenomenon. The context of emergency places a premium on fast automatic techniques for discriminating between changed and unchanged contents in large image time series. SOM-QE has been shown to detect changed content, even when the change is small, and it accomplishes this within a short time.

On the basis of statistical regression analysis, it has been shown that SOM-QE output provides a statistically significant sensitivity to systematic variations in the spatial content of images. Just like the brain maps in animals, SOM-QE uses specialized units to detect changes in corresponding input data. This makes it an effective clustering tool that can be used as a detector of changes between images.

This thesis has addressed some of the advantages and limitations of approaches developed to detect change and has brought to the fore some of its major implications for both science and society.

In SOM-QE, a new image content variation measure has been developed to determine the status of images within a time series dataset. When the images are from the same object, this measure tracks down the changes that have taken place within the object with time.



This new method of change detection comes with features that makes it suite the needs of its users. In modern times, accurate results are demanded from the analysis of big data, requiring that computational techniques work fast to avoid delays. Such a technique has the potential to save lives, and enable swift decision making among administrators that leads to improving the living and working conditions of the humanity. An additional feature that makes SOM-QE stand out among its peers is the ability to detect changes even when they are small and/or obscured by nuisance noise. Besides, SOM-QE locates the area within the image that is affected by the detected changes. This comes in handy for radiologist and surgeons who are enabled to make the right decision early in a patient's treatment and care.

SOM-QE results on a time series of images provide a way of predicting the status of the object in future. This is done with 100% accuracy, providing a new and reliable method to generate prediction data. Such data finds use among weather forecasting team, city administrators and many others.

New aspects that make up the contribution to knowledge by this thesis are as follows:

1. Unsupervised machine learning architecture composed of SOM and QE determination is proposed. It outperforms human experts and other techniques suggested in literature on the task of change detection while remaining suitably lightweight and fast.
2. Change detection by SOM-QE is at pixel level of the image. This enables

changed areas within the ROI to be spotted and located even when they are very small.

3. Detector of change even among noised situations. Even when true changes within the object are accompanied by noise, SOM-QE performs better than other techniques in separating true changes from the nuisance changes.
4. New method to calculate QE for a set of time series images is proposed. When parameters established for each pixel location are kept constant and used for each image in a series, changes between images are larger, allowing more accurate determination of smaller changes.
5. The data generated by SOM-QE from a time series set of images of a scene carries useful information. This data can be used to predict changes in the scene. The future status of a scene can be determined from available images.

# Bibliography

Kilian M Pohl, Ender Konukoglu, Sebastian Novellas, Nicholas Ayache, Andriy Fedorov, Ion-Florin Talos, Alexandra Golby, William M Wells, Ron Kikinis, and Peter M Black. A New Metric for Detecting Change in Slowly Evolving Brain Tumors: Validation in Meningioma Patients:. *Operative Neurosurgery*, 68:ons225–ons233, March 2011a. ISSN 2332-4252. doi: 10.1227/NEU.0b013e31820783d5. URL <http://content.wkhealth.com/linkback/openurl?sid=WKPTLP:landingpage&an=01787389-201103001-00030>.

P. R. Oliveira and R. F. Romero. A comparison between PCA neural networks and the JPEG standard for performing image compression. In *Proceedings II Workshop on Cybernetic Vision*, pages 112–116, December 1996. doi: 10.1109/CYBVIS.1996.629449.

Nikhil R. Pal and Sankar K. Pal. A review on image segmentation techniques. *Pattern Recognition*, 26(9):1277–1294, 1993. ISSN 0031-3203. doi: 10.1016/0031-3203(93)90135-J.

- Michael Egmont-Petersen, Dick de Ridder, and Heinz Handels. Image processing with neural networks—a review. *Pattern recognition*, 35(10):2279–2301, 2002.
- A. Adler and R. Guardo. A neural network image reconstruction technique for electrical impedance tomography. *IEEE Transactions on Medical Imaging*, 13(4):594–600, December 1994. ISSN 02780062. doi: 10.1109/42.363109. URL <http://ieeexplore.ieee.org/document/363109/>.
- GH Griffiths. Monitoring urban change from Landsat TM and SPOT satellite imagery by image differencing. In *ESA, Proceedings of the 1988 International Geoscience and Remote Sensing Symposium(IGARSS 1988) on Remote Sensing: Moving Towards the 21 st Century*, volume 1, 1988.
- D. Jiang. A SOM algorithm based procedure for MRI image processing under significant Rician noise. In *2013 Australian Control Conference*, pages 14–19, November 2013. doi: 10.1109/AUCC.2013.6697241.
- Yuan Jiang and Zhi-Hua Zhou. SOM Ensemble-Based Image Segmentation. *Neural Processing Letters*, 20(3):171–178, November 2004. ISSN 1370-4621, 1573-773X. doi: 10.1007/s11063-004-2022-8. URL <http://link.springer.com/10.1007/s11063-004-2022-8>.
- Jieh-Haur Chen, Mu-Chun Su, Ruijun Cao, Shu-Chien Hsu, and Jin-Chun Lu. A self organizing map optimization based image recognition and processing model for bridge crack inspection. *Automation in Construction*, 73: 58–66, January 2017. ISSN 0926-5805. doi: 10.1016/j.autcon.2016.08.

033. URL <http://www.sciencedirect.com/science/article/pii/S092658051630187X>.

R. J. Radke, S. Andra, O. Al-Kofahi, and B. Roysam. Image change detection algorithms: a systematic survey. *IEEE Transactions on Image Processing*, 14(3):294–307, March 2005a. ISSN 1057-7149. doi: 10.1109/TIP.2004.838698.

Ken Sakurada and Takayuki Okatani. Change Detection from a Street Image Pair using CNN Features and Superpixel Segmentation. pages 61.1–61.12. British Machine Vision Association, 2015. ISBN 978-1-901725-53-7. doi: 10.5244/C.29.61. URL <http://www.bmva.org/bmvc/2015/papers/paper061/index.html>.

Elsa D. Angelini, Jamal Atif, Julie Delon, Emmanuel Mandonnet, Hugues Duffau, and Laurent Capelle. Detection of glioma evolution on longitudinal MRI studies. In *2007 4th IEEE International Symposium on Biomedical Imaging: From Nano to Macro*, pages 49–52. IEEE, 2007. URL [http://ieeexplore.ieee.org/xpls/abs\\_all.jsp?arnumber=4193219](http://ieeexplore.ieee.org/xpls/abs_all.jsp?arnumber=4193219).

Elsa D. Angelini, Julie Delon, Laurent Capelle, and Emmanuel Mandonnet. Contrast mapping and statistical testing for low-grade glioma growth quantification on brain mri. In *2010 IEEE International Symposium on Biomedical Imaging: From Nano to Macro*, pages 872–875. IEEE, 2010. URL [http://ieeexplore.ieee.org/xpls/abs\\_all.jsp?arnumber=5490125](http://ieeexplore.ieee.org/xpls/abs_all.jsp?arnumber=5490125).

Ender Konukoglu, William M. Wells, Sébastien Novellas, Nicholas Ayache, Ron Kikinis, Peter M. Black, and Kilian M. Pohl. Monitoring slowly evolving tumors. In *2008 5th IEEE International Symposium on Biomedical Imaging: From Nano to Macro*, pages 812–815. IEEE, 2008. URL [http://ieeexplore.ieee.org/xpls/abs\\_all.jsp?arnumber=4541120](http://ieeexplore.ieee.org/xpls/abs_all.jsp?arnumber=4541120).

Daniel Crispell, Joseph Mundy, and Gabriel Taubin. A Variable-Resolution Probabilistic Three-Dimensional Model for Change Detection. *IEEE Transactions on Geoscience and Remote Sensing*, 50(2):489–500, February 2012. ISSN 0196-2892, 1558-0644. doi: 10.1109/TGRS.2011.2158439. URL <http://ieeexplore.ieee.org/document/5958599/>.

A. Huertas and R. Nevatia. Detecting changes in aerial views of man-made structures. In *Sixth International Conference on Computer Vision (IEEE Cat. No.98CH36271)*, pages 73–80, Jan 1998. doi: 10.1109/ICCV.1998.710703.

Ibrahim Eden and David B. Cooper. Using 3d Line Segments for Robust and Efficient Change Detection from Multiple Noisy Images. In *ECCV*, 2008.

Aparna Taneja, Luca Ballan, and Marc Pollefeys. Image based detection of geometric changes in urban environments. pages 2336–2343. IEEE, November 2011. ISBN 978-1-4577-1102-2 978-1-4577-1101-5 978-1-4577-1100-8. doi: 10.1109/ICCV.2011.6126515. URL <http://ieeexplore.ieee.org/document/6126515/>.

Grant Schindler and Frank Dellaert. Probabilistic temporal inference on reconstructed 3d scenes. pages 1410–1417. IEEE, June 2010. ISBN 978-1-4244-6984-0. doi: 10.1109/CVPR.2010.5539803. URL <http://ieeexplore.ieee.org/document/5539803/>.

Kevin Matzen and Noah Snavely. Scene Chronology. In *Proc. European Conf. on Computer Vision*, 2014.

Aparna Taneja, Luca Ballan, and Marc Pollefeys. City-Scale Change Detection in Cadastral 3d Models Using Images. pages 113–120. IEEE, June 2013. ISBN 978-0-7695-4989-7. doi: 10.1109/CVPR.2013.22. URL <http://ieeexplore.ieee.org/document/6618866/>.

Ken Sakurada, Takayuki Okatani, and Koichiro Deguchi. Detecting Changes in 3d Structure of a Scene from Multi-view Images Captured by a Vehicle-Mounted Camera. pages 137–144. IEEE, June 2013. ISBN 978-0-7695-4989-7. doi: 10.1109/CVPR.2013.25. URL <http://ieeexplore.ieee.org/document/6618869/>.

Simon Stent. Detecting Change for Multi-View, Long-Term Surface Inspection. page 12, 2015.

T Kohonen. Automatic formation of topological maps of patterns in a self-organizing system. In *2nd Scand. Conf. on Image Analysis*, pages 214–220, Espoo, Finland, 1981a.

Kurt Skifstad and Ramesh Jain. Illumination Independent Change Detection for Real World Image Sequences. *Computer Vision, Graphics, and Image processing*, 46:387–399, 1989. URL <https://deepblue.lib.umich.edu/bitstream/handle/2027.42/27921/0000345.pdf%3Bjsessionid%3DDF98484E3E199A844479FEA34529E466?sequence%3D1>.

Murugeswari Palanivel and Manimegalai Duraisamy. Color Textured Image Segmentation Using ICICM - Interval Type-2 Fuzzy C-Means Clustering Hybrid Approach. *Engineering Journal*, 16(5):115–126, October 2012. ISSN 01258281. doi: 10.4186/ej.2012.16.5.115. URL <http://www.engj.org/index.php/ej/article/view/252/199>.

Ashbindu Singh. Review Article Digital change detection techniques using remotely-sensed data. *International Journal of Remote Sensing*, 10(6):989–1003, June 1989. ISSN 0143-1161, 1366-5901. doi: 10.1080/01431168908903939. URL <http://www.tandfonline.com/doi/abs/10.1080/01431168908903939>.

Ibrahim Rizk Hegazy and Mosbeh Rashed Kaloop. Monitoring urban growth and land use change detection with GIS and remote sensing techniques in Daqahlia governorate Egypt. *International Journal of Sustainable Built Environment*, 4(1):117–124, June 2015. ISSN 2212-6090. doi: 10.1016/j.ijsbe.2015.02.005. URL <http://www.sciencedirect.com/science/article/pii/S2212609015000060>.



Narayan Kayet and Khanindra Pathak. Remote sensing and GIS based land use/land cover change detection mapping in Saranda Forest, Jharkhand, India. *Int Res J Earth Sci*, 3(10):1–6, 2015. URL [https://www.researchgate.net/profile/Narayan\\_Kayet3/publication/298424808\\_Remote\\_Sensing\\_and\\_GIS\\_Based\\_Land\\_useLand\\_cover\\_Change\\_Detection\\_Mapping\\_in\\_Saranda\\_Forest\\_Jharkhand\\_India/links/56e9668408ae77f87278fc05.pdf](https://www.researchgate.net/profile/Narayan_Kayet3/publication/298424808_Remote_Sensing_and_GIS_Based_Land_useLand_cover_Change_Detection_Mapping_in_Saranda_Forest_Jharkhand_India/links/56e9668408ae77f87278fc05.pdf).

Shlomo Angel, Alejandro M Blei, Jason Parent, and et al. *{Atlas} of {Urban}{Expansion}{}}{}*. 2016. ISBN 978-0-9981758-0-5 (PDF). URL <http://www.lincolninst.edu/sites/default/files/pubfiles/atlas-of-urban-expansion-2016-volume-1-full.pdf>.

Richard Guthmann, Nancy Davis, Matthew Brown, and Jose Elizondo. Visit Frequency and Hypertension. *The Journal of Clinical Hypertension*, 7(6):327–332, June 2005. ISSN 1524-6175, 1751-7176. doi: 10.1111/j.1524-6175.2005.04371.x. URL <http://doi.wiley.com/10.1111/j.1524-6175.2005.04371.x>.

Gordon Schectman, Gary Barnas, Prakash Laud, Laura Cantwell, Monica Horton, and Edwin J. Zarling. Prolonging the return visit interval in primary care. *The American journal of medicine*, 118(4):393–399, April 2005. ISSN 0002-9343 0002-9343. doi: 10.1016/j.amjmed.2005.01.003.

Lisa M Schwartz, Steven Woloshin, John H Wasson, Roger A Renfrew, and

- H Gilbert Welch. Setting the Revisit Interval in Primary Care. *Journal of General Internal Medicine*, 14(4):230–235, April 1999. ISSN 0884-8734. doi: 10.1046/j.1525-1497.1999.00322.x. URL <http://www.ncbi.nlm.nih.gov/pmc/articles/PMC1496560/>.
- Teuvo Kohonen. Essentials of the self-organizing map. *Neural Networks*, 37:52–65, January 2013. ISSN 08936080. doi: 10.1016/j.neunet.2012.09.018. URL <http://linkinghub.elsevier.com/retrieve/pii/S0893608012002596>.
- Vernon B. Mountcastle. MODALITY AND TOPOGRAPHIC PROPERTIES OF SINGLE NEURONS OF CAT'S SOMATIC SENSORY CORTEX. *Journal of Neurophysiology*, 20(4):408–434, July 1957. ISSN 0022-3077. doi: 10.1152/jn.1957.20.4.408. URL <https://doi.org/10.1152/jn.1957.20.4.408>.
- D H Hubel and T N Wiesel. Receptive fields, binocular interaction and functional architecture in the cat's visual cortex. *The Journal of Physiology*, 160(1):106–154.2, January 1962. ISSN 0022-3751. URL <http://www.ncbi.nlm.nih.gov/pmc/articles/PMC1359523/>.
- M. M. Merzenich, J. H. Kaas, J. Wall, R. J. Nelson, M. Sur, and D. Felleman. Topographic reorganization of somatosensory cortical areas 3b and 1 in adult monkeys following restricted deafferentation. *Neuroscience*, 8(1):33–55, January 1983. ISSN 0306-4522 0306-4522.

- S. Grossberg. On the development of feature detectors in the visual cortex with applications to learning and reaction-diffusion systems. *Biological cybernetics*, 21(3):145–159, January 1976. ISSN 0340-1200 0340-1200.
- M. M. Nass and L. N. Cooper. A theory for the development of feature detecting cells in visual cortex. *Biological cybernetics*, 19(1):1–18, August 1975. ISSN 0340-1200 0340-1200.
- Rafael Perez, Leon Glass, and Robert Shlaer. Development of Specificity in the Cat Visual Cortex. *Journal of mathematical biology*, 13:275–288, 1975.
- N. Suga and W. E. O’Neill. Neural axis representing target range in the auditory cortex of the mustache bat. *Science (New York, N.Y.)*, 206(4416):351–353, October 1979. ISSN 0036-8075 0036-8075.
- A. R. TUNTURI. Physiological determination of the arrangement of the afferent connections to the middle ectosylvian auditory area in the dog. *The American journal of physiology*, 162(3):489–502, September 1950. ISSN 0002-9513 0002-9513. doi: 10.1152/ajplegacy.1950.162.3.489.
- Archie R. Tunturi. A Difference in the Representation of Auditory Signals for the Left and Right Ears in the Iso-Frequency Contours of the Right Middle Ectosylvian Auditory Cortex of the Dog. *American Journal of Physiology-Legacy Content*, 168(3):712–727, February 1952. ISSN 0002-9513. doi: 10.1152/ajplegacy.1952.168.3.712. URL <https://doi.org/10.1152/ajplegacy.1952.168.3.712>.

- S. Zeki. The representation of colours in the cerebral cortex. *Nature*, 284:412, April 1980. URL <http://dx.doi.org/10.1038/284412a0>.
- STUART P LLOYD. Least Squares Quantization in PCM. *IEEE TRANSACTIONS ON INFORMATION THEORY*, . IT-28(2):9, March 1982. URL <http://www-evasion.imag.fr/people/Franck.Hetroy/Teaching/ProjetsImage/2007/Bib/lloyd-1982.pdf>.
- Forgy, E.W. Cluster Analysis of Multivariate Data: Efficiency vs Interpretability of Classifications. *Biometrics*, (21):768–780, 1965.
- Teuvo Kohonen. Self-organized formation of topologically correct feature maps. *Biological cybernetics*, 43(1):59–69, 1982. URL <http://link.springer.com/article/10.1007/BF00337288>.
- T. Kohonen. *Self-Organizing Maps*. Springer Series in Information Sciences 30. Springer Berlin Heidelberg, 3 edition, 1995. ISBN 978-3-642-97612-4 978-3-642-97610-0. URL <https://www.springer.com/la/book/9783642976100>.
- Vahid Moosavi. Computing With Contextual Numbers. *arXiv.org e-Print archive*, 2014. URL <http://arxiv.org/abs/1408.0889>.
- Afra Zomorodian. Topological data analysis, 2011.
- J. B. Kruskal. Multidimensional scaling by optimizing goodness of fit to a non-metric hypothesis. *Psychometrika*, 29(1):1–27, March 1964. ISSN 0033-3123,

1860-0980. doi: 10.1007/BF02289565. URL <http://link.springer.com/10.1007/BF02289565>.

Sam T. Roweis and Lawrence K. Saul. Nonlinear Dimensionality Reduction by Locally Linear Embedding. *Science*, 290(5500):2323, December 2000. doi: 10.1126/science.290.5500.2323. URL <http://science.sciencemag.org/content/290/5500/2323.abstract>.

J. B. Tenenbaum. A Global Geometric Framework for Nonlinear Dimensionality Reduction. *Science*, 290(5500):2319–2323, December 2000. ISSN 00368075, 10959203. doi: 10.1126/science.290.5500.2319. URL <http://www.sciencemag.org/cgi/doi/10.1126/science.290.5500.2319>.

Gurjeet Singh, Facundo Mémoli, and Gunnar Carlsson. Topological Methods for the Analysis of High Dimensional Data Sets and 3d Object Recognition. *Eurographics Symposium on Point-Based Graphic*, page 11, 2007.

H K Hartline, Henry G Wagner, and Floyd Ratliff. INHIBITION IN THE EYE OF LIMULUS. *The Journal of General Physiology*, 39(5):651–673, May 1956. ISSN 0022-1295. URL <http://www.ncbi.nlm.nih.gov/pmc/articles/PMC2147566/>.

Teuvo Kohonen. Automatic Formation of Topological Maps of Patterns in a Self-Organizing System. 1981b. URL <http://www.citeulike.org/group/1480/article/793951>.

Mat Buckland. Kohonen's Self Organizing Feature Maps. 2005. URL <http://www.ai-junkie.com/ann/som/som1.html>.

Teuvo Kohonen. *MATLAB Implementations and Applications of the Self-Organizing Map*. Unigrafia Bookstore Helsinki, 2014a. ISBN 978-952-60-3678-6. URL [http://docs.unigrafia.fi/publications/kohonen%7B\\_%7Dteuvo/](http://docs.unigrafia.fi/publications/kohonen%7B_%7Dteuvo/).

R. Martin and K. Obermayer. Self-Organizing Maps A2 - Squire, Larry R. In *Encyclopedia of Neuroscience*, pages 551–560. Academic Press, Oxford, 2009. ISBN 978-0-08-045046-9. doi: 10.1016/B978-008045046-9.01431-5. URL <https://www.sciencedirect.com/science/article/pii/B9780080450469014315>.

Teuvo Kohonen. The Self-Organizing Map, a Possible Model of Brain Maps. page 4, 1996.

R. Gray. Vector quantization. *IEEE ASSP Magazine*, 1(2):4–29, April 1984. doi: 10.1109/MASSP.1984.1162229. URL <http://ieeexplore.ieee.org/articleDetails.jsp?arnumber=1162229>.

Georg Pözlbauer. Survey and Comparison of Quality Measures for Self-Organizing Maps. *Proceedings of the Fifth Workshop on Data Analysis WDA'04*, pages 67–82, 2004. ISSN 80-89066-87-9.

R.J. Radke, S. Andra, O. Al-Kofahi, and B. Roysam. Image change detection algorithms: a systematic survey. *IEEE Transactions on Image Processing*, 14

(3):294–307, March 2005b. ISSN 1057-7149. doi: 10.1109/TIP.2004.838698.  
URL <http://ieeexplore.ieee.org/document/1395984/>.

Yi Wang, Pierre-Marc Jodoin, Fatih Porikli, Janusz Konrad, Yannick Benezeth, and Prakash Ishwar. CDnet 2014: an expanded change detection benchmark dataset. In *Proceedings of the IEEE Conference on Computer Vision and Pattern Recognition Workshops*, pages 387–394, 2014.

David Rey, Gérard Subsol, Hervé Delingette, and Nicholas Ayache. Automatic detection and segmentation of evolving processes in 3d medical images: Application to multiple sclerosis. *Medical Image Analysis*, 6(2):163 – 179, 2002a. ISSN 1361-8415. doi: [https://doi.org/10.1016/S1361-8415\(02\)00056-7](https://doi.org/10.1016/S1361-8415(02)00056-7). URL <http://www.sciencedirect.com/science/article/pii/S1361841502000567>.

John Mwangi Wandeto, Henry Nyongesa, Yves Rémond, and Birgitta Dresplangley. Detection of small changes in medical and random-dot images comparing self-organizing map performance to human detection. *Informat-ics in Medicine Unlocked*, 7:39–45, 2017. ISSN 23529148. doi: 10.1016/j.imu.2017.03.001. URL <http://linkinghub.elsevier.com/retrieve/pii/S2352914817300059>.

Kilian M. Pohl, Ender Konukoglu, Sebastian Novellas, Nicholas Ayache, Andriy Fedorov, Ion-Florin Talos, Alexandra Golby, William M. Wells, Ron Kikinis, and Peter M. Black. A New Metric for Detecting Change in Slowly

Evolving Brain Tumors: Validation in Meningioma Patients. *Neurosurgery*, 68(1 Suppl OPERATIVE):225–233, March 2011b. ISSN 0148-396X. doi: 10.1227/NEU.0b013e31820783d5. URL <http://www.ncbi.nlm.nih.gov/pmc/articles/PMC3099129/>.

Swets John A. David M. Green. *Signal detection theory and psychophysics*. John Wiley & Sons, Inc., New York, 1966.

Birgitta Dresch, Séverine Durand, and Stephen Grossberg. Depth perception from pairs of overlapping cues in pictorial displays. *Spatial Vision*, 15(3):255–276, 2002. ISSN 0169-1015. doi: 10.1163/15685680260174038. URL <http://booksandjournals.brillonline.com/content/journals/10.1163/15685680260174038>.

David Rey, Gérard Subsol, Hervé Delingette, and Nicholas Ayache. Automatic detection and segmentation of evolving processes in 3d medical images: Application to multiple sclerosis. *Medical image analysis*, 6(2):163–179, 2002b. URL <http://www.sciencedirect.com/science/article/pii/S1361841502000567>.

van Riel, S.J., Sánchez C.I., Bankier A.A., Naidich D.P., and 10 others. Observer Variability for Classification of Pulmonary Nodules on Low-Dose CT Images and Its Effect on Nodule Management. *Radiology*, 277(3):863–871, December 2015. doi: 10.1148/radiol.2015142700. URL <https://www.ncbi.nlm.nih.gov/pubmed/26020438>.



Julia Patriarche and Bradley Erickson. Part 2. Automated Change Detection and Characterization Applied to Serial MR of Brain Tumors may Detect Progression Earlier than Human Experts. *Journal of Digital Imaging*, 20(4): 321–328, December 2007. ISSN 0897-1889, 1618-727X. doi: 10.1007/s10278-006-1039-0. URL <http://link.springer.com/10.1007/s10278-006-1039-0>.

Teuvo Kohonen. *MATLAB Implementations and Applications of the Self-Organizing Map*. 2014b. ISBN 978-952-60-3678-6. URL [http://docs.unigrafia.fi/publications/kohonen\\_teuvo/](http://docs.unigrafia.fi/publications/kohonen_teuvo/).

Sezgin Kaçar and Ünal Sakoğlu. Design of a Novel Biomedical Signal Processing and Analysis Tool for Functional Neuroimaging. *Comput. Methods Prog. Biomed.*, 125(C):46–57, March 2016. ISSN 0169-2607. doi: 10.1016/j.cmpb.2015.11.011. URL <http://dx.doi.org/10.1016/j.cmpb.2015.11.011>.

Aimee Mavratzakis, Cornelia Herbert, and Peter Walla. Emotional facial expressions evoke faster orienting responses, but weaker emotional responses at neural and behavioural levels compared to scenes: A simultaneous EEG and facial EMG study. *NeuroImage*, 124(Pt A):931–946, January 2016. ISSN 1095-9572 1053-8119. doi: 10.1016/j.neuroimage.2015.09.065.

Paul L Rosin and Efstathios Ioannidis. Evaluation of global image thresholding for change detection. *Pattern Recognition Letters*, 24(14):2345–2356, October 2003. ISSN 01678655. doi: 10.1016/S0167-8655(03)

00060-6. URL <http://linkinghub.elsevier.com/retrieve/pii/S0167865503000606>.

NOBUYUKI OTSU. A Threshold Selection Method from Gray-Level Histograms. *EEE TRANSACTIONS ON SYSTEMS, MAN, AND CYBERNETICS*, VOL SMC-9(NO. 1):5, January 1979.

J. N. Kapur, P. K. Sahoo, and A. K. C. Wong. A new method for gray-level picture thresholding using the entropy of the histogram. *Computer Vision, Graphics, and Image Processing*, 29(3):273 – 285, 1985. ISSN 0734-189X. doi: [https://doi.org/10.1016/0734-189X\(85\)90125-2](https://doi.org/10.1016/0734-189X(85)90125-2). URL <http://www.sciencedirect.com/science/article/pii/S0734189X85901252>.

Jay L Devore. *Probability and statistics for engineering and the sciences*. Belmont, Calif. : Thomson-Brooks/Cole, 6th ed edition, 2004. ISBN 0-534-39933-9.

P. Thévenaz, U.E. Ruttimann, and M. Unser. A Pyramid Approach to Sub-pixel Registration Based on Intensity. *IEEE Transactions on Image Processing*, 7(1):27–41, January 1998. URL <http://bigwww.epfl.ch/publications/thevenaz9801.html>.

Marit Jentoft-Nilsen, Matthew Radcliff, James Irons, and Aries Keck. Las Vegas, 1972-2013 Released on March 5, 2012, NASA/Goddard Space Flight Center Landsat images obtained from USGS Earth Explorer. The Landsat Program is

a series of Earth-observing satellite missions jointly managed by NASA and the U.S. Geological Survey. Technical Report ID: 10721, March 2012. URL <http://svs.gsfc.nasa.gov/10721>.

Kenji Suzuki. Pixel-Based Machine Learning in Medical Imaging. *International Journal of Biomedical Imaging*, 2012:1–18, 2012. ISSN 1687-4188, 1687-4196. doi: 10.1155/2012/792079. URL <http://www.hindawi.com/journals/ijbi/2012/792079/>.

Avery M Guest and George H Nelson. Central City/Suburban Status Differences: Fifty Years of Change. *The Sociology Quarterly*, 19:7–23, 1978.

Luke J Juday. The Changing Shape of American Cities. *Demographics Research Group, University of Virginia*, page 20, February 2015.

K.W. Thoning, D.R. Kitzis, and A. Crotwell. NOAA ESRL Global Monitoring Division. 2016, updated annually. Atmospheric Carbon Dioxide Dry Air Mole Fractions from quasi-continuous measurements at Mauna Loa, Hawaii. 2017. doi: <http://dx.doi.org/10.7289/V54X55RG>. URL [ftp://aftp.cmdl.noaa.gov/data/trace\\_gases/co2/in-situ/surface/mlo/co2\\_mlo\\_surface-insitu\\_1\\_ccgg\\_DailyData.txt](ftp://aftp.cmdl.noaa.gov/data/trace_gases/co2/in-situ/surface/mlo/co2_mlo_surface-insitu_1_ccgg_DailyData.txt).

Ali Osman Ulusoy and Joseph L Mundy. Image-based 4-d Reconstruction Using 3-d Change Detection. In *Computer Vision – ECCV 2014*, Lecture Notes in Computer Science, pages 31–45. Springer International Publishing, September 2014.

R. Finman, T. Whelan, M. Kaess, and J. J. Leonard. Toward lifelong object segmentation from change detection in dense RGB-D maps. In *2013 European Conference on Mobile Robots*, pages 178–185, September 2013. doi: 10.1109/ECMR.2013.6698839.

# Appendix A

## List of publications the thesis has produced

### 1. Articles:

Wandeto, JM, Nyongesa, HKO, Remond, Y, Dresp-Langley, B (2017), Detection of small changes in medical and random-dot images comparing self-organizing map performance to human detection. *Informatics in Medecine Unlocked*, 7, 39-45. Retrieved from URL: <https://www.sciencedirect.com/science/article/pii/S2352914817300059> on 11<sup>th</sup> June 2018.

### 2. Book chapters:

Dresp-Langley, B; Wandeto, JM; Nyongesa, HKO (2018). Using the quan-

tization error from Self-Organizing Map *SOM* output for fast detection of critical variations in image time series. ISTE OpenScience, Volume "From data to decisions"- "Des données aux décisions". Wiley and Sons, London,. Retrieved from URL: <https://www.openscience.fr/Using-the-quantization-error-from-Self-Organizing-Map-SOM-output-> on 11<sup>th</sup> June 2018.

### 3. Conference abstracts

- (a) Wandeto, JM, Nyongesa HKO, Dresp-Langley, B (2016). A biologically inspired technique to track a patient's condition through extraction of information from images, 2nd DEKUT International Conference on Science, Technology, Innovation and Entrepreneurship, Nyeri, Kenya, November 2016.
- (b) Wandeto, J. M., Nyongesa, H.K.O., Dresp-Langley, B. (2017, August). Detection of smallest changes in complex images comparing self-organizing map and expert performance. Poster presented at the European Conference on Visual Perception 2017, Berlin, Germany. Page 166. Retrieved from URL: <http://journals.sagepub.com/page/pec/collections/ecvp-abstracts/index/ecvp-2017> on 11<sup>th</sup> June 2018.

### 4. Open Archive Library ArXiv

- (a) rXiv:1710.10648 [pdf]

Using the quantization error from Self-Organized Map (SOM) output for detecting critical variability in large bodies of image time series in less than a minute, Birgitta Dresp-Langley, John Mwangi Wandeto. Subjects: Computers and Society (cs.CY); Computer Vision and Pattern Recognition (cs.CV). retrieved from URL: <https://arxiv.org/abs/1710.10648> on 11<sup>th</sup> June 2018.

(b) arXiv:1709.02292 [pdf]

On the detectability by novices, radiologists, and computer algorithms of smallest increases in local single dot size in random-dot images, Birgitta Dresp-Langley, John Wandeto. Subjects: Computers and Society (cs.CY). Retrieved from URL: <https://arxiv.org/abs/1709.02292> on 11<sup>th</sup> June 2018.

(c) arXiv:1803.11125 [pdf]

Detection of Structural Change in Geographic Regions of Interest by Self Organized Mapping: Las Vegas City and Lake Mead across the Years, John M. Wandeto, Henry O. Nyongesa, Birgitta Dresp-Langley. Subjects: Computers and Society (cs.CY); Computer Vision and Pattern Recognition (cs.CV). Retrieved from URL: <https://arxiv.org/abs/1803.11125> on 11<sup>th</sup> June 2018.

## Appendix B

### Sample code: The Python code used in section 2.7

```
from math import sqrt
from numpy import (array, unravel_index, nditer, linalg,
random, subtract, power, exp, pi, zeros, arange, outer,
meshgrid, dot)
from collections import defaultdict
from warnings import warn

def fast_norm(x):
    """Returns norm-2 of a 1-D numpy array.
```



```
* faster than linalg.norm in case of 1-D arrays (numpy  
1.9.2rc1).
```

```
"""
```

```
return sqrt(dot(x, x.T))
```

```
class MiniSom(object):
```

```
def __init__(self, x, y, input_len, sigma=1.0,
```

```
learning_rate=0.5, decay_function=None, random_seed=3000):
```

```
    """
```

```
Initializes a Self Organizing Maps.
```

```
x,y – dimensions of the SOM
```

```
input_len – number of the elements of the  
vectors in input
```

```
sigma – spread of the neighborhood function  
(Gaussian), needs to be adequate to the  
dimensions of the map.
```

```
(at the iteration t we have  $\sigma(t) = \sigma$   
/ (1 + t/T) where T is #num_iteration/2)
```

```
learning_rate – initial learning rate
```

```
(at the iteration t we have  $\text{learning\_rate}(t) =$   
learning_rate / (1 + t/T) where T is  
#num_iteration/2)
```

```
decay_function, function that reduces
```

```

        learning_rate and sigma at each iteration
        default function: lambda
        x, current_iteration, max_iter:
        x/(1+ current_iteration/max_iter) random_seed,
        random seed to use.
    """
    if sigma >= x/2.0 or sigma >= y/2.0:
        warn('Warning: sigma is too high for the dimension of the
    if random_seed:
        self.random_generator = random.RandomState
        (random_seed)
    else:
        self.random_generator = random.RandomState
        (random_seed)
    if decay_function:
        self._decay_function = decay_function
    else:
        self._decay_function = lambda x, t, max_iter:
            x/(1+t/max_iter)
    self.learning_rate = learning_rate
    self.sigma = sigma
    self.weights = self.random_generator.rand
    (x,y,input_len)*2-1 # random initialization

```

```

for i in range(x):
    for j in range(y):
        self.weights[i,j] = self.weights[i,j] /
            fast_norm(self.weights[i,j])
            # normalization

self.activation_map = zeros((x,y))
self.neigx = arange(x)
self.neigy = arange(y)
# used to evaluate the neighborhood function
self.neighborhood = self.gaussian

def _activate(self, x):
    """ Updates matrix activation_map, in this
matrix the element i,j is the response of the
neuron i,j to x """
    s = subtract(x, self.weights) #  $x - w$ 
    it = nditer(self.activation_map, flags=
['multi_index'])
    while not it.finished:
        self.activation_map[it.multi_index] =
            fast_norm(s[it.multi_index]) #  $\|x - w\|$ 
        it.iternext()

```

```

def activate(self, x):
    """ Returns the activation map to x """
    self._activate(x)
    return self.activation_map

def gaussian(self, c, sigma):
    """ Returns a Gaussian centered in c """
    d = 2*pi*sigma*sigma
    ax = exp(-power(self.neigx-c[0], 2)/d)
    ay = exp(-power(self.neigy-c[1], 2)/d)
    return outer(ax, ay) # the external
    product gives a matrix

def winner(self, x):
    """ Computes the coordinates of the winning neuron
    for the sample x """
    self._activate(x)
    return unravel_index(self.activation_map.argmax(),
    self.activation_map.shape)

def update(self, x, win, t):
    """
        Updates the weights of the neurons.

```

```

        x – current pattern to learn
        win – position of the winning neuron for x (array
        or tuple).
        t – iteration index
    """
    eta = self._decay_function(self.learning_rate , t ,
        self.T)
    sig = self._decay_function(self.sigma , t , self.T) #
    sigma and learning rate decrease with the same rule
    g = self.neighborhood(win , sig)*eta # improves the
    performances
    it = nditer(g, flags=['multi_index'])
    while not it.finished:
        # eta * neighborhood_function * (x-w)
        self.weights[it.multi_index] += g[it.multi_index]*
        (x-self.weights[it.multi_index])
        # normalization
        self.weights[it.multi_index] = self.weights
        [it.multi_index] / fast_norm(self.weights
        [it.multi_index])
        it.iternext()

def random_weights_init(self , data):

```

```

""" Initializes the weights of the SOM picking random
samples from data """
it = nditer(self.activation_map , flags=
['multi_index'])
while not it.finished:
    self.weights[it.multi_index] = data
    [self.random_generator.randint(len(data))]
    self.weights[it.multi_index] = self.weights
    [it.multi_index]/fast_norm(self.weights
    [it.multi_index])
    it.iternext()

def train_random(self , data , num_iteration):
    """ Trains the SOM picking samples at random from
    data """
    self._init_T(num_iteration)
    for iteration in range(num_iteration):
        rand_i = self.random_generator.randint(len(data))
        # pick a random sample
        self.update(data[rand_i] , self.winner(data
        [rand_i]) , iteration)

def train_batch(self , data , num_iteration):

```

```

""" Trains using all the vectors in data sequentially
"""

self._init_T(len(data)*num_iteration)

iteration = 0

while iteration < num_iteration:

    idx = iteration % (len(data)-1)

    self.update(data[idx], self.winner(data[idx]),
                iteration)

    iteration += 1

def _init_T(self, num_iteration):

    """ Initializes the parameter T needed to adjust the
    learning rate """

    self.T = num_iteration/2

def quantization_error_compare(self, data):

    """

    Returns the quantization error computed as the
    average distance between

    each input sample and its best matching unit.

    """

    error = 0

    err_ind = []

```

```

    pix = []
    for x in data:
        err = fast_norm(x-self.weights[self.winner(x)])
        err_ind.append(err)
        pix.append(x)

    return err_ind, pix

from pylab import
imread, imshow, show, subplots, NullFormatter, NullLocator
from numpy import reshape, unravel_index
import time

start_time = time.time()

# read the train image
img = imread('train.png')

# ... and reshaping the pixels matrix

pixels = reshape(img, (img.shape[0]*img.shape[1], 3))

# SOM initialization and training

```



```

print ('training ... ')
som = MiniSom(4,4,3,sigma=1.2,learning_rate=0.02)
som.random_weights_init(pixels)
som.train_batch(pixels,10000)

print '... done'

print 'Begin change detection ... '
print '.... collect QE details of first image'
im1 = imread('first.png')
pixI = reshape(im1,(im1.shape[0]*im1.shape[1],3))
qe1,pix1 = som.quantization_error_compare(pixI)

print '.... for the second image'
im2 = imread('second.png')
pixII = reshape(im2,(im2.shape[0]*im2.shape[1],3))
qe2,pix2 = som.quantization_error_compare(pixII)

print

print 'Compare the two QE for similar QE in the two images'
qe_equal = []

```

```

for ti in range(0, img.shape[0]):
    if qe1[ti] == qe2[ti]:
        qe_equal.append(qe1)
        pix1[ti] = [0,0,0]
    else: pix1[ti] = [1,1,1]

print 'Unchanged pixels are: ', len(qe_equal)
print 'out of: ', im1.shape[0]*im1.shape[1]

print('building the change mask image...')
im1_label = zeros(im1.shape)
for i,q in enumerate(pix1): # place the new pixels values
into a new image
    im1_label[unravel_index(i, dims=(im1.shape[0], im1.shape[1]))]
    = q

print('done.')

print 'Prepare the figures...'
# show the result

f, (ax1, ax2, ax3) = subplots(1,3, sharey=True)

```

```

ax1.yaxis.set_major_locator(NullLocator())
ax1.xaxis.set_major_formatter(NullFormatter())
ax1.imshow(im1)
ax1.set_title('Uniform_image')

ax2.yaxis.set_major_locator(NullLocator())
ax2.xaxis.set_major_formatter(NullFormatter())
ax2.imshow(im2)
ax2.set_title('Non-uniform_image')

ax3.yaxis.set_major_locator(NullLocator())
ax3.xaxis.set_major_formatter(NullFormatter())
ax3.imshow(im1_label)
ax3.set_title('Change_mask')

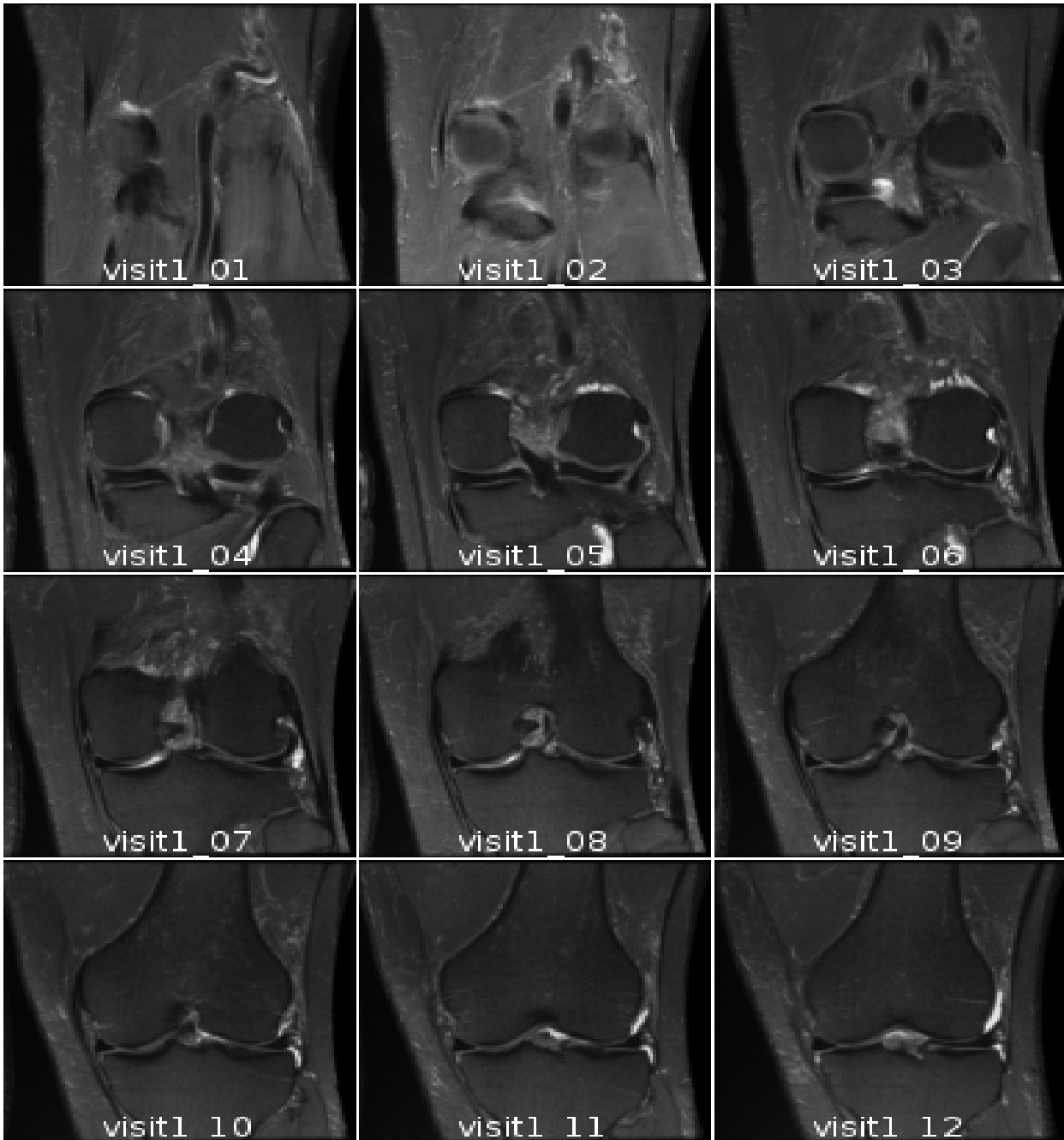
print "The_end."
print ("——_%s_seconds_——" % round(time.time() - start_time ,
2))

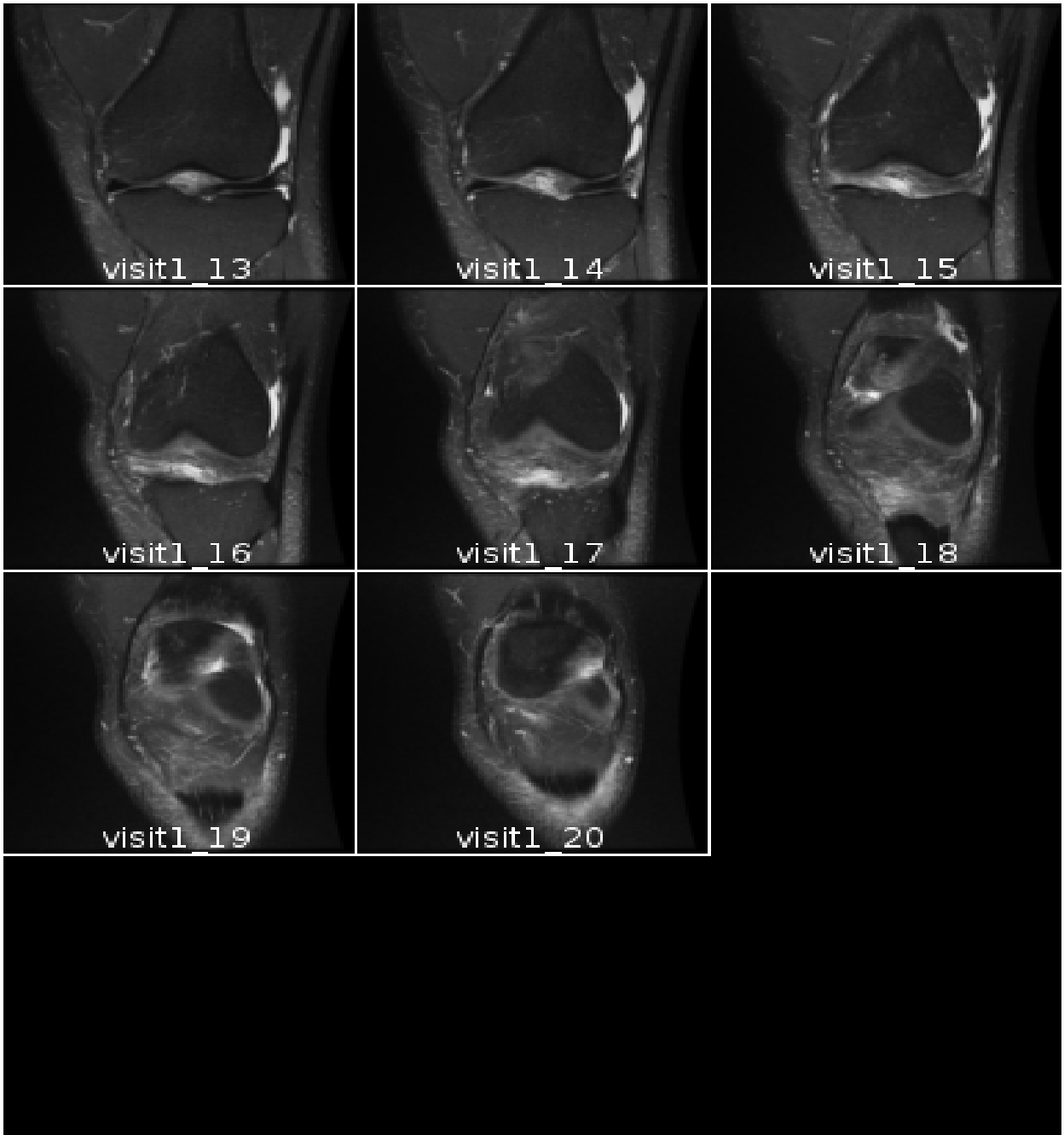
show()

```

# **Appendix C**

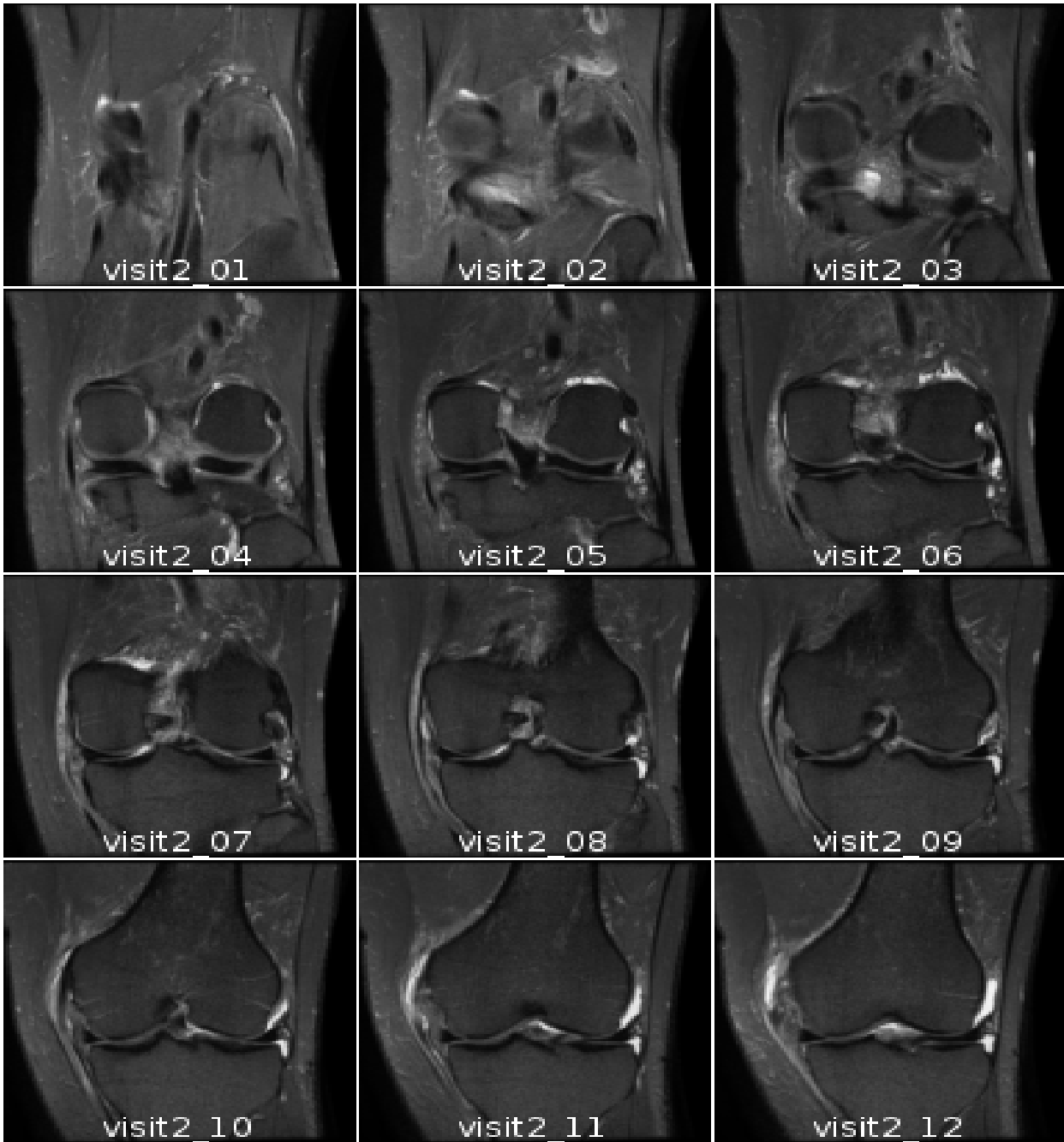
## **Real medical images: set 1**



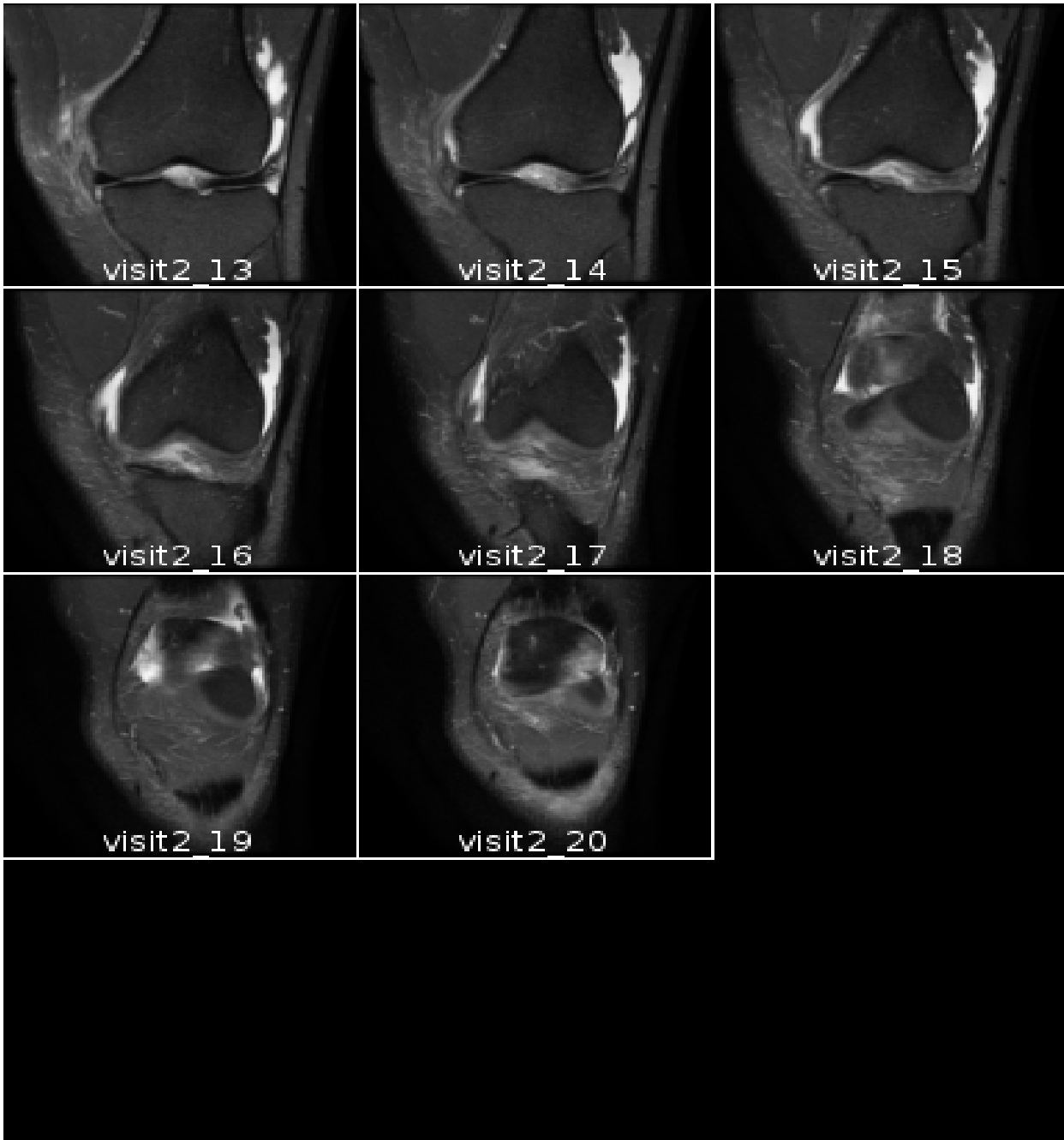


## **Appendix D**

### **Real medical images: set 2**

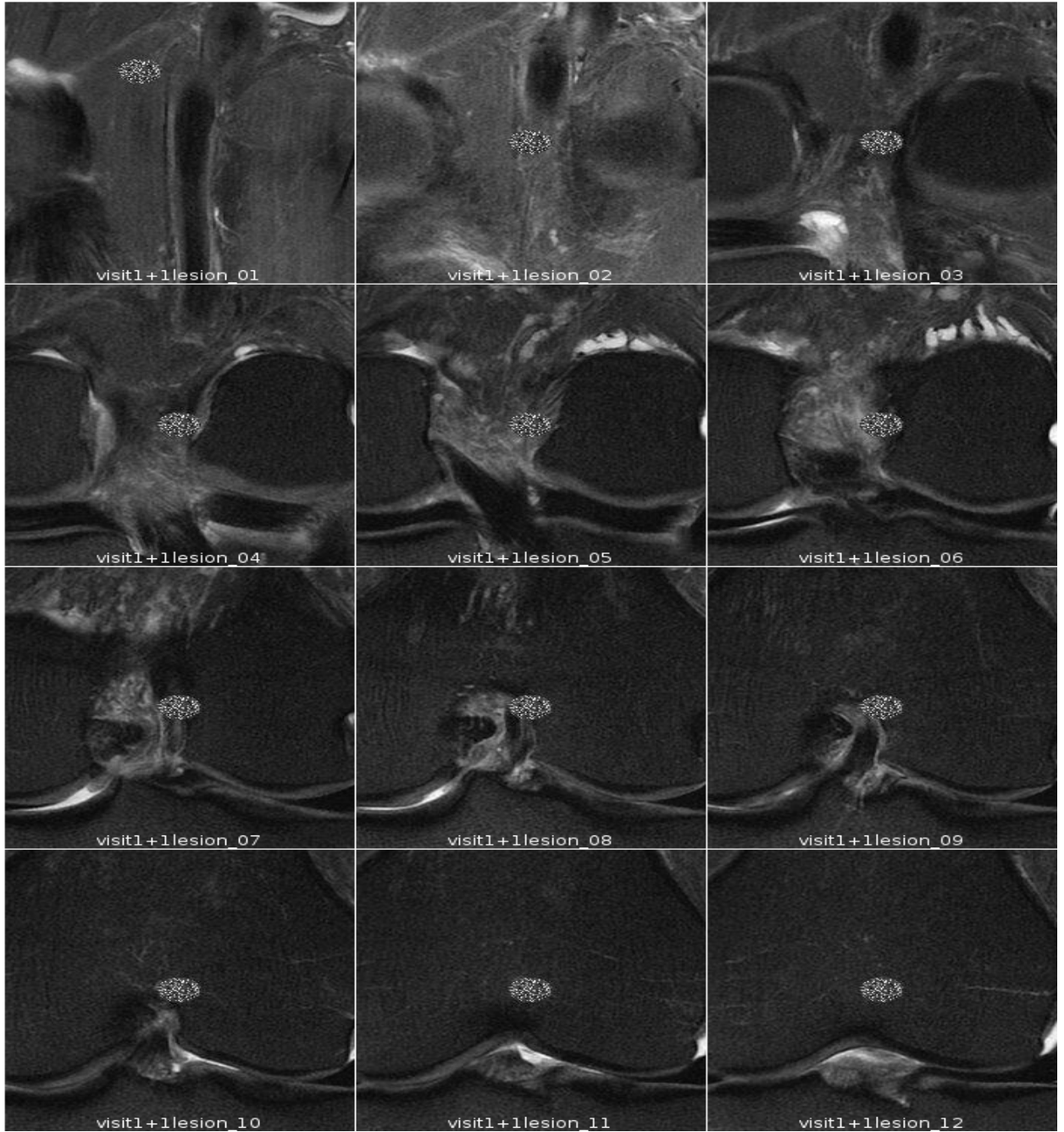


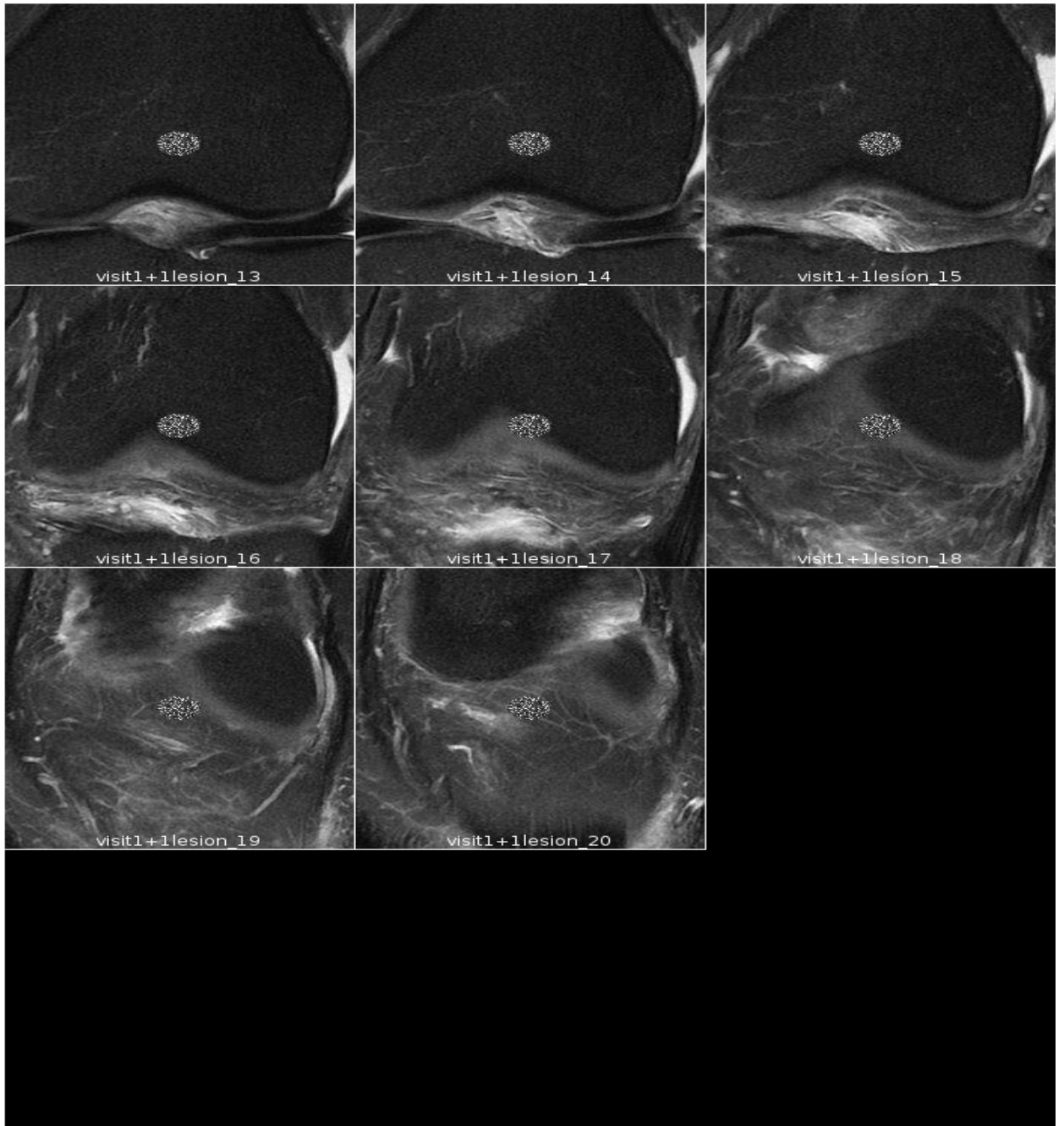




## **Appendix E**

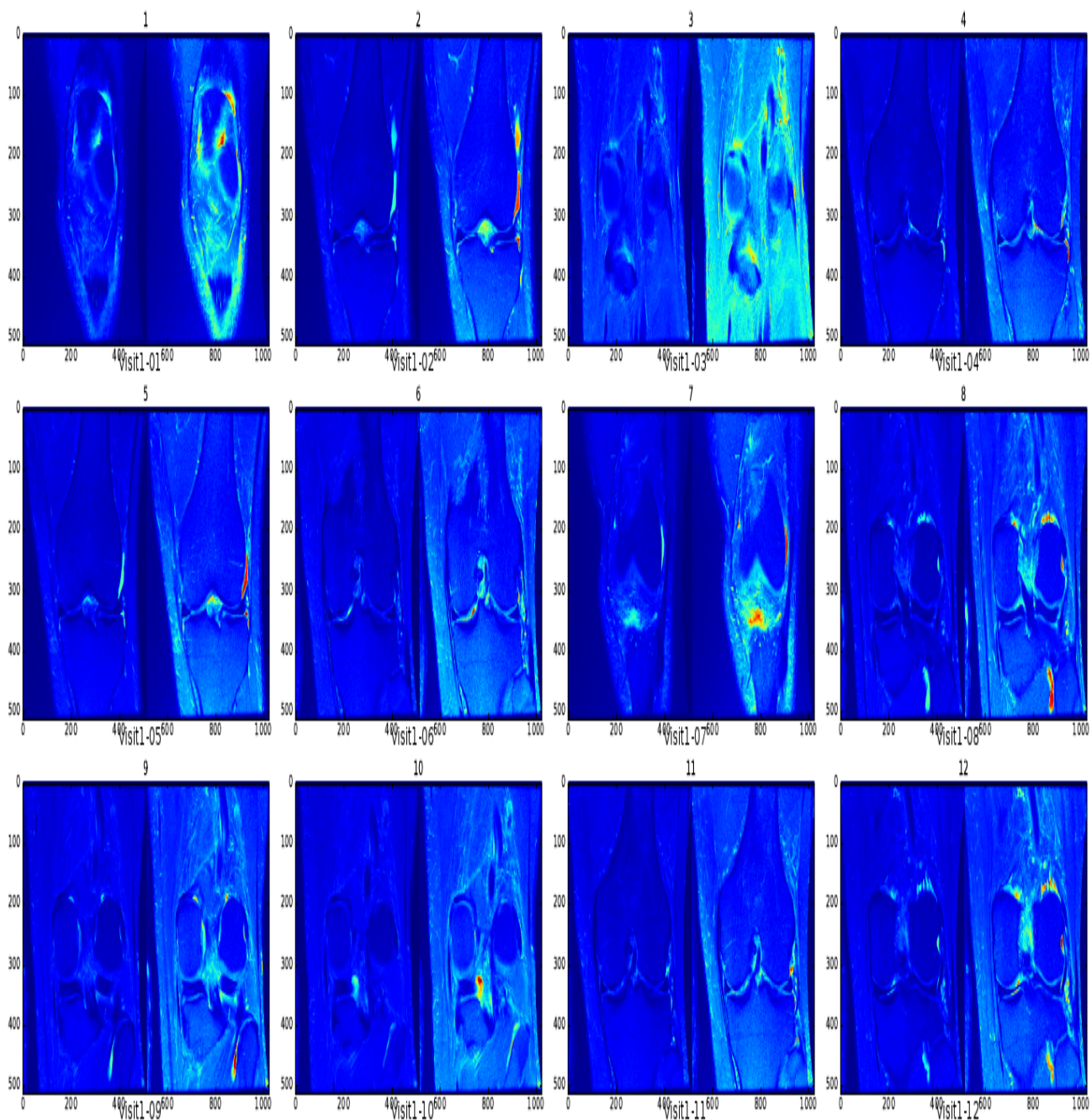
### **Real medical images with added 1 'lesion'**

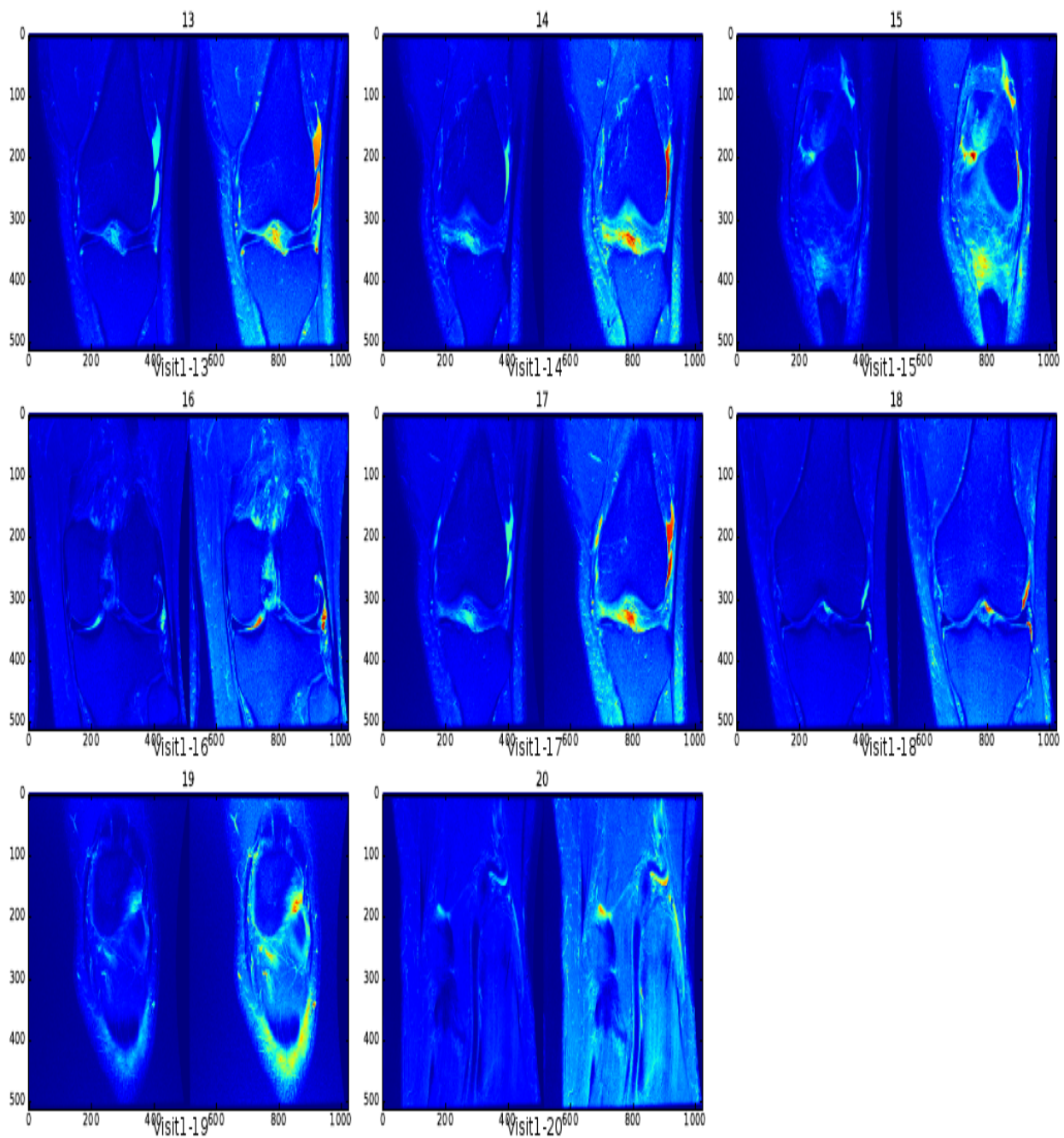




## **Appendix F**

### **Real medical images with global 'lesions'**



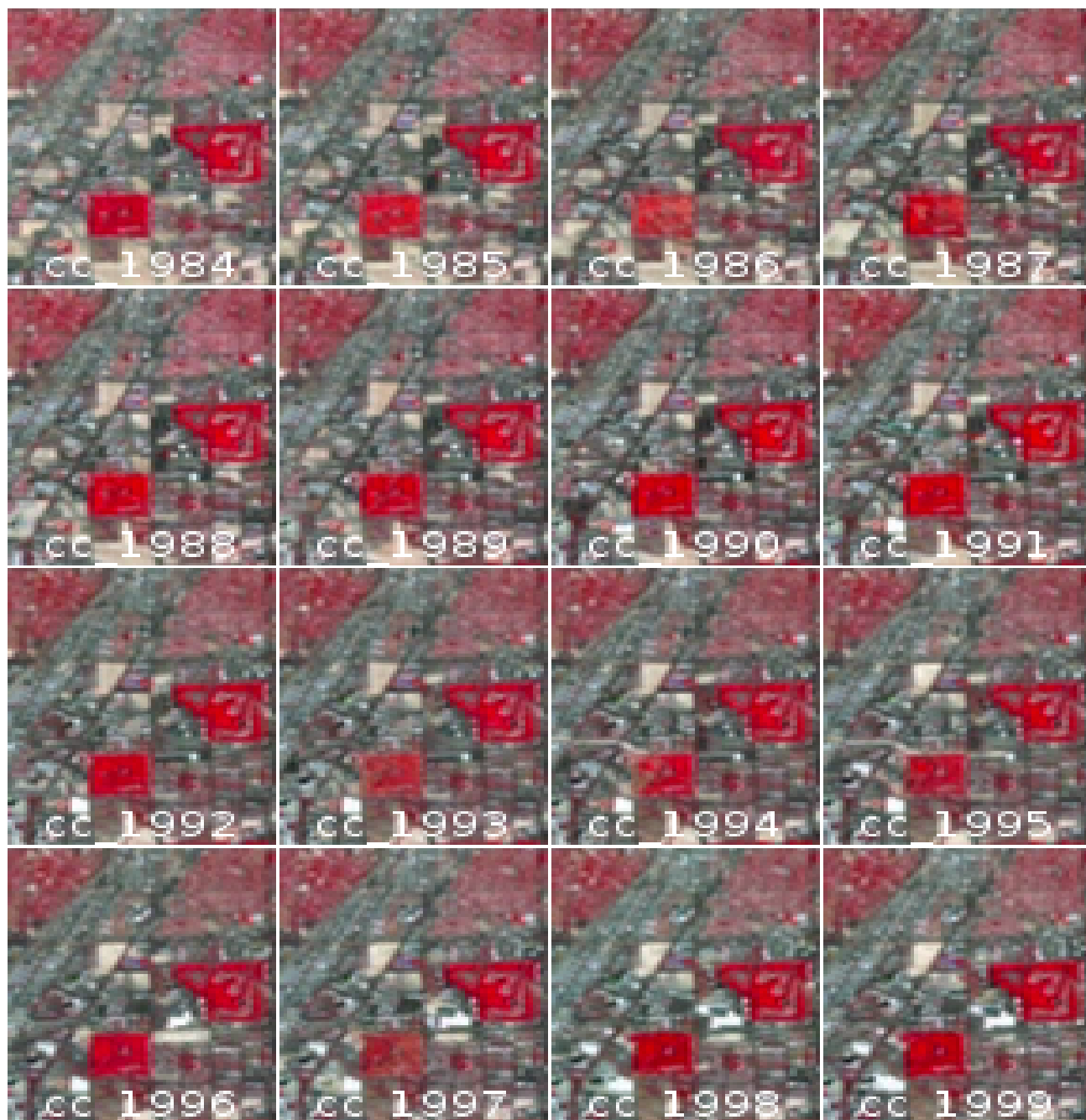


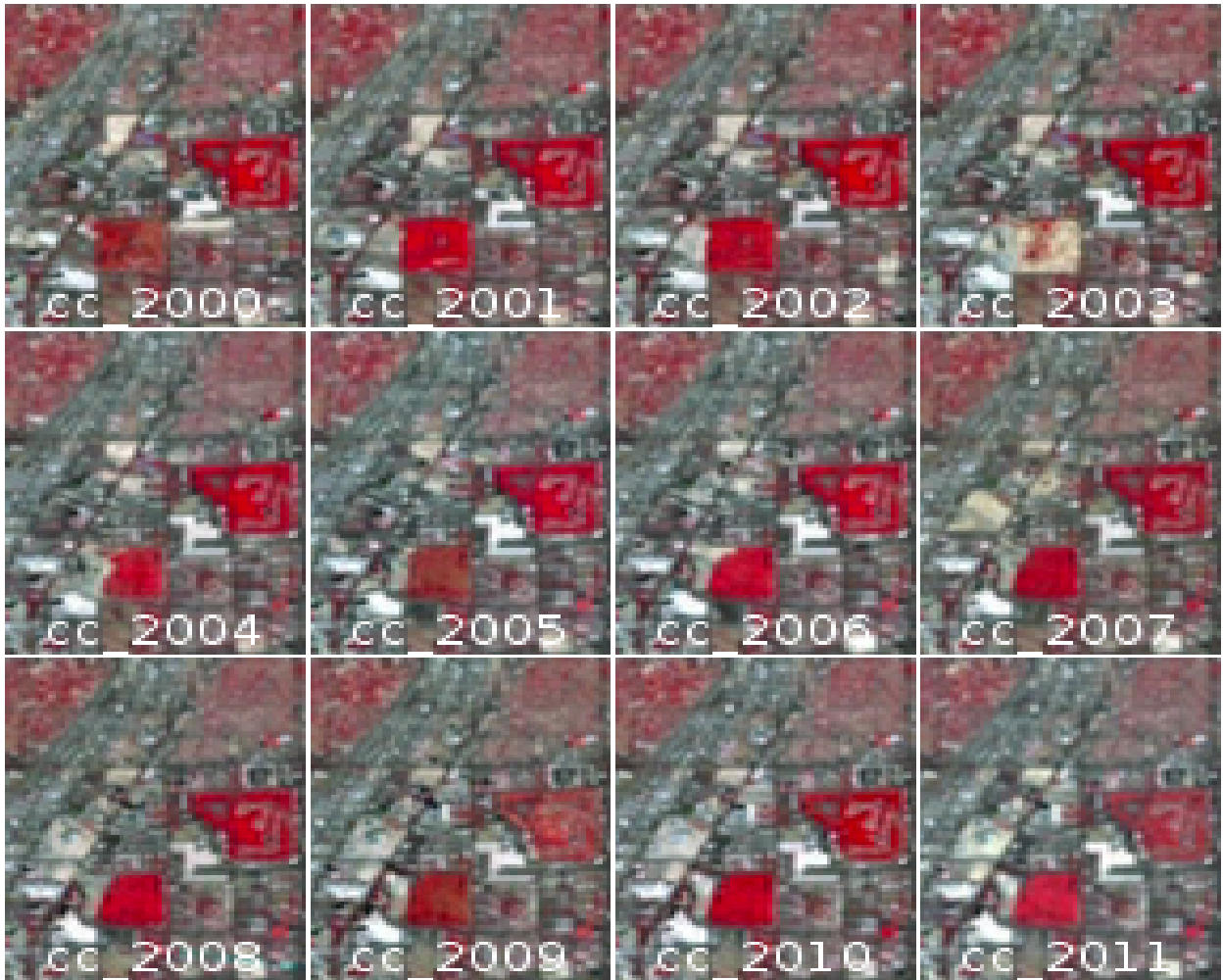
## **Appendix G**

**Satellite images: Las Vegas City**

**Center ROI**

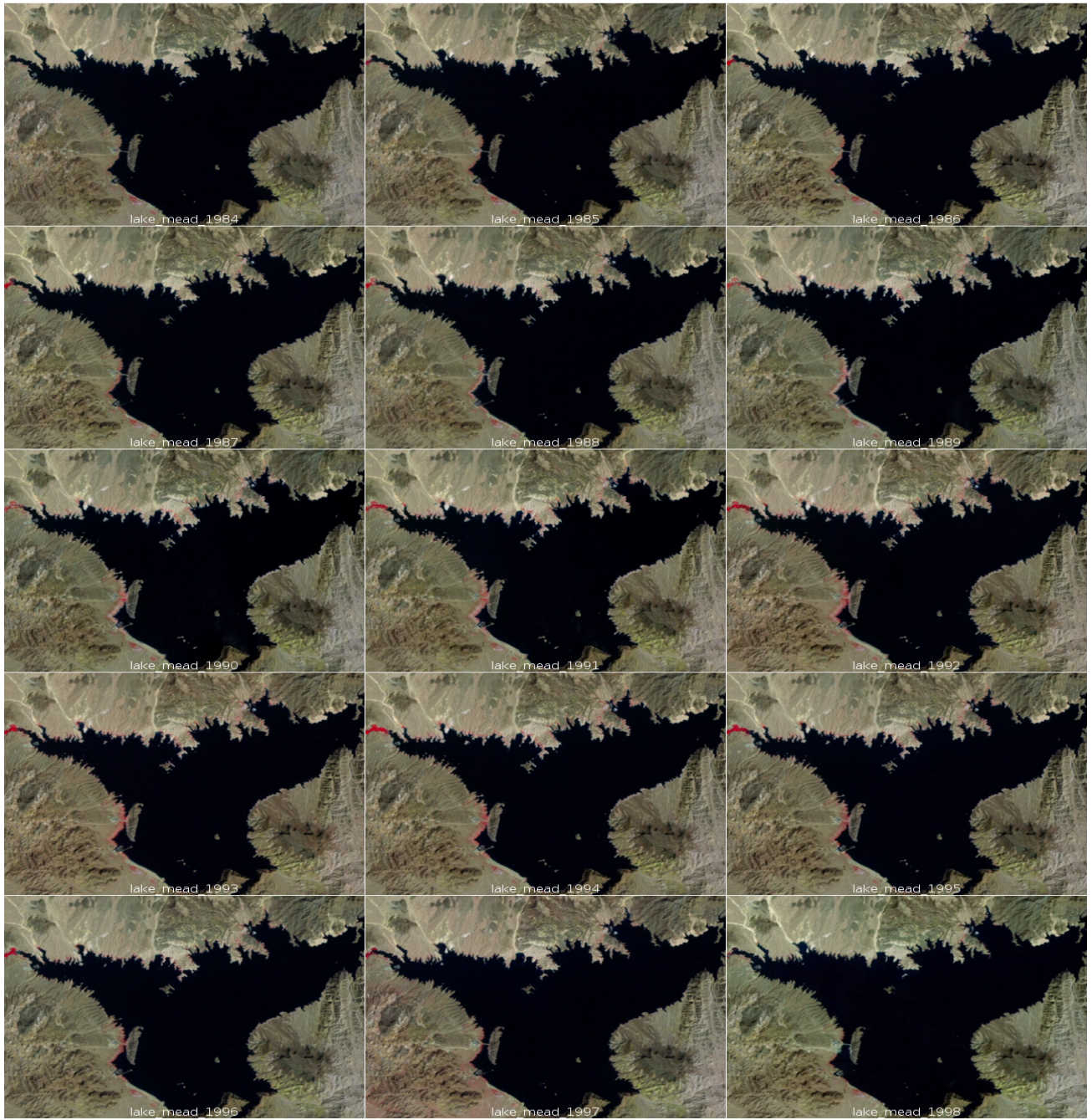


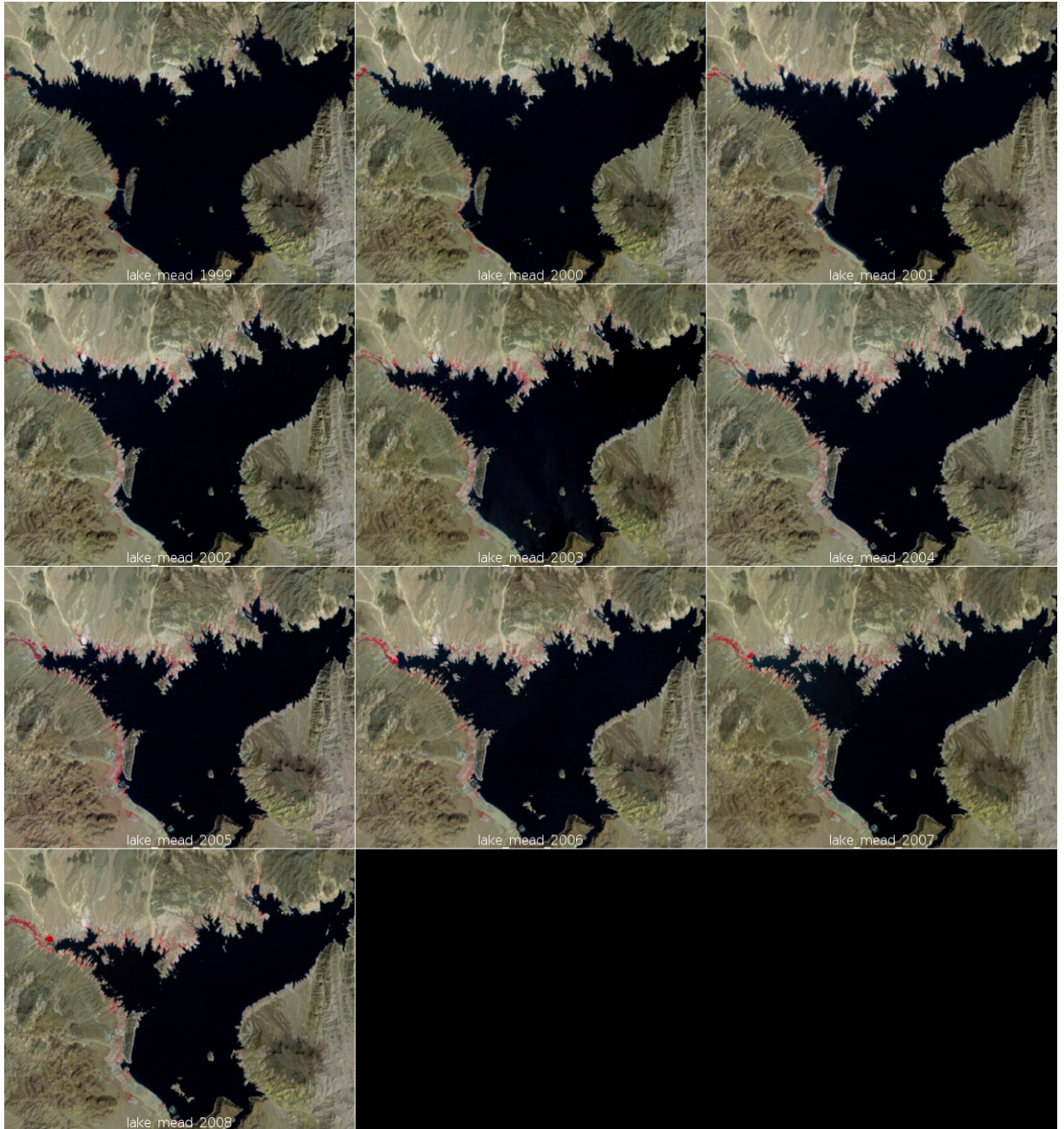




## **Appendix H**

### **Satellite images: Lake Mead ROI**





# **Appendix I**

## **Satellite images: Residential North of Las Vegas ROI**









JOHN MWANGI



WANDETO

# DÉTECTION AUTOMATISÉE DE VARIATIONS CRITIQUES DANS DES SÉRIES TEMPORELLES D'IMAGES PAR ALGORITHMES NON-SUPERVISÉES DE KOHONEN

## I.1 Résumé

Une façon de déterminer le changement d'un objet à différents moments est d'analyser les images de l'objet prises à différents moments. De tels besoins surviennent dans le domaine médical où les radiologues et les chirurgiens peuvent vouloir suivre l'évolution d'un patient. Ils sont intéressés à déterminer si un patient réagit positivement ou négativement à une ordonnance. Ils obtiennent donc les images du patient lors des visites cliniques et les utilisent pour comparer l'état de chacun d'eux afin de déterminer si la maladie ou l'état est en cours de progression, de rémission ou de régression. De même, les administrateurs municipaux peuvent souhaiter connaître les changements qui se produisent dans les différentes zones de la ville. Les changements, comme les nouveaux

bâtiments à venir, peuvent être capturés dans le but de déterminer s'ils sont légaux ou non ou généralement pour surveiller le taux d'urbanisation, les taux de boisement/déboisement, entre autres sur les différentes sections de la ville. Plusieurs approches ont été suggérées au fil des ans sur la façon de déterminer les différences entre les images d'un objet.

Les travaux de recherche de cette thèse portent sur une nouvelle approche computationnelle pour la détection du changement dans les images complexes. L'approche commence par la détermination de la variation à l'intérieur d'une image qu'elle utilise pour étiqueter l'image. Lorsqu'une série d'images d'un même objet sont étiquetées, la différence dans les étiquettes correspond aux changements entre les images. Ceci reflète à son tour les changements qui se sont produits dans l'objet entre les temps des images capturées. L'idée peut ensuite être utilisée par un radiologue pour vérifier le changement chez le patient, grâce à l'utilisation d'images prises lors de différentes visites cliniques. De même, les administrateurs municipaux peuvent utiliser la même technique pour étudier les changements qui se produisent au fil du temps dans la ville.

La variation au sein d'une image est calculée en soumettant l'image à un processus d'apprentissage machine. Ensuite, la différence entre les résultats du processus d'apprentissage et l'image réelle donne la variation souhaitée. Cette différence est appelée quantization error (QE) et l'algorithme d'apprentissage machine utilisé est une self-organizing map (SOM). SOM est une technique de calcul bien documentée introduite au début des années 80 par Teuvo Kohonen en

tant qu'architecture de artificial neural networks (ANN) inspirée biologiquement. Dans la catégorie de l'apprentissage compétitif non supervisé, le SOM produit une représentation discrète et discrète des vecteurs d'entrée (généralement un ou deux dimensions). Les sorties SOM sont organisées selon une structure cartographique dans le même ordre topologique que les données d'entrée, ce qui les différencie des autres techniques d'apprentissage machine.

Pour configurer et appliquer SOM, l'utilisateur doit déterminer la taille de la carte, la distance du quartier, le taux d'apprentissage et le nombre d'itérations à effectuer pendant le processus d'apprentissage. La carte est constituée d'unités d'apprentissage dont le nombre détermine la taille. Les unités d'apprentissage se comportent différemment lorsqu'on leur présente les mêmes stimuli - une adaptation du style d'apprentissage du cerveau humain, où différentes sections sont connues pour apprendre des stimuli environnementaux spécifiques mieux que d'autres. Chaque unité d'apprentissage prend une position sur la carte, formant une grille hexagonale ou rectangulaire régulière. Les unités reçoivent des valeurs initiales - qui peuvent être prises au hasard à partir de l'image - à utiliser pour commencer le processus d'apprentissage.

Pendant le processus d'apprentissage, un vecteur d'entrée de l'image est présenté à la carte. Ceci déclenche un processus de comparaison entre le vecteur d'entrée et chacune des unités d'apprentissage. Le but de la comparaison est de déterminer l'unité d'apprentissage qui est plus similaire au vecteur d'entrée que les autres. Une telle unité est considérée comme étant le vainqueur du vecteur

d'entrée, et elle devient sa best matching unit (BMU).

Avant d'introduire un autre vecteur d'entrée, la BMU est ajustée de telle sorte que ses valeurs se rapprochent de celles du vecteur d'entrée qu'elle a gagné. En outre, et c'est ce qui distingue SOM des autres processus d'apprentissage machine, les unités voisines de la BMU sont également ajustées. Les voisins sont les unités qui se situent dans le rayon du quartier déterminé au début du processus d'apprentissage. Avec le BMU comme centre, la distance de voisinage forme une zone "circulaire" autour du BMU sur la carte. Toute unité d'apprentissage qui se trouve dans la zone circulaire est alors considérée comme se trouvant dans le voisinage de l'BMU.

L'ajustement des valeurs dans les unités d'apprentissage constitue l'"apprentissage" de la carte. Il est fait de telle sorte que les valeurs de BMU sont ajustées (apprendre) plus que les autres unités du quartier. La quantité d'apprentissage diminue au fur et à mesure que l'on s'éloigne de la BMU dans la zone de voisinage et est régie par la relation suivante :

$$W(t + 1) = W(t) + \Theta(t)L(t)(V(t) - W(t)) \quad (\text{I.1})$$

C'est la méthode d'apprentissage de SOM, où  $t$  est le pas de temps et  $L$  est une petite variable appelée le taux d'apprentissage, qui diminue avec le temps. A partir de cette équation, le nouveau poids ajusté pour l'unité est égal à l'ancien poids ( $W$ ), plus une fraction de la différence, ( $L$  et  $\theta$ ), entre l'ancien poids et le

vecteur d'entrée ( $V$ ).

Elle ressemble de près à la sensation qu'une personne ressent lorsqu'un objet pointu, comme un stylo, est pressé sur la peau. La sensation est plus intense au point de contact et diminue à mesure que la distance de ce point augmente, jusqu'à ce qu'elle ne soit pas ressentie à des distances éloignées. Dans ce cas, la BMU représente le point de contact tandis que les unités du quartier représentent la région qui éprouvera le sentiment. De cette façon, le processus d'apprentissage SOM imite le comportement humain en créant une fondation qui le rendra supérieur dans l'application de détection de changement.

Ce processus d'apprentissage se fait pour chaque vecteur d'entrée de l'image. Au fur et à mesure que les unités cartographiques apprennent, leurs valeurs se rapprochent de plus en plus de celles des vecteurs d'entrée qu'ils ont gagnés et de celles qui leur ressemblent de plus en plus. Chaque unité d'apprentissage devient une zone qui s'associe et attire certains vecteurs d'intrants. Tout vecteur d'entrée sera toujours incliné vers une zone donnée, faisant de SOM un algorithme de clustering. Après que tous les vecteurs d'entrée ont été exposés au SOM, le processus est répété encore et encore, jusqu'à ce que le nombre prédéterminé de répétitions soit atteint.

Au fur et à mesure que l'apprentissage progresse, la distance entre les quartiers diminue et, par conséquent, le nombre d'unités affectées par les vecteurs d'entrée diminue également. Cela a pour effet d'assurer que l'unité ne gagne que les vecteurs d'entrée dont les valeurs sont plus proches des siennes et aussi celles qui

lui sont proches.

Un autre paramètre SOM qui est initialement fourni par l'utilisateur et qui diminue au fur et à mesure que le processus d'apprentissage progresse est le taux d'apprentissage. Il fournit la fraction utilisée pour ajuster les valeurs existantes des unités.

Lorsque le processus d'apprentissage est terminé, une comparaison entre le SOM appris et les vecteurs d'entrée originaux est faite pour fournir l'EQ. Chaque vecteur d'entrée a son propre QE, qui est la différence du vecteur avec son BMU. Ainsi, le QE détermine fondamentalement "à quel point SOM était proche d'atteindre les valeurs d'image d'origine".

Après avoir déterminé le QE pour chaque vecteur d'entrée, on calcule le QE moyen pour tous les vecteurs de l'image, voir l'équation I.2.

$$QE = 1/N \sum_{i=1}^N ||x_i - (BMU_i)|| \quad (I.2)$$

où N est le nombre de vecteurs en X, l'ensemble des vecteurs de données d'image et BMU est l'unité dont le vecteur de poids est le plus similaire au vecteur d'entrée x, pour tous les vecteurs de poids de SOM. partir de cette relation, l'QE ne tient pas compte de la topologie et de l'alignement de la carte, ce qui lui permet d'être universellement applicable.

Cette valeur QE devient l'étiquette de l'image qui sera utilisée pour suivre les

changements qui se produisent dans l'image avec le temps.

L'QE est un sous-produit du SOM et est traditionnellement utilisé pour déterminer l'exactitude des résultats produits par la carte. Dans l'utilisation traditionnelle de QE, plusieurs configurations SOM avec des paramètres variables sont exécutées sur un seul jeu de données et à la fin de chaque exécution, le QE est déterminé. Le but est de trouver une combinaison de paramètres qui donne la valeur la plus basse de QE, qui est considéré comme l'ensemble optimal à utiliser pour qu'un SOM transforme cet ensemble de données d'entrée.

Dans ce travail, ce produit de SOM, connu sous le nom de SOM-QE, est utilisé d'une nouvelle manière qui quantifie et détermine les variations des vecteurs de caractéristiques d'entrée comme mesure de l'uniformité au sein de l'ensemble de données. Le SOM-QE fournit une mesure des variations à l'intérieur de l'image à une instance dans le temps, et lorsqu'il est comparé aux valeurs des images subséquentes du même objet, il révèle une visualisation transitoire des changements dans l'objet d'étude. Ainsi, SOM-QE est proposé comme une nouvelle technique pour détecter et quantifier les changements transitoires dans les images d'objets.

Les images médicales et satellitaires sont prises en compte dans ce travail. Il est démontré que l'approche SOM-QE est capable de détecter des changements qui sont trop petits pour être détectés par des observateurs humains, ou qui n'étaient pas détectables par d'autres approches dans des études précédentes. En outre, il

s'avère qu'il est moins coûteux en termes de calcul et qu'il prend moins de temps.

Les changements qui se sont produits dans les objets d'intérêt, comme les nouveaux bâtiments dans une ville ou la progression des maladies, intéressent particulièrement les scientifiques et les ingénieurs. SOM-QE fournit un nouveau moyen de détection automatique de tels changements, fournissant des informations opportunes pour une planification ou une intervention appropriée. Par exemple, grâce au SOM-QE, les radiologues et les chirurgiens n'ont pas besoin d'attendre longtemps avant de programmer des patients pour une chirurgie ou des visites cliniques de suivi pour vérifier la progression d'une maladie. SOM-QE constitue un indicateur statistiquement fiable des petits changements locaux potentiellement critiques sur les images d'une série chronologique. Il est facile à mettre en œuvre et il a été démontré que les temps de calcul sont compris entre 18 et 350 secondes pour générer des données à partir d'ensembles de données de 20 à 25 images médicales ou Landsat. Il est en outre démontré que le SOM-QE atteint une sensibilité élevée et une spécificité élevée sur les images médicales. Il a fait preuve d'une grande robustesse dans la détection des variations systématiques du contraste d'intensité dans les images spatiales.

Pour démontrer le fonctionnement et l'efficacité de l'algorithme SOM-QE proposé, diverses simulations ont été effectuées sur différentes catégories d'images dans les domaines d'étude.

Avant d'effectuer les simulations, les images ont été préparées pour être utilisées



en les soumettant à une procédure de prétraitement. Cela a rendu les résultats SOM-QE plus fiables et reflète la position réelle des images comparées. Cela élimine d'autres causes possibles de changement qui pourraient mener à l'affichage de faux résultats. Par exemple, les images doivent être alignées de la même manière et les changements causés par un éclairage différent sur l'objet sont corrigés. De cette façon, l'effet des changements sans importance et / ou bruyants sur l'exactitude des résultats obtenus est minimisé.

Pour confirmer le concept SOM-QE, des expériences et des simulations avec des images réelles et artificielles ont été réalisées. Les résultats de chaque expérience / simulation ont été comparés aux résultats escomptés et il a été constaté que l'EQ-SOM-QE donne des résultats fiables. Statistiquement, il a été confirmé que les résultats étaient fiables et cohérents.

Par exemple, une simulation a été faite avec deux images de base dont les différences pouvaient être facilement tracées visuellement par l'homme. Lorsque SOM-QE a été appliqué pour donner les différences entre ces deux images, il a produit des résultats qui étaient corrects et correspondaient à ceux observés par un humain visuellement. En outre, l'application des techniques connues et couramment utilisées pour déterminer le contenu des données d'image - histogramme et calcul de variance - a donné des résultats qui correspondent à ceux donnés par SOM-QE. Les histogrammes sont utilisés pour donner une distribution précise des données numériques. Étant donné qu'une image est un ensemble de données de ce genre, il s'agissait d'un outil approprié à utiliser et à

comparer avec les résultats du SOM-QE. La variance, par contre, mesure dans quelle mesure les valeurs des données sont écartées de leur moyenne. Il donne la variation à l'intérieur d'un ensemble de données, tout comme SOM-QE. En donnant des résultats qui correspondent à ceux de ces méthodes standard, SOM-QE se qualifie pour entrer dans leur ligue et donc concourir et compléter les méthodes existantes.

Dans une simulation ultérieure, SOM-QE permet de détecter avec précision les variations contrôlées de la taille d'un seul point local à l'intérieur d'images à points aléatoires. Il s'est mieux comporté que les observateurs humains, qui comprenaient des personnes non formées et des radiologues experts. Des expériences de détection visuelle ont été mises en place, en utilisant des images à points aléatoires dans une procédure psychophysique "même différence". Une paire d'images a été présentée à l'observateur à un moment donné. La tâche de l'observateur était de dire si les deux images étaient identiques ou différentes. La paire d'images présentées a été composée à partir d'un ensemble de données de 4 images différentes. La première image était une image pointillée originale, avec des points de taille égale et répartis au hasard dans l'image. Les deuxième, troisième et quatrième images avaient un point dont la taille a été modifiée. Dans la deuxième image, la taille du point a été augmentée de 5% et de 10% et 30% dans les troisième et quatrième images respectivement. Les observateurs humains ont eu des difficultés à noter ces changements, en particulier celui de 5%. Mais SOM-QE a clairement produit les différences requises. Les résultats

ont montré que les petits changements détectés par SOM-QE sont indétectables par les observateurs humains, tant les novices que les radiologues experts. Sur la base de cette preuve de concept, il est postulé que SOM-QE fournit un indicateur statistiquement fiable de petits changements dans les séries d'images qui peuvent être indétectables par la vision naturelle humaine.

Ensuite, le SOM-QE a été appliqué à des images d'IRM réelles prises d'un patient blessé au genou dont les résultats correspondaient au développement clinique du patient. Lorsqu'il est appliqué à un ensemble de données d'image utilisé par une autre approche discutée dans la littérature, SOM-QE affiche de meilleurs résultats, en particulier en ce qui concerne la détection d'une croissance plus faible dans la série d'images.

Lorsque des impuretés sont systématiquement ajoutées à un ensemble d'images réelles, SOM-QE renvoie des résultats qui correspondent à l'effet des impuretés ajoutées dans les images, et les résultats sont également statistiquement cohérents. Les impuretés ont été ajoutées de deux façons. Tout d'abord, ils ont été ajoutés pour se comporter comme des croissances locales dans l'image. C'est-à-dire qu'elles ont causé des changements dans des régions particulières des images, comme le font les lésions en croissance. Dans la seconde manière, les impuretés ont été ajoutées à travers les images se comportant comme des impuretés globales.

Lorsqu'une " lésion " a été ajoutée sur chaque image de l'ensemble de données pour former un autre ensemble de données, les résultats de l'EQ-SOM reflétaient

cet ajout de lésion. Les résultats étaient également statistiquement importants. Lorsqu'une deuxième lésion est ajoutée pour former un troisième ensemble de données d'images et que le SOM-QE est appliqué, l'ajout de la lésion est également reflété par les résultats du SOM-QE. Si ces séries d'images étaient réelles, prises lors de 3 visites cliniques consécutives du patient, alors SOM-QE aura indiqué aux radiologues et chirurgiens que les lésions étaient en augmentation, ce qui devrait déclencher un changement dans la prise en charge de l'état du patient. Ainsi, l'EQ-SOM peut dire quand une lésion ou une tumeur augmente ou diminue dans l'organe d'un patient, ce qui incite le radiologue à prendre les mesures appropriées.

Les résultats de la série de simulations décrites dans ce travail suggèrent que l'analyse SOM-QE semble bien adaptée à la détection de changements rapides dans de grandes quantités d'images médicales de patients. Il permet la détection automatique de changements subtils mais significatifs dans les séries temporelles d'images susceptibles de refléter des lésions en croissance ou en recul. Dans la pratique clinique, il peut être très difficile de trouver des preuves d'une croissance subtile par l'inspection visuelle de l'imagerie en série. C'est particulièrement vrai pour les scanners effectués à des intervalles relativement courts (moins d'un an). L'inspection visuelle rate souvent l'évolution lente parce que le changement peut être obscurci par des variations dans la position du corps, la position des tranches ou le profil d'intensité entre les balayages. Dans certains cas, le changement peut être trop petit pour être remarqué. Les chirurgiens et les

oncologues calculent fréquemment la variation du volume tumoral en comparant les mesures des scanners consécutifs. Lorsque le changement de volume de la tumeur est trop faible et donc difficile à détecter entre deux scanners séquentiels, les radiologues ont tendance à comparer le dernier scan avec l'image la plus ancienne disponible pour trouver des preuves visibles d'une évolution de la tumeur. L'analyse qui en résulte ne reflète toutefois pas l'évolution actuelle de la tumeur, mais plutôt une perspective rétrospective de l'évolution de la tumeur, comme nous l'avons souligné précédemment. Cette étude aborde ce problème, car le SOM rapide pourrait être facilement mis en œuvre pour aider les cliniciens à décider du traitement. Le processus d'exécution du code pour déterminer la distribution QE pour une série de vingt images prend environ 40 secondes. Ceci implique la lecture des images DICOM à partir d'un dossier, l'exécution du SOM et la détermination du QE pour chaque image, l'affichage de l'image à l'écran et l'enregistrement de la valeur QE dans un fichier texte. En résumé, chaque fois que les valeurs SOM-QE des images prises à des moments consécutifs augmentent, c'est une indication potentielle que des lésions ou d'autres changements pathologiques de l'organe à l'étude peuvent se développer, tandis qu'une diminution de la valeur SOM-QE peut indiquer qu'une pathologie est en recul. Au meilleur de notre connaissance, notre approche est la première à détecter automatiquement les changements locaux potentiellement critiques chez un patient en comparant des images prises lors de visites cliniques subséquentes sans se fier à une inspection visuelle ou à des annotations manuelles. La méthode SOM-QE détecte rapidement ces changements avec un temps de calcul minimal

en utilisant des images consécutives d'un organe sans avoir à se fier à des qualités d'image dérivées comme c'est le cas pour les méthodes de soustraction d'image, par exemple. La méthode SOM-QE représente également un avantage certain par rapport à la surveillance d'un état, par exemple la progression ou la rémission du cancer, en utilisant des techniques de segmentation manuelle sur chaque image d'une séquence d'MRI, ce qui prend beaucoup de temps.

D'autres simulations sur l'application du SOM-QE ont été réalisées à l'aide d'images satellitaires capturées par Landsat. La détection et la caractérisation des changements critiques dans les espaces publics de l'environnement naturel ou bâti reflétés par les changements dans les séries temporelles d'images à partir de données d'images télédéteectées peuvent être d'une importance considérable pour les politiques d'atténuation des risques et la sensibilisation du public. Les résultats de SOM-QE à cette fin ont confirmé qu'il s'agit d'une technique automatique rapide qui permet de distinguer les contenus modifiés et inchangés dans les grandes séries temporelles d'images, ce qui a fait défaut, comme le rapporte la littérature. Les tendances changeantes de la croissance sur l'urbanisation des régions au sein de la ville de Las Vegas aux États-Unis ont été étudiées. Entre 1984 et 2008, l'urbanisation de la ville s'est développée pour couvrir une grande partie de ce qui était auparavant un désert. SOM-QE a couvert ce phénomène de façon fiable, la corrélation de Pearson montrant des corrélations statistiquement significatives entre la valeur SOM-QE et le nombre de visiteurs et le total de la population pour la période. Au niveau des pixels - qui

se traduisent par des endroits spécifiques dans la ville - SOM-QE a retourné des résultats montrant les endroits qui ont connu des changements et ceux qui n'ont pas connu de changements au cours d'une période spécifique. Bien que certaines approches de détection des changements dans l'utilisation et la couverture du sol reposent sur le changement de la taille d'une zone d'utilisation du sol d'une période à l'autre, l'SOM-QE a démontré que même les changements qui n'ont pas entraîné de réduction ou d'augmentation de la taille de la zone d'utilisation du sol sont détectables. Une zone d'utilisation du sol et de couverture de taille fixe pour toutes les images à l'étude a été utilisée pour le démontrer. Pour l'instant, lorsqu'une maison supplémentaire est construite dans une zone bâtie, un changement se produit, mais la taille de l'utilisation du sol / couverture de la zone bâtie n'a pas changé. Ainsi, SOM-QE peut détecter les objets changeants à l'intérieur d'une scène, comme un nouveau bâtiment qui arrive, en fournissant aux gestionnaires de la ville des informations pour, par exemple, détecter les bâtiments illégaux en construction.

La ville voisine de Las Vegas est le lac Mead qui a vu son niveau d'eau changer au cours de cette période. SOM-QE a également fait état de ces résultats de manière fiable. La statistique de corrélation de Pearson calculée sur les distributions appariées pour l'SOM-QE et les niveaux d'eau signalait une corrélation statistiquement significative, pour la période 1984-2008.

L'efficacité de la technique SOM-QE pour déterminer les changements tels qu'ils sont représentés par les images satellites a été évaluée à l'aide d'un ensemble de

données d'images. Lors de la détection de changements entre deux images à partir de cet ensemble de données, SOM-QE a retourné des résultats qui correspondaient parfaitement aux résultats de vérité de terrain fournis. La détection de changement dans les images temporelles à l'aide de SOM-QE, ouvre de nouvelles possibilités de traitement automatique rapide pour lequel une décision rapide sur le changement ou pas de changement doit être prise. Les résultats indiquent que les valeurs SOM-QE varient de façon constante, fiable et prévisible en fonction des variations locales des signaux de contraste spatialement distribués dans les images à points aléatoires et dans les séries d'images avec des contrastes spatiaux régulièrement distribués (configurations géométriques). Sur la base de ces variations systématiques, SOM-QE est un indicateur très sensible et fiable de l'homogénéité des images locales et globales : à mesure que les images d'une série temporelle deviennent plus hétérogènes dans le contenu spatial, SOM-QE augmente ; inversement, à mesure que les images deviennent plus homogènes dans le contenu spatial, SOM-QE diminue constamment, à condition que l'intensité du contraste soit constante à travers les images d'une série donnée.

En conclusion, il n'existe, à notre connaissance, aucune méthode rapportée qui a obtenu des résultats supérieurs sur des problèmes similaires. Le travail est important car il introduit une nouvelle façon d'envisager la détection automatique des changements lorsqu'il s'agit de très petits changements locaux dans les images. La méthode proposée est facile à mettre en œuvre, rapide et



robuste. La méthode vise à fournir des résultats en temps quasi réel pour la détection et/ou la classification d'images. Il s'agit donc d'une technique prometteuse et non coûteuse pour la classification automatique des images médicales ou le suivi des changements dans l'information paysagère à partir d'un grand nombre de données d'images. Dans les applications médicales, il peut s'agir de scanners pris dans le temps sur un même patient pour une condition donnée dont l'évolution peut être lente mais progressive et donc difficilement détectable par les experts humains. Cela ouvre de nouvelles portes pour la surveillance de la progression et de la rémission du cancer. Dans l'étude de l'imagerie par satellite terrestre, les études longitudinales des données chronologiques des régions d'intérêt sont essentielles pour une planification adéquate des villes et autres espaces urbains futurs.

Les résultats suivants montrent comment SOM-QE peut suivre les changements d'objets dans le ROI. La QE d'un vecteur de caractéristiques d'entrée est surveillée entre les images pour déterminer les changements. Voir Tableau I.1 et Figure I.1.

Certains objets ont changé en augmentant leurs valeurs SOM-QE, d'autres ont diminué tandis que d'autres n'ont pas changé comme indiqué dans la dernière colonne du tableau I.1. La figure I.1 montre les objets dans le ROI, avec des points noirs - pixels - indiquant les régions qui n'ont pas changé entre les images sur chaque ligne. Tous les autres objets ont subi des changements.

Une autre conclusion de cette thèse est qu'étant donné une série de valeurs

	Input vector position index	SOM-QE value 1984 image	SOM-QE value 1985 image	Change in QE
	353	0.3316	0.3316	0
	362	0.3314	0.3314	0
	1284	0.2896	0.2896	0
	2501	0.1551	0.1551	0
[h]	3001	0.0534	0.0566	-0.0033
	3587	0.0411	0.0362	0.0049
	3955	0.0711	0.0649	0.0062
	7065	0.1681	0.1427	0.0254
	11689	0.1287	0.1260	0.0027
	17587	0.24211	0.2421	0

Table I.1: Samplé SOM-QE des régions du RCI résidentiel Nord sur la même position des images capturées en 1984 et 1985. La dernière colonne indique l'ampleur et la direction du changement dans la région, tel que déterminé par le SOM-QE. Notez les deux positions, 2501 et 17587, avec des valeurs SOM-QE de 0,1551 et 0,2421 respectivement et dont les positions sont indiquées dans la Figure I.1.

SOM-QE d'un objet/scène, il est possible de déterminer des valeurs SOM-QE futures et donc de prédire les changements qui sont susceptibles de se produire dans l'objet/scène.

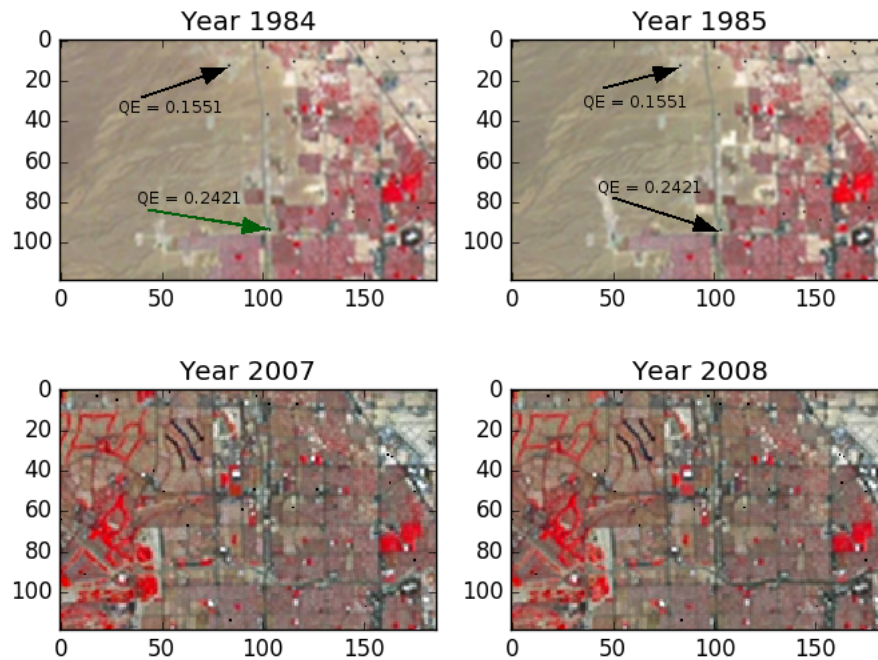


Figure I.1: Les petits points noirs dans l'image de chaque année sont des zones qui n'ont pas subi de changements entre les deux années de chaque rangée. Le reste de l'image a subi quelques changements. Sur la ligne du haut, deux zones spécifiques sont illustrées. L'une a une valeur SOM-QE de 0,2421, la seconde a une valeur SOM-QE de 0,1551 pour les deux années, 1984 et 1985. La ligne du bas montre également les zones où il n'y a pas eu de changement entre 2007 et 2008. Il faut 7,1 secondes pour détecter les changements et étiqueter les régions entre les deux paires d'images, ce qui rend cette approche appropriée à la tâche.

Une visualisation des données SOM-QE calculées à partir d'un ensemble de 28 images de séries temporelles a indiqué que ces points de données calculés dans le temps par SOM-QE ont une structure interne qui peut être prise en compte.

Lorsqu'elles sont tracées, la valeur actuelle de SOM-QE par rapport à l'observation à l'étape précédente, les observations tombent le long d'une ligne diagonale. Il s'agit d'une confirmation que le jeu de données SOM-QE est corrélé à l'intérieur de celui-ci, ce qui permet de l'utiliser à des fins de prédiction. Ainsi, la nouvelle technique, SOM-QE, génère des données qui peuvent être appliquées pour déterminer le changement futur, sa direction et son ampleur.

Lorsqu'un modèle de prédiction est formé et exécuté sur ces données, tous les changements représentés par SOM-QE entre les images sont correctement prédits par ce modèle. La détection de changement est vue dans le même sens (augmentation ou pas de changement ou diminution) que les valeurs réelles.

Pour évaluer la performance du SOM-QE en tant que détecteur de changement et en tant que fournisseur de données de prévision, il a été testé sur deux ensembles de données. Le premier ensemble de données était constitué de mesures réelles capturées par des instruments, qui sont comparées aux valeurs SOM-QE obtenues à partir d'images correspondantes pour déterminer la précision. Les mesures portent sur le cycle annuel du gaz carbonique ( $CO_2$ ) dans l'hémisphère Nord, couvrant la période du 1er janvier au 31 décembre 2012 et indiquent la hausse et la baisse distinctes des niveaux de dioxyde de carbone sur une période d'un an.

L'unité utilisée pour enregistrer les données sur les gaz est le nombre de parties par million (ppm), c'est-à-dire le nombre de molécules de  $CO_2$  présentes dans chaque million de molécules d'air. La tendance annuelle est causée par l'absorption et le rejet de  $CO_2$  provenant de la croissance saisonnière des plantes sur les vastes masses continentales de l'hémisphère Nord. La concentration annuelle maximale de  $CO_2$  dans l'hémisphère Nord se situe autour du mois de mai. L'accumulation printanière se produit parce que les plantes en décomposition ont libéré du carbone tout au long de l'hiver. La concentration minimale annuelle se produit autour d'octobre, après que la nouvelle croissance a retiré  $CO_2$  de l'air pendant la photosynthèse.

L'ensemble de données peut être utilisé dans ce cas parce que, lorsque les molécules de polluants augmentent, la variation à l'intérieur du million de molécules d'air augmente également. Cela signifie que pour les ppm faibles, SOM-QE devrait augmenter/réduire avec augmentation/réduction de la quantité de  $CO_2$ .

La performance de SOM-QE en tant que détecteur de changement a été calculée comme suit :

$$\text{précision, } p = 8 \div 11 = 0,727$$

$$\text{rappel, } r = 8 \div 11 = 0,727$$

$$\text{et F1 score de } (2 \times p \times r) \div (p + r) = 0.727$$

Il s'agit d'un meilleur score que ceux rapportés dans la littérature connexe. Par exemple, on rapporte que les meilleurs résultats affichés par divers détecteurs de changement 2D étaient un score de  $F1$  de 0,723.

Les 12 images mensuelles ont été utilisées pour former un prédicteur. La prédiction de la valeur SOM-QE de l'image suivante a été déterminée comme suit : 0.224166

C'est-à-dire que l'image de janvier 2013 aura une valeur SOM-QE de 0,2242, en hausse par rapport à celle de décembre 2012 à 0,2023, soit un changement de + 0,0219. Par contre, le montant de  $CO_2$  enregistré pour janvier 2013 est de 395,5 ppm en hausse par rapport aux 394,82 ppm enregistrés pour décembre 2012, soit une variation de + 0,68. Il s'agit d'un " hit ", ce qui signifie que SOM-QE prédit correctement que le montant de  $CO_2$  dans l'air a augmenté en janvier 2013.

Le deuxième ensemble de données utilisé pour évaluer et comparer SOM-QE avec d'autres techniques était ce qui a été décrit dans la littérature comme un " ensemble de données d'images de détection des changements difficiles ". Cet ensemble de données comprend une catégorie d'images appelée PTZ - caméra panoramique avec zoom et panoramique - catégorie qui nécessite différentes techniques de détection des changements par rapport aux vidéos de caméras statiques.

On rapporte qu'un total de 14 méthodes de détection des changements disponibles dans la littérature ont été testées et la mesure F pour chaque méthode

a été calculée. En particulier, la catégorie PTZ a affiché la performance la plus faible, un fait attribué à ses défis uniques posés par la nature zoomée/zoomée des images concernées.

Chacune des 14 méthodes a affiché des scores de mesure F1 inférieurs à 0,30. Quand SOM-QE a été appliqué à cette catégorie, il a obtenu une note F1 de 0,39, battant nettement les autres qui sont parmi les meilleures méthodes de la littérature.

Dans la catégorie PTZ, tout mouvement de caméra (panoramique, inclinaison ou zoom) provoquait des faux positifs majeurs pour chaque méthode, mais SOM-QE les minimisait, voir Figure I.2.

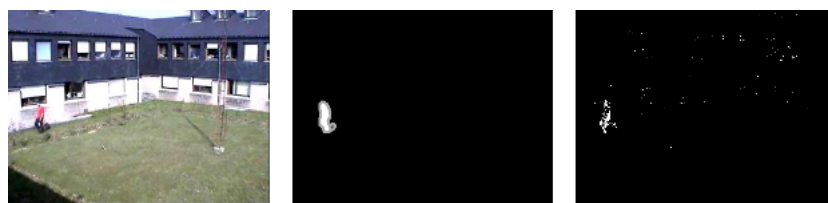


Figure I.2: Sur la gauche et au milieu se trouvent des images d'entrée de l'échantillon et des images de la vérité au sol, respectivement de l'ensemble de données du CDnet 2014, catégorie PTZ. A droite se trouve l'image produite par SOM-QE lors de la détection des changements entre l'image d'entrée et son image suivante sur la vidéo. La catégorie d'images PTZ posait des défis uniques en matière de détection des changements, les autres méthodes de la littérature géant un score F1 inférieur à 0,30. SOM-QE a obtenu un score F1 de 0,39, ce qui est le meilleur score dans cette catégorie.

Enfin, dans cette thèse, une nouvelle méthode de détermination de l'EQ dans les images de séries temporelles est proposée. La nouvelle méthode tient compte du fait qu'une BMU pour un vecteur d'entrée spécifique peut changer le long de la série temporelle des images.

Dans la détermination traditionnelle de QE, la différence entre le vecteur d'entrée original,  $x$ , et son gagnant, le BMU, est utilisée, voir l'équation I.3. Le BMU est l'un des poids finaux du SOM entraîné et est choisi pour être le plus proche du vecteur d'entrée.

$$QE = x - BMU \quad (I.3)$$

Pour un ensemble d'images de séries temporelles où le changement doit être détecté, le gagnant du vecteur peut ne pas être le même sur l'ensemble des images. C'est inhérent au principe de l'apprentissage compétitif que SOM pratique. Les unités de la carte SOM se disputent le droit de répondre au vecteur de données d'entrée - l'unité dont la ressemblance est la plus proche gagne et devient sa BMU. Par conséquent, si les valeurs en vecteur ont changé entre les images et qu'il est soumis à la concurrence, n'importe laquelle des unités SOM peut devenir sa BMU. Selon les changements dans, il peut se retrouver avec un nouveau gagnant parmi les unités de poids SOM et cela affectera les résultats affichés par l'équation I.3.

Dans la détection de changement, l'intérêt est dans le changement qui s'est



produit entre les images subséquentes dans un ensemble de données de séries temporelles. C'est le changement qui résulte du changement d'état de l'objet dont les images ont été acquises à des moments différents. Lorsque l'objet a subi des changements, nous nous attendons à ce que les changements soient reflétés dans le vecteur d'entrée  $x$ . L'ensemble des poids finaux de SOM, à partir duquel le gagnant de  $x$ 's est déterminé, porte des valeurs différentes et ne sont pas nécessairement égaux. Cela implique donc que lorsque  $x$  change de gagnant, cela affecte les résultats donnés par l'équation I.3 car cela inclut non seulement le changement dans  $x$ , mais aussi les changements dus à l'utilisation d'un gagnant différent. La déclaration d'un changement de cette manière peut être inexacte, car elle inclut les résultats de deux sources : premièrement, la différence réelle entre le vecteur d'entrée dans le premier ensemble de données et celui du deuxième ensemble de données, et deuxièmement, l'utilisation d'un *BMU* différent pour calculer l'EQ pour le vecteur dans les deux ensembles de données différents. Pour maintenir l'exactitude, il faut éliminer cette deuxième source de changement.

Par exemple, supposons que nous ayons deux images avec les vecteurs d'entrée correspondants  $x_{t1}$  et  $x_{t2}$ , c'est-à-dire  $x$  au temps 1 et  $x$  au temps 2. Les deux images sont capturées à des moments différents et sont prétraitées pour assurer l'uniformité de l'alignement et de l'exposition à la lumière. Le vecteur d'entrée  $x_{t1}$  et  $x_{t2}$  proviennent de la même position dans les deux images, c'est-à-dire qu'ils représentent le même objet dans l'image. A partir d'un SOM formé,  $x_{t1}$

peut être gagné par poids  $w_1$  tandis que  $x_2$  est gagné par poids  $w_2$ . Ainsi,  $w_1$  devient la BMU pour  $x_{t1}$  ( $BMU_1$ ) tandis que  $w_2$  devient la BMU pour  $x_{t2}$  ( $BMU_2$ ). La méthode traditionnelle de calcul de l'EQ consiste à trouver la différence entre le vecteur d'entrée et son BMU. Dans ce cas, en appliquant l'équation I.3, le QE pour les deux instances devient :

$$QE_1 = x_{t1} - BMU_1 \quad (I.4)$$

et,

$$QE_2 = x_{t2} - BMU_2 \quad (I.5)$$

et pour l'ensemble du stock de données, les valeurs QE de l'objet forment un ensemble :

$$QE_{object} = \{x_{t1} - BMU_1, x_{t2} - BMU_2, x_{t3} - BMU_3, \dots\} \quad (I.6)$$

c'est-à-dire que l'objet a des valeurs QE de chaque image de la série qui n'est pas calculée à partir de la même BMU.

Dans le cas d'un ensemble de données de séries chronologiques, cela soulève un problème. Les vecteurs d'entrée  $x_{t1}$  et  $x_{t2}$  représentent le même objet, seulement que leur représentation est à des moments différents. Il est donc logique que  $QE_1$  et  $QE_2$  soient déterminés à partir d'un point de référence commun ( $BMU$ ) afin qu'ils soient mathématiquement comparables et ainsi déterminer avec précision

si un changement s'est produit dans l'objet ou non.

La proposition est donc de restreindre le processus de détection de changement pour changer en  $x$  entre les images. Pour ce faire, on s'assure que le vecteur d'entrée  $x$  est associé au même gagnant dans l'ensemble des données de l'image. Pour ce faire, les gagnants déterminés lors de la phase de formation du SOM sont maintenus pour chaque  $x$ . L'indice de  $x$  dans les données de formation est utilisé pour l'extraire sur les images d'essai et son gagnant initial à partir des données de formation utilisées pour déterminer l'QE.

$$QE = x - originalBMUofx \quad (I.7)$$

et donc équation I.6 devient:

$$QE_{object} = \{x_{t1} - BMU, x_{t2} - BMU, x_{t3} - BMU, \dots\} \quad (I.8)$$

Lorsque SOM-QE est déterminé à l'aide des deux méthodes - la méthode traditionnelle et la nouvelle méthode suggérée ici - les résultats présentés à la Figure I.3 sont obtenus.

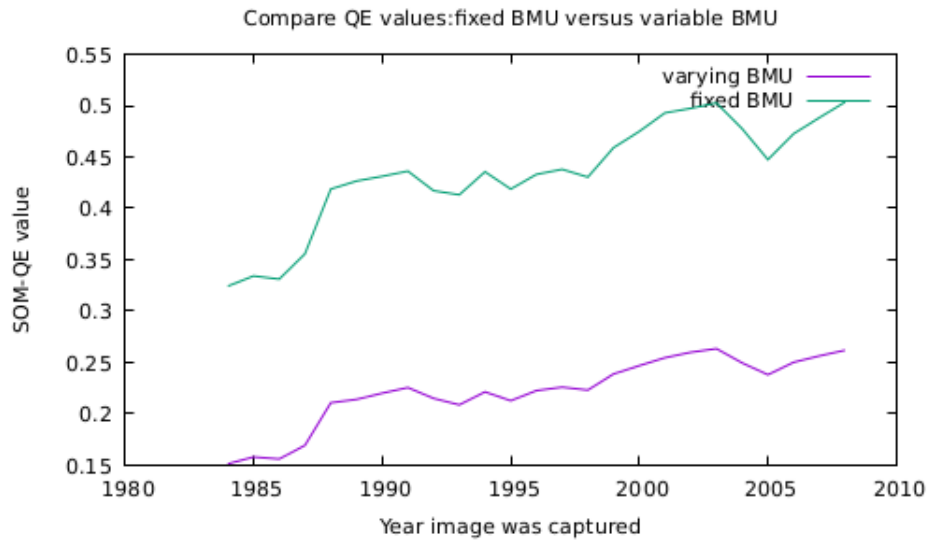


Figure I.3: Les deux graphiques montrent le résultat du calcul des valeurs SOM-QE à l'aide des deux méthodes. En bas, le résultat obtenu en appliquant l'équation 9 où le BMU du vecteur d'entrée à une image particulière est utilisé pour trouver le QE. Le graphique du haut montre les résultats obtenus par la nouvelle méthode où la BMU obtenue pour chaque vecteur d'entrée à la fin de la formation SOM est conservée et utilisée pour déterminer la QE pour ce vecteur particulier tout au long de la série temporelle d'images, comme dans l'équation I.7. Il y a un modèle commun dans les deux résultats, mais lorsque la BMU fixe est utilisée, la différence SOM-QE entre les images est plus grande et donc plus prononcée. Des images d'une section de Las Vegas capturées entre 1984 et 2008 ont été utilisées dans cette simulation.

Dans les deux cas, la tendance à l'évolution des valeurs SOM-QE est similaire.

Mais les valeurs SOM-QE plus élevées obtenues lorsqu'une valeur BMU fixe est appliquée la rendent plus sensible au changement. La quantité de changement détectée par SOM-QE lorsqu'une BMU fixe pour un vecteur d'entrée est appliquée est plus grande que lorsqu'une BMU variable est utilisée, voir Figure I.4.

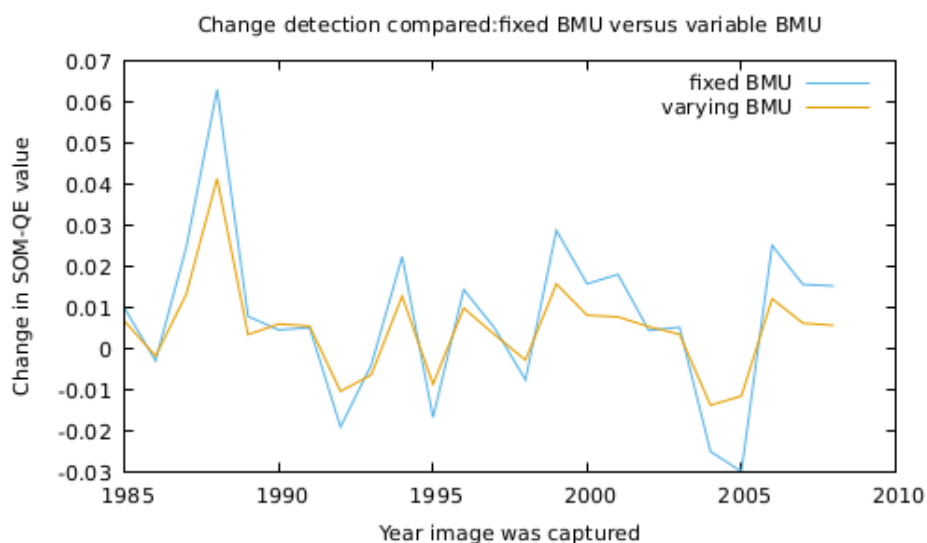


Figure I.4: Les changements qui se sont produits dans le ROI tel que reflété dans les images sont montrés ici pour les deux méthodes de détermination de SOM-QE. La méthode BMU fixe montre qu'un changement plus important s'est produit entre les images consécutives de la série que la méthode BMU variable. Pour noter le changement, considérez la distance du point à partir de 0 (pas de changement de point, sur l'axe des y) sur les deux courbes. Par exemple, en 2005, le changement est de 0,03 unité pour la nouvelle méthode et légèrement supérieur à 0,01 unité pour la méthode traditionnelle.

Ainsi, la nouvelle méthode fournit une mesure du changement à plus grande échelle que la méthode traditionnelle et se révèle plus sensible aux changements que la méthode traditionnelle. Cela le place dans une meilleure position pour détecter les changements, en particulier les petits changements, entre les images.



JOHN MWANGI



WANDETO

# SELF-ORGANIZING MAP QUANTIZATION ERROR APPROACH FOR DETECTION OF TEMPORAL VARIATIONS WITHIN IMAGE SETS

## I.1 Résumé en anglais

One way to determine change in an object at different times is to analyse images of the object taken at the different times. Such needs occur in the medical field where radiologists and surgeons may want to monitor the developments in a patient. They are interested in determining whether a patient is responding positively or negatively to some prescription. They, therefore, obtain the patient's images during clinical visits and use them to compare the status of each in view of determining if the disease/condition is on progression, remission or regression. Similarly, city administrators may wish to know changes occurring in various zones of the city. Changes, like new buildings coming up, can be captured with the aim of determining whether they are legal or not or generally to monitor the

urbanization rate, the afforestation/deforestation rates, among others on the various sections of the city. Several approaches have been suggested over the years on how to determine the differences between images of an object.

The research work in this thesis deals with a new computational approach to detection of change in complex images. The approach starts by determining the variation within an image which it uses to label the image. When a series of images of the same object are labelled, the difference in the labels is found to correspond to the changes between the images. This in turn reflects the changes that have occurred in the object between the times of the images captured. The idea can then be used by a radiologist to check for change in the patient; done through use of images taken at different clinical visit. Similarly, city administrators can employ the same technique to study changes that occur over time within the city.

Variation within an image is calculated by subjecting the image to a machine learning process. Then, the difference between the results of the learning process and the actual image gives the desired variation. This difference is called the quantization error (QE) and the machine learning algorithm used is self-organizing maps (SOM). SOM is a well-documented computational technique introduced in early 80s by Teuvo Kohonen as a biologically inspired artificial neural network (ANN) architecture. Under the unsupervised competitive learning category, SOM produces low-dimensional (usually, one or two-dimensional), discretized representation of the input vectors. SOM output



are arranged in a map structure in the same topological order as that of the input data, making it different from other machine learning techniques.

To set-up and apply SOM, the user is required to determine the map size, the neighbourhood distance, the learning rate and the number of iterations to be made during the learning process. The map is made up of learning units whose number determines its size. Learning units behave differently when presented with the same stimuli – an adaptation of the human brain learning style, where different sections have been known to learn specific environmental stimuli better than others. Each learning unit takes up a position on the map, forming a regular hexagonal or rectangular grid. The units are given initial values – which can be taken randomly from the image – to be used to start off the learning process.

During the learning process, an input vector from the image is presented to the map. This triggers a comparison process between the input vector and each of the learning unit. The aim of the comparison is to determine the learning unit that is more similar to the input vector than the others. Such a unit is taken to be the winner of the input vector, and it becomes its best matching unit (BMU).

Before bringing in another input vector, the BMU is adjusted such that its values become closer to those of the input vector it won. Besides, and this is what set SOM apart from other machine learning processes, units that neighbour the BMU are also adjusted. The neighbours are those units that fall within the neighbourhood radius that was determined at the beginning of the learning process. With the BMU as the center, the neighbourhood distance forms a

“circular” area around the BMU on the map. Any learning unit that is within the circular area is then taken to be in the neighbourhood of the BMU.

The adjustment of the values in the learning units constitute the “learning” of the map. It is done in such a way that the BMU values are adjusted (learn) more than the other units in the neighbourhood. The amount of learning reduces as one moves away from the BMU within the neighbourhood zone and is governed by the following relation:

$$W(t + 1) = W(t) + \Theta(t)L(t)(V(t) - W(t)) \quad (I.9)$$

This is SOM’s learning method, where  $t$  is the time step and  $L$  is a small variable called the learning rate, which decreases with time. From this equation, the new adjusted weight for the unit is equal to the old weight ( $W$ ), plus a fraction of the difference, ( $L$  and  $\theta$ ), between the old weight and the input vector ( $V$ ).

It resembles closely to the feeling a person gets when a sharp object, like a pen, is pressed on the skin. The feeling is more intense at the point of touch and reduces as distance from this point increases, until it is not felt at far distances. In this case, the BMU represents the point of touch while the units within the neighbourhood represent the region that will experience the feeling. This way, SOM learning process imitates the human behaviour creating a foundation that will make it superior in change detection application.

This learning process is done for each input vector from the image. As the map

units learn, their values become closer and closer to those of the input vectors they have won and also to those that have closer resemblance to them. Each learning unit becomes a zone that will associate and attract certain input vectors. Any input vector will always be inclined to a given zone, making SOM a clustering algorithm. After all the input vectors have been exposed to the SOM, the process is repeated over and over again, until the predetermined number of repetition is reached.

As the learning progresses, the neighbourhood distance reduces, and hence the number of units affected by the input vectors reduces too. This has the effect of ensuring that the unit wins only those input vectors whose values are closer to its own and also those that are closely located to it.

Another SOM parameter that is initially provided by the user and reduces as the learning process progresses is the learning rate. It provides the fraction used to adjust the existing values of units.

When the learning process is complete, a comparison between the learned SOM and the original input vectors is done to provide the QE. Each input vector has its own QE, which is the vector's difference with its BMU. Thus, the QE basically determines "how close SOM was to attaining the original image values". After the QE for each input vector is determined the average QE for all the vectors in the image is calculated, see equation I.10.

$$QE = 1/N \sum_{i=1}^N ||x_i - (BMU_i)|| \quad (I.10)$$

where N is the number of vectors in  $X$ , the set of image data vectors and BMU is the unit whose vector of weights is most similar to the input vector  $x$ , for all weight vectors of SOM. From this relation, QE disregards map topology and alignment, allowing it to be universally applicable.

This QE value becomes the label for the image which will be used to track changes that occur within the image with time.

QE is a by-product of SOM and is traditionally used to determine the accuracy of the results produced by the map. In the traditional usage of QE, several SOM set-ups with varying parameters are run on one dataset and at the end of each run, the QE is determined. The aim is to find a combination of parameters that gives the lowest value of QE, which is taken to be the optimal set to be used for a SOM to transform that input dataset.

In this work, this product of SOM, known as SOM-QE, is used in a novel way that quantifies and determines the variations in input feature vectors as a measure of uniformity within the dataset. The SOM-QE provides a measure of variations within the image at an instance in time, and when compared with the values from subsequent images of the same object, it reveals a transient visualization of changes in the object of study. Thus, SOM-QE is proposed as a new technique to detect and quantify transient changes in object images.

Medical and satellite imageries are considered in this work. It is shown that the SOM-QE approach is able to detect changes that are too small to be detected by human observers, or that were not detectable by other approaches in previous studies. In addition, it is shown to be less computationally expensive and less time consuming.

Changes that have occurred in objects of interest, such as new buildings in a city or progression of illnesses, are of particular interest to scientists and engineers. SOM-QE provides a new way for automatic detection of such changes, providing timely information for appropriate planning or intervention. For instance, by use of SOM-QE, radiologists and surgeons do not have to wait for long periods before scheduling patients for surgery or follow up clinical visits to check on progression of an illness. SOM-QE is shown to constitute a statistically reliable indicator of small potentially critical local changes across images of a time series. It is easily implemented and has been shown to have computation times of between 18 and 350 seconds for generating output from datasets of between 20 to 25 medical or Landsat images. It is further shown that SOM-QE achieves high sensitivity and high specificity on medical images. It showed significant robustness in detecting of systematic variations in intensity contrast in spatial images.

To demonstrate the working and effectiveness of the proposed SOM-QE algorithm various simulations were carried out on different categories of images in the domains of study.

Before performing the simulations, the images were prepared for use by subjecting them to a pre-processing procedure. This made the SOM-QE results more reliable and reflect the true position of images being compared. This eliminates other possible causes of change that could lead to posting of false results. For instance, the images need to be aligned in a similar way and that changes caused by different illumination on the object are corrected. This way, the effect of unimportant and / or noisy changes on the accuracy of results obtained is minimized.

To confirm the SOM-QE concept, experiments and simulations with real and artificial images were conducted. Each experiment / simulation's results were compared with the expected results and SOM-QE was found to give reliable results. Statistically, it was confirmed that the results were reliable and consistent.

For example, a simulation was done with two basic images whose differences could easily be traced visually by human. When SOM-QE was applied to give the differences between these two images, it produced results that were correct and matched those observed by a human visually. Besides, applying known and commonly used techniques of determining image data content – histogram and variance calculation - gave results that correspond to those given by SOM-QE. Histogram are used to give accurate distribution of numerical data. Since an image is a dataset of such data, it was an appropriate tool to employ and to compare to SOM-QE's findings. Variance, on the other hand, measures how far data values are spread from their mean. It gives the variation within a dataset,

just like SOM-QE. By giving results that correspond to those of these standard methods, SOM-QE qualifies to enter into their league and hence compete and complement the existing methods.

In further simulation, SOM-QE is shown to accurately sense controlled variations in the size of a single local dot within random-dot images. It performed better than human observers, who included untrained persons and also trained expert radiologists. Visual detection experiments were set-up, using random-dot images in a psychophysical "same-different" procedure. A pair of images was presented to the observer at a time. The observer's task was to tell whether the two images were the same or different. The pair of images presented was composed from a dataset of 4 different images. The first image was an original dot-image, with dots that were equal in size and were randomly spread within the image. The second, third and fourth images had a dot that was altered in size. In the second image, the size of the dot was increased by 5% and by 10% and 30% in the third and fourth images respectively. The human observers had difficulties noting these changes, especially the 5% one. But SOM-QE clearly produced the required differences. The results showed that the small changes detected by SOM-QE are undetectable by the human observers, both the novices and the expert radiologists. On the basis of this proof of concept, it is postulated that SOM-QE provides a statistically reliable indicator of small changes in image series that may be undetectable by the human natural vision.

Then, SOM-QE was applied to real MRI images taken from a patient with an

injured knee where its results corresponded with the clinical development within the patient. When applied to an image dataset used by another approach discussed in literature, SOM-QE posts better results especially on detection of smaller growth in the image series.

When impurities are consistently added to a set of real images, SOM-QE returns results that correspond to the effect of added impurities in the images, and the results are statistically consistent too. The impurities were added in two ways. First they were added to behave like local growths in the image. That is, they impurities caused changes in particular regions of the images, like growing lesions do. In the second way, the impurities were added throughout the images behaving like global impurities.

When one 'lesion' was added on each image in the dataset to form another dataset, SOM-QE results reflected this addition of lesion. The results were also statistically important. When a second lesion is added to form a third dataset of images and which SOM-QE is applied, the addition of the lesion is reflected by the SOM-QE results too. If these image datasets were real, taken during 3 consecutive clinical visits by the patient, then SOM-QE will have indicated to the radiologists and surgeons that the lesions were increasing, which should trigger a change in management of the patient's condition. Thus, SOM-QE can tell when a lesion or tumour is increasing or decreasing in size in a patient's organ, triggering the radiologist to take appropriate action.

The results from the series of simulations described in this work suggest that



SOM-QE analysis seems well-tailored for fast change detection in large bodies of medical images from patients. It allows the automatic detection of subtle but significant changes in time series of images likely to reflect growing or receding lesions. In clinical practice, finding evidence for subtle growth through visual inspection of serial imaging can be very difficult. This is especially true for scans taken at relatively short intervals (less than a year). Visual inspection often misses the slow evolution because the change may be obscured by variations in body position, slice position, or intensity profile between scans. In some cases, the change can be too small to be noticed. Surgeons and oncologists frequently compute the change in tumour volume by comparing the measurements from consecutive scans. When the change in tumour volume is too small and hence difficult to detect between two sequential scans, radiologists tend to compare the most recent scan with the earliest available image to find any visible evidence for an evolution of the tumour. The resulting analysis does, however, not reflect the current development of the tumour but rather a retrospective perspective of tumour evolution, as pointed out earlier. This study addresses this problem, as fast SOM could be easily implemented to aid clinicians in deciding about treatment. The process of executing the code to determine the QE distribution for a series of twenty images takes about 40 seconds. This involves reading the DICOM images from a folder, running the SOM and determining the QE for each image, displaying the image on the screen and saving the QE value in a text file. In summary, whenever SOM-QE values of images taken at consecutive times rises, it is a potential indication that lesions or other pathological changes

of the organ under study may be developing, while a decrease of the SOM-QE value may indicate that a pathology is receding. To the best of our knowledge, our approach is the first to automatically detect potentially critical local changes in a patient by comparing images taken from subsequent clinical visits without relying on visual inspection or manual annotations. The SOM-QE method detects these changes rapidly with a minimal computation time using consecutive images of an organ without having to rely on derived image qualities as is the case for image subtraction methods, for example. The SOM-QE method also represents a clear advantage compared with monitoring a condition, for example cancer progression or remission, using manual segmentation techniques on each image from an MRI sequence, which is prohibitively time consuming.

Other simulations on the application of SOM-QE were done using satellite images captured by Landsat. The detection and characterization of critical changes in public spaces of the natural or the built environment reflected by changes in image time series from remotely sensed image data may be of considerable importance for risk mitigation policies and public awareness. SOM-QE results on this end confirmed it to be a fast automatic technique that discriminates between changed and unchanged contents in large image time series, something that has been lacking as reported in literature. The changing trends of growth on urbanization of regions within Las Vegas city in USA was studied. Between 1984 to 2008, urbanization in the city grew to cover much of what was previously a desert. SOM-QE reliably covered this phenomenon, with

Pearson's correlation showing statistically significant correlations between SOM-QE value and the number of visitors and the population totals for the time period. At the pixel level – which translate to specific locations within the city – SOM-QE returned results that showed locations that experienced change and those that did not experience changes within a specific period. While some approaches of detecting changes in land use / cover rely on changing size of particular land use zone from one time to another, SOM-QE demonstrated that even changes that did not result to reduction or increase in the size of land use zone are detectable. A fixed-size land use / cover zone for all images under consideration was used to demonstrate this. For instant, when an additional house is built in a built-up zone, a change occurs yet the land-use / cover size of the built up zone has not changed. Thus SOM-QE can detect changing objects within a scene, like new building coming up, equipping the city managers with information to, for instance, potentially detect illegal building being constructed.

Neighbouring Las Vegas city is Lake Mead which has seen its water level change within this period. SOM-QE reliably reported this results too. Pearson's correlation statistic computed on the paired distributions for SOM-QE and water levels signalled a statistically significant correlation, for the time period 1984-2008.

The effectiveness of the SOM-QE technique to determine changes as portrayed by satellite images was evaluated using a dataset of images. When detecting changes between two images from this dataset, SOM-QE returned results that

fully corresponded with the ground truth results provided. Detection of change in temporal images using SOM-QE, opens new possibilities for fast automatic processing for which a quick decision about change or no change needs to be made. Results indicate that SOM-QE values varies consistently, reliably, and predictably with local variations in spatially distributed contrast signals in random-dot images, and in image series with regularly distributed spatial contrasts (geometric configurations). On the grounds of these systematic variations, SOM-QE is a highly sensitive and reliable indicator of local and global image homogeneity: as images from a time series become more heterogeneous in spatial contents, SOM-QE increases; conversely, as images become more homogeneous in spatial contents, SOM-QE consistently decreases, provided the intensity of contrast is constant across images of a given series.

In conclusion, there is, to our knowledge, no reported method that has achieved superior results on similar problems. The work is important as it introduces a new way of looking at automatic change detection when dealing with very small local changes in images. The method proposed is easy to implement, fast, and robust. The method is aimed to provide near real time results in detection and or classification of images. Thus, it represents a promising and non-expensive technique for the automatic classification of medical images or tracking changes in landscape information from large bodies of image data. In the medical applications, these could be scans taken over time from the same patient for a given condition whose evolution may be slow but progressive and therefore not

easily detectable by human experts. This opens new doors for monitoring of cancer progression and remission. In the study of land satellite imagery, longitudinal studies of time-series data of regions of interest is essential for proper planning of future cities and other urban spaces.

The next results, show how SOM-QE can track changing objects within the ROI. The QE of an input feature vector is monitored between images to determine the changes. See Table I.2 and Figure I.5.

Input vector position index	SOM-QE value 1984 image	SOM-QE value 1985 image	Change in QE
353	0.3316	0.3316	0
362	0.3314	0.3314	0
1284	0.2896	0.2896	0
2501	0.1551	0.1551	0
3001	0.0534	0.0566	-0.0033
3587	0.0411	0.0362	0.0049
3955	0.0711	0.0649	0.0062
7065	0.1681	0.1427	0.0254
11689	0.1287	0.1260	0.0027
17587	0.24211	0.2421	0

Table I.2: Sampled SOM-QE values of regions within the Residential North ROI on the same position of images captured in 1984 and 1985. The last column indicates the amount and direction of change in the region as determined by SOM-QE. Note the two positions, 2501 and 17587, with SOM-QE values of 0.1551 and 0.2421 respectively and whose positions are labelled in Figure I.5.

Some objects changed by increasing their SOM-QE values, others decreased while others did not change as shown in the last column of Table I.2. Figure I.5 shows the objects within the ROI, with black dots – pixels- indicating the regions that did not change between the images on each row. All other objects changed.

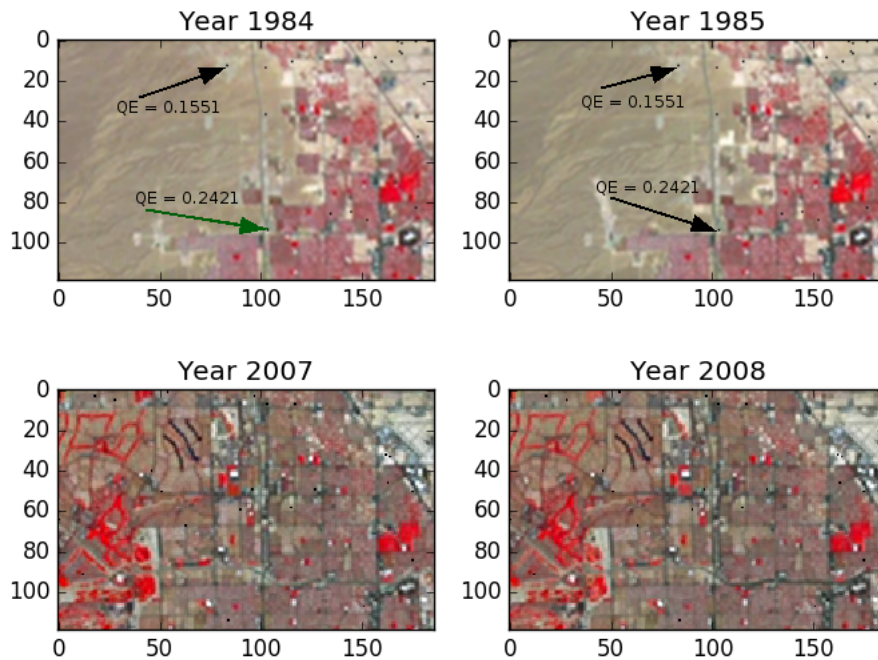


Figure I.5: The small, black dots in each year's image are areas that did not experience changes between the two years in each row. The rest of the image had some changes taking place. On the top row, two specific areas are shown out for illustration. One has a SOM-QE value of 0.2421, the second has SOM-QE of 0.1551 in both years, 1984 and 1985. The bottom row also shows areas of no-change between the years 2007 and 2008. It takes 7.1 seconds to detect changes and label regions between the two pairs of images, making this approach appropriate for the task.

Another finding in this thesis, is that given a series of SOM-QE values of an object/scene, it is possible to determine future SOM-QE values and hence predict the changes that are likely to occur in the object/scene.

A visualization of SOM-QE data calculated from a set of 28 time series images indicated that this data points calculated over time by SOM-QE have an internal structure that can be accounted for. When plotted, current SOM-QE value against the observation at the previous time step, the observations fall along a diagonal line. This is a confirmation that the SOM-QE dataset has correlation within it, hence it can be used for prediction purposes. Thus, the new technique, SOM-QE, generates data that can be applied to determine future change, its direction and its magnitude.

When a prediction model is trained and run on this data, all changes depicted by SOM-QE between images are correctly predicted by this model. The change detection is seen to be on the same direction (increase or no-change or decrease) with the actual values.

To evaluate SOM-QE performance as a change detector and as a provider of prediction data, it was tested on two datasets. The first dataset was of real measurements captured by instruments, which are compared with SOM-QE values obtained from corresponding images to determine the accuracy. The measurements are of the annual cycle of carbon dioxide gas ( $CO_2$ ) in the Northern Hemisphere, covering the period from January 1 to December 31, 2012 and indicate the distinct rise and fall of carbon dioxide levels over a year's time.

The unit used to record the gas data is parts per million (ppm), which is the number of  $CO_2$  molecules present in every million molecules of air. The annual pattern is caused by the uptake and release of  $CO_2$  from seasonal plant growth on the vast landmasses of the Northern Hemisphere. The annual maximum  $CO_2$  concentration in the Northern Hemisphere occurs around May. The spring build-up happens because decaying plants have been releasing carbon throughout the winter. The annual minimum concentration occurs around October, after new growth has withdrawn  $CO_2$  from the air during photosynthesis.

The dataset is suitable for use in this instance because, when the pollutants molecules increase the variation within the 1 million molecules of air increases too. This means for low ppm, SOM-QE should increase/reduce with increase/reduction of the amount of  $CO_2$ .

The performance of SOM-QE as a change detector was calculated as:

$$\text{precision, } p = 8 \div 11 = 0.727$$

$$\text{recall, } r = 8 \div 11 = 0.727$$

$$\text{and F1 score of } (2 \times p \times r) \div (p + r) = 0.727$$

This is a better score than those reported in related literature. For instance, it is reported that the best results posted by various 2D change detectors was an  $F1$  score of 0.723. This is below that posted by SOM-QE above.

The 12 monthly images were used to train a predictor. The prediction for



SOM-QE value of next image was determined as: 0.224166

That is, January 2013 image will have a SOM-QE value of 0.2242, up from that of December 2012 image at 0.2023, a + 0.0219 change. On the other hand the recorded  $CO_2$  for January 2013 is 395.5 ppm up from 394.82 ppm recorded for December 2012, a + 0.68 change. This is a 'hit', meaning that SOM-QE correctly predicts that the amount of  $CO_2$  in air increased in January 2013.

The second dataset used to evaluate and compare SOM-QE with other techniques was what was described in literature as a 'challenging change-detection image dataset'. This dataset has a category of images called the PTZ - pan-tilt-zoom camera - category which requires different type of change detection techniques in comparison to static camera videos.

It is reported that a total of 14 change detection methods available in literature were tested and the F-measure for each method was calculated. In particular, the PTZ category showed the lowest performance, a fact attributed to its unique challenges posed by the zoomed-in/zoomed-out nature of the images involved.

Each of the 14 methods posted F1-measure scores of under 0.30. When SOM-QE was applied to this category, it scored an F1 of 0.39, clearly beating the rest which are among the best methods in literature.

In the PTZ category, any camera motion (pan, tilt or zoom) caused major false positives from each method, but SOM-QE minimized them, see Figure I.6.



Figure I.6: On the left and at the middle are sample input and ground truth images respectively from the 2014 CDnet dataset, PTZ category. To the right is the image produced by SOM-QE on detecting the changes between the input image and its next image frame on the video. The PTZ category of images posed unique challenges on change detection, with other methods in the literature managing F1 score of less than 0.30. SOM-QE scored an F1 score of 0.39, which is the best score in this category.

Finally, in this thesis, a new method to determine QE in time series images is proposed. The new method considers the fact that a BMU for a specific input vector may change along the time series of images.

In the traditional determination of QE, the difference between the original input vector,  $x$ , and its winner, the BMU, is used, see equation I.11. The BMU is one of the final weights in the trained SOM and is chosen to be the closest to the input vector.

$$QE = x - BMU \quad (I.11)$$

For a set of time series images where change is to be detected, the winner of vector may not be the same across the images. This is inherent from the principle of competitive learning which SOM practices. Units in the SOM map compete for the right to respond to the input data vector – the unit with the closest resemblance wins, and becomes its BMU. Consequently, if the values in vector

changed between images and it is subjected to the competition, any of the SOM units can become its BMU. Depending on the changes in  $x$ , it may find itself having a new winner among the SOM weight units and this will affect results posted by equation I.11.

In change detection, the interest is in the change that has occurred in between subsequent images in a time series dataset. This is the change that is as a result of changing status of the object whose images were acquired at different times.

When the object has undergone some changes, we expect the changes to be reflected in the input vector  $x$ . The set of SOM final weights, from which  $x$ 's winner is determined from, carries different values and are not necessarily equal. It therefore implies that when  $x$  switches winners, it affects the results given by equation I.11 as it include not only the change in  $x$ , but also the changes due to the use of a different winner. Reporting change in this manner may be inaccurate, as it includes the results from two sources: first the actual difference between the input vector in the first dataset and that of the second dataset, and secondly the use of a different *BMU* to calculate the QE for the vector in the two different datasets. To maintain accuracy, this second source of change need to be eliminated.

For example, suppose we have two images with corresponding input vectors  $x_{t1}$  and  $x_{t2}$ , that is,  $x$  at time 1 and  $x$  at time 2. The two images are captured at different times and are preprocessed to ensure uniformity in alignment and lighting exposure. Input vector  $x_{t1}$  and  $x_{t2}$  are from the same position in the two

images, that is, they represent the same object within the image. From a trained SOM,  $x_{t1}$  may be won by weight  $w_1$  while  $x_2$  is won by weight  $w_2$ . Thus,  $w_1$  becomes the BMU for  $x_{t1}$  ( $BMU_1$ ) while  $w_2$  becomes the BMU for  $x_{t2}$  ( $BMU_2$ ). The traditional method to calculate QE is to find the the difference of the input vector and its BMU. In this case, on applying equation I.11, the QE for the two instances becomes:

$$QE_1 = x_{t1} - BMU_1 \quad (I.12)$$

and,

$$QE_2 = x_{t2} - BMU_2 \quad (I.13)$$

and for the entire dataset the QE values for the object form a set:

$$QE_{object} = \{x_{t1} - BMU_1, x_{t2} - BMU_2, x_{t3} - BMU_3, \dots\} \quad (I.14)$$

that is, the object has QE values from each image in the series that is not calculated from the same BMU.

For a time series dataset this raises an issue. Input vectors  $x_{t1}$  and  $x_{t2}$  represent the same object, only that their representation is at different times. It is therefore logical that  $QE_1$  and  $QE_2$  be determined from a common reference point ( $BMU$ ) in order for them to be mathematically comparable and hence

accurately determine whether change has occurred in the object or not.

The proposal is, therefore, to restrict the change detection process to change in  $x$  between images. This is done by ensuring that input vector  $x$  is associated to the same winner across the image dataset. To attain this, the winners determined during the training phase of SOM are maintained for each  $x$ . The index of  $x$  in the training data is used to extract it on testing images and its initial winner from the training data used to determine QE.

$$QE = x - originalBMUofx \quad (I.15)$$

and thus equation I.14 becomes:

$$QE_{object} = \{x_{t1} - BMU, x_{t2} - BMU, x_{t3} - BMU, \dots\} \quad (I.16)$$

When SOM-QE is determined using the two methods – the traditional method and the new method suggested here - the results shown in Figure I.7 are obtained.

In both results, the trend in changing SOM-QE values is similar. But the larger SOM-QE values obtained when a fixed BMU value is applied make it more sensitive to change. The amount of change sensed by SOM-QE when a fixed BMU for an input vector is applied is bigger than when a varying BMU is used, see Figure I.8.

Thus, the new method provides a bigger scale of change measurement than the

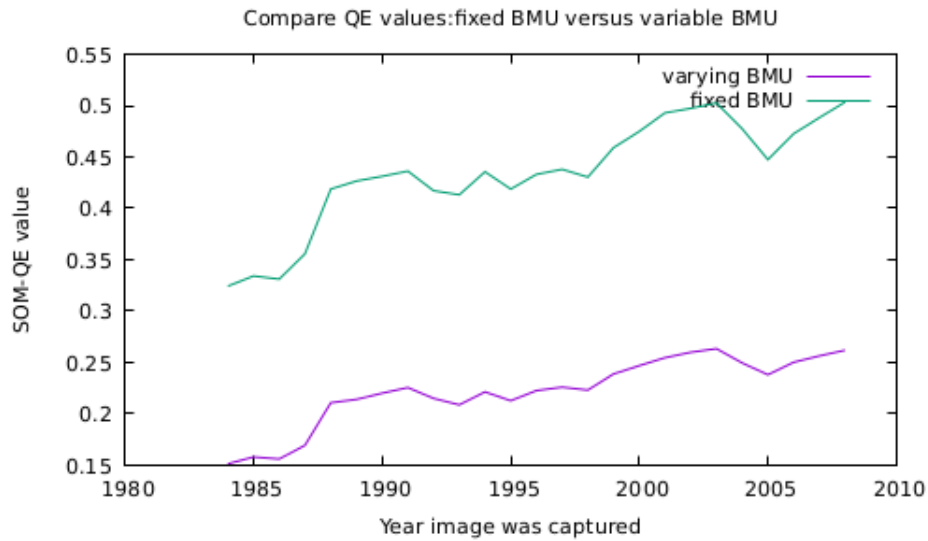


Figure I.7: The two plots show the result of calculating SOM-QE values using the two methods. At the bottom is the result obtained by applying equation 9 where the BMU of the input vector at a particular image is used to find the QE. The plot on top shows results obtained by the new method where the BMU obtained for every input vector at the end of SOM training is retained and used to determined QE for that particular vector throughout the time series of images, as in equation I.15. There is a common pattern in the two results, but when the fixed BMU is used, the difference in SOM-QE between images is bigger and hence more pronounced. Images of a section of Las Vegas as captured between year 1984 and 2008 were used in this simulations.

traditional method, and is found to be more sensitive to changes than the traditional method. This places it in a better position to detect changes, especially small changes, between images.

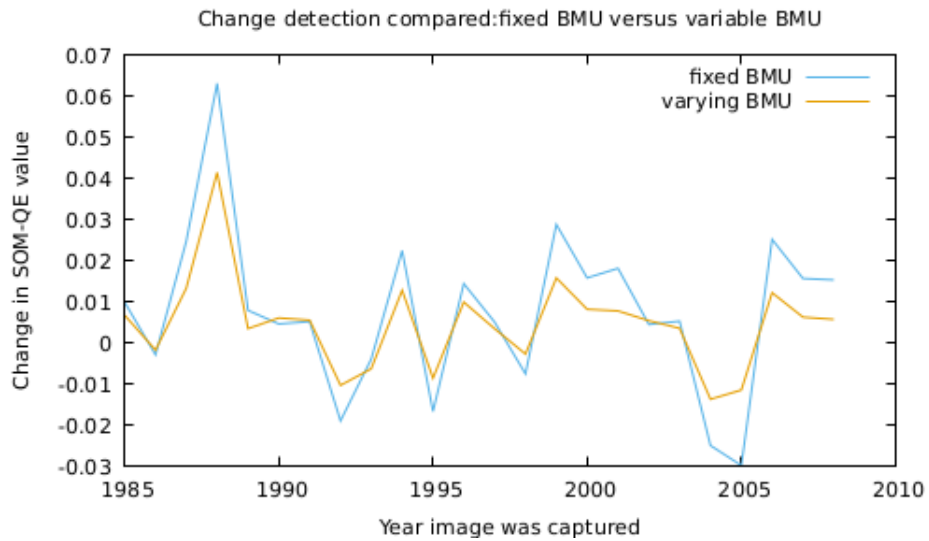


Figure I.8: The changes that occurred in the ROI as reflected in images are shown here for the two methods of determination of SOM-QE. The fixed BMU method shows bigger change occurred between consecutive images in the series than the varying BMU method. To note change, consider the point's distance from 0 (no-change-point, on y-axis) on the two curves. For instance in year 2005, the change is 0.03 units for the new method and slightly above 0.01 units for the traditional method.